AD-A080 227 NORTHROP CORP HAWTHORNE CA AIRCRAFT GROUP F/G 20/4
TRANSONIC KERNEL FUNCTION METHOD FOR UNSTEADY FLOW CALCULATIONS--ETC(U)
MAY 79 D D LIU, W S PI, M T LANDAHL F33615-78-C-3202
UNCLASSIFIED NOR-79-52 AFFDL-TR-79-3085 NL

1 OF 2
AD A080227

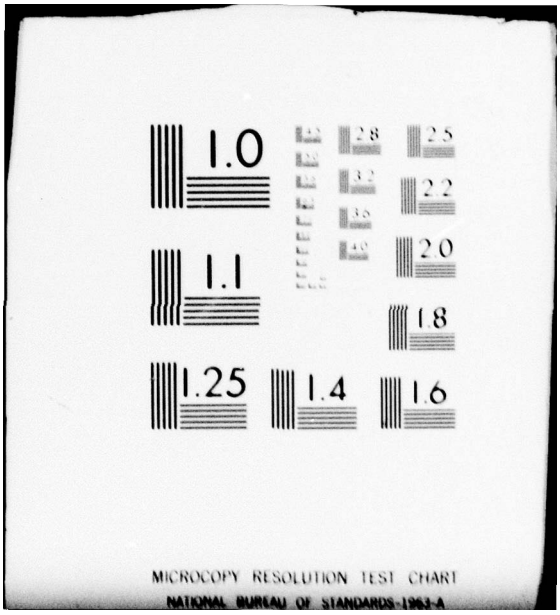
1.0
1.1
1.25
1.4
1.6
2.8
2.5
2.2
2.0
1.8
MICROCOPY RESOLUTION TEST CHART
NATIONAL BUREAU OF STANDARDS-1963-A

LEVEL II

AFFDL-TR-79-3085

TRANSONIC KERNEL FUNCTION METHOD FOR UNSTEADY FLOW CALCULATIONS USING A UNIFIED LINEAR PRESSURE PANEL PROCEDURE

NORTH CORPORATION
AIRCRAFT GROUP
HAWTHORNE, CALIFORNIA 90250

OCTOBER 1979

TECHNICAL REPORT AFFDL-TR-79-3085
Final Report for period 1 March 1978 – 31 May 1979

Approved for public release, distribution unlimited.

AIR FORCE FLIGHT DYNAMICS LABORATORY
AIR FORCE WRIGHT AERONAUTICAL LABORATORIES
AIR FORCE SYSTEMS COMMAND
WRIGHT-PATTERSON AIR FORCE BASE, OHIO 45433

NOTICE

When Government drawings, specifications, or other data are used for any purpose other than in connection with a definitely related Government procurement operation, the United States Government thereby incurs no responsibility nor any obligation whatsoever; and the fact that the government may have formulated, furnished, or in any way supplied the said drawings, specifications, or other data, is not to be regarded by implication or otherwise as in any manner licensing the holder or any other person or corporation, or conveying any rights or permission to manufacture, use, or sell any patented invention that may in any way be related thereto.

This report has been reviewed by the Information Office (OI) and is releasable to the National Technical Information Service (NTIS). At NTIS, it will be available to the general public, including foreign nations.

This technical report has been reviewed and is approved for publication.

S. J. Pollock

S. J. POLLOCK
Project Engineer
Aeroelastic Group
Analysis & Optimization Branch

Fred A. Picchioni

FREDERICK A. PICCHIONI, Lt Col, USAF
Chief, Analysis & Optimization Br
Structures and Dynamics Division

FOR THE COMMANDER

Ralph L. Kuster Jr

RALPH L. KUSTER, JR., Colonel, USAF
Chief, Structures & Dynamics Division

"If your address has changed, if you wish to be removed from our mailing list, or if the addressee is no longer employed by your organization please notify AFFDL/FBR *, W-PAFB, OH 45433 to help us maintain a current mailing list".*

Copies of this report should not be returned unless return is required by security considerations, contractual obligations, or notice on a specific document.

AIR FORCE/56780/22 January 1980 — 150

UNCLASSIFIED

SECURITY CLASSIFICATION OF THIS PAGE (When Data Entered)

(19) **REPORT DOCUMENTATION PAGE**

READ INSTRUCTIONS BEFORE COMPLETING FORM

1. REPORT NUMBER (18) AFFDL-TR-79-3085	2. GOVT ACCESSION NO. / 3. RECIPIENT'S CATALOG NUMBER
4. TITLE (and Subtitle) (6) TRANSONIC KERNEL FUNCTION METHOD FOR UNSTEADY FLOW CALCULATIONS USING A UNIFIED LINEAR PRESSURE PANEL PROCEDURE	5. TYPE OF REPORT & PERIOD COVERED FINAL - 1 March 1978 - 30 May 1979
	6. PERFORMING ORG. REPORT NUMBER (14) NOR-79-52
7. AUTHOR(s) (10) D. D. Liu, W. S. Pi, M. T. Landahl	8. CONTRACT OR GRANT NUMBER(s) (15) F33615-78-C-3202
9. PERFORMING ORGANIZATION NAME AND ADDRESS Northrop Corporation, Aircraft Group 3901 W. Broadway Blvd. Hawthorne, CA 90250	10. PROGRAM ELEMENT, PROJECT, TASK AREA & WORK UNIT NUMBERS (12) 1486
11. CONTROLLING OFFICE NAME AND ADDRESS Air Force Flight Dynamics Laboratory/FBR Air Force Systems Command Wright-Patterson Air Force Base, Ohio 45433	(11) 12. REPORT DATE May 1979 / 13. NUMBER OF PAGES
14. MONITORING AGENCY NAME & ADDRESS (if different from Controlling Office) (9) Final rept. 1 Mar 78 - 30 May 79,	15. SECURITY CLASS. (of this report) Unclassified / 15a. DECLASSIFICATION/DOWNGRADING SCHEDULE

16. DISTRIBUTION STATEMENT (of this Report)

Approved for public release; distribution unlimited

17. DISTRIBUTION STATEMENT (of the abstract entered in Block 20, if different from Report)

18. SUPPLEMENTARY NOTES

19. KEY WORDS (Continue on reverse side if necessary and identify by block number)

Subsonic Flow
Transonic Flow
Supersonic Flow
Unsteady Aerodynamics
Kernel Function Method
Panel Methods

20. ABSTRACT (Continue on reverse side if necessary and identify by block number)

A transonic kernel function method for unsteady flow calculations has been developed. A unified linear pressure panel procedure is established to solve for two-dimensional problems in the subsonic, transonic, and supersonic flow regimes; consequently, a TLP2D computer code is developed. Numerical results are presented for pitching or flapping airfoils in these linear and nonlinear flow regimes. The mixed kernel function procedure is applied to a pitching Guderley airfoil in sonic flow. Comparisons with other results and

DD FORM 1 JAN 73 1473 EDITION OF 1 NOV 65 IS OBSOLETE

UNCLASSIFIED

SECURITY CLASSIFICATION OF THIS PAGE (When Data Entered)

410 275

20. ABSTRACT

discussions are given. Additional analytical studies include Landahl's general formulation of the phase correction method and the kernel function formulation of the Eckhaus-Landahl shock-jump model. Finally, assessments of and recommendations for the present work are given.

FOREWORD

This report was prepared by Northrop Corporation, Aircraft Group, for the Analysis and Optimization Branch, Structures and Dynamics Division, Air Force Flight Dynamics Laboratory (AFFDL), Wright-Patterson Air Force Base, Ohio. The research study was performed under contract F33615-78-C-3202, entitled "Mixed Kernel Function Method for Unsteady Transonic Flow Calculations." Mr. Sam Pollock of AFFDL/FBR was the Air Force Task Engineer.

At Northrop, the principal investigator was Dr. D. D. Liu and the co-investigator was Dr. W. S. Pi; Professor M. T. Landahl of MIT/KTH was the consultant. The report was submitted in May 1979 to cover research conducted from March 1978 to May 1979.

The authors express their appreciation to Professor M. F. Platzer of the Naval Postgraduate School for technical discussions and for providing them a number of check cases. Ms. K. Dorsey's and Mrs. P. Barnes' effort in preparation of the graphics and typing of the manuscript are acknowledged.

CONTENTS

ILLUSTRATIONS

ILLUSTRATIONS (continued)

ILLUSTRATIONS (continued)

LIST OF SYMBOLS

Symbol	Definition
a_n	coefficients of the curve fit polynomials for C_{p_o}
A, B, F	variant coefficients of Eq (2.10)
$\bar{A}, \bar{B}, \bar{C}$	coefficients of the curve-fit parabola for F_m's
$\bar{c}$	physical chord length
c_m	associated constants of the two-dimensional kernel functions, Eq (3.13) m = o,1,2
C_m	associated constants of the three-dimensional kernel functions
C_{p_o}	pressure coefficient of steady mean-flow
$\Delta C_p'$	in-phase pressure distribution, real part of p
$\Delta C_p''$	out-of-phase pressure distributions, imaginary part of p
D_{ji}	the kernel matrix element
ΔD_{ji}	integrated D_{ji} for the ith or (i+1)th element
$f_i(\xi)$	assumed functions for $p(\xi)$ in the panel method
$F_m(x_j - \xi)$	regular functions; m = 0,1,2
$H(X)$	unit step function
$H_0^{(2)}(\lvert X\rvert), H_1^{(2)}(\lvert X\rvert)$	Hankel functions of zeroth and first order of the second kind
i	$= \sqrt{-1}$
$J_0(X), J_1(X)$	Bessel functions of zeroth and first order
k	$= \omega\bar{c}/(2U_\infty)$, the reduced frequency
$K_0(X), K_1(X)$	modified Bessel functions
$K_m(X,O)$	transonic kernel functions m = o,1 and 2 for sonic, transonic/supersonic, and transonic/subsonic flow regimes

ℓ	total normalized chord length
m_0	$= \sqrt{M^2 - 1}$
m_∞	$= \sqrt{M_\infty^2 - 1}$
M	local Mach number
M_∞	freestream Mach number
$p(\xi)$	the unsteady pressure function
r	$= Y^2 + z^2$ ($r = z$ for two-dimensional flow)
R	$= \sqrt{X^2 + \beta_0^2 r^2}$
t	$= \bar{t} U_\infty / \bar{c}$
$\bar{t}$	true time
$\hat{t}$	one-half of the maximum airfoil thickness
$Sgn(X)$	$= 1$, if $X > 0$ $= -1$, if $X < 0$
U_∞	freestream velocity
$W(x)$	downwash function
$(\bar{x},\bar{y},\bar{z})$	physical cartesian coordinates
(x,y,z)	normalized cartesian coordinates
x_i	the control point (or the receiving point)
x_s	shock point location
X	$= x - \xi$
Y	$= y - \eta$

Greek Symbols

α	$= \dfrac{2kM_\infty^2}{1 - M^2(x_s^+)}$ see Eq (B.1)
α_0	see Eq (3.10)
$\tilde{\alpha}_0$	see Eqs (3.25) and (3.26)
β_0	$= \sqrt{1 - M_\infty^2 - \lambda}$

β_∞	$= \sqrt{1 - M_\infty^2}$
γ	specific heat ratio of the gas, 1.4 for air
$\delta(X)$	Dirac's delta function
δ_i	see Appendix A, Eq (A.1)
θ	the phase angle of the local solution
$\hat{\theta}$	wedge apex angle
	$= kM_\infty/\beta_\infty$
λ	$= (\gamma + 1)M_\infty^2 \phi_x$
μ	$= (\gamma + 1)M_\infty^2 \phi_{xxx}$
ν	wave front angle, see Addendum
ν_∞	$= (\gamma + 1)M_\infty^2$
(ξ, η, ζ)	running coordinate of (x,y,z)
ξ_i	the sending point for the DL method; or the leading edge of the ith panel for LPP method
π	$= 3.14159\cdots$
ρ	see Eq (3.11)
σ	see Eq (3.11)
τ	$= \hat{t}/\ell$ for an airfoil
	$\simeq \hat{\theta}/2$ for a wedge
ϕ	perturbed steady velocity potential
φ	perturbed oscillatory velocity potential
$\bar{\Phi}$	perturbed velocity potential
Φ	$= \bar{\Phi}/(U_\infty \bar{c})$
χ	see Eq (3.12)
Ψ	total acceleration potential
Ψ_0	steady acceleration potential
ψ	oscillatory acceleration potential
$\bar{\Omega}$	total time-dependent velocity potential
ω	true angular frequency of pitching or flapping motion

SECTION 1

INTRODUCTION

Current interests in aeroelastic problems in the transonic range demand viable methods for unsteady flow calculations. At present, there are two classes of numerical methods in progress: first, computation based on flow field 'meshes' or 'elements', and second, computation based on wing planform elements. The method in the first class, known as the 'computational method', relies mainly on the finite difference scheme (References 1 through 6) and on the finite element scheme (Reference 7). Although these methods in many cases provide accurate details of the transonic flow field, their applications to the three-dimensional flutter calculation appear to be still too costly in practice. Besides, there are some frequency restrictions in these methods due to either equation simplification (e.g., Reference 5) or requirements in convergence (e.g., Reference 1).

The methods in the second class are based on the lifting-surface theory formulation. In terms of the paneling scheme, these methods require considerably fewer elements and hence are potentially more cost-effective.

Ever since Küssner (Reference 8) formulated the classical lifting surface theory, there has been a long-standing research effort devoted to the development of the kernel function methods (e.g., Reference 9). In the last decade, this method was advanced and adopted by various aircraft industries as a common practice for flutter calculation purposes (Reference 10). As the method is based on a pressure formulation, it has the advantage that the calculation domain can safely exclude the upstream and the wake regimes without any loss of generality (see Figure 1). Moreover, the method is proven to be flexible in incorporating various modes into the flutter calculation scheme in a fairly wide frequency range. The scope of this method, however, has yet to be explored further in two important areas. First, the method was largely

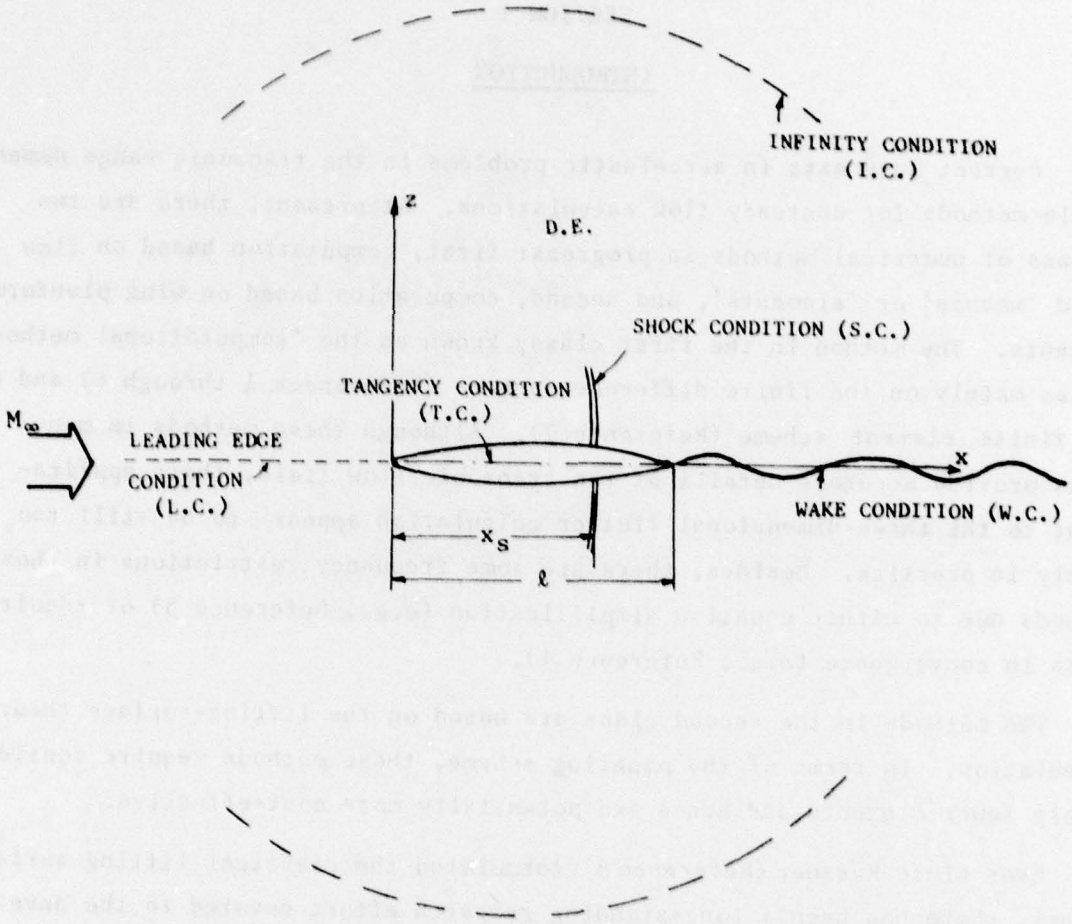

Figure 1. Oscillatory Transonic Airfoil as a Boundary Value Problem

restricted to the linearized subsonic and supersonic flow regimes, whereas its application in the transonic flow regime only until recently was uncertain. Second, the applications of the kernel function formulation have been successfully combined with the use of the pressure-mode method (References 11 and 12), which, however, lacks the flexible and versatile feature of that of the panel methods, e.g., the doublet lattice (DL) scheme (Reference 13).

Although the pressure-mode method has been worked out in the purely subsonic and supersonic regimes, the panel method has been limited to the subsonic regime and its supersonic unsteady counterpart has never been completely worked out. In recent years, the kernel function method was extended to the transonic range by Tijdeman and Zwaan (Reference 14), and by A. Cunningham (Reference 15). These methods are, however, based on the modification of the classical purely subsonic and/or the purely supersonic kernel functions in which the steady flow nonuniformity was not formally considered. Some good results were produced by these methods as a result of the partial inclusion of the receding-wave effects, but the formal expressions of the transonic kernel functions and the calculation procedures remain to be established.

More recently, Liu and his associates (References 16 through 19) have proposed a Mixed Kernel Function (MKF) method for unsteady transonic flow calculations. In these publications, mixed procedures of various types of kernel functions in combination with the panel method were proposed. The method was aimed at a unified three-dimensional approach, which would bridge the classical subsonic and supersonic lifting surface methods through the transonic regime, including the effect of the oscillatory shock wave. The only provision of the MKF approach is that the mean flow structure in the proximity of the planform must be supplied by either experiments or other means of computations.

To tackle the three-dimensional problem as such, however, requires a firm understanding of the basic MKF procedure. Hence, it is the purpose of this report to investigate the basic issues related to the MKF procedure for two-dimensional flow. The present work consists of two goals. On one hand, the transonic acceleration potential equation is derived and the transonic

kernel functions in various flow regions are established. The formulation of the MKF method is then followed by the numerical evaluations of these transonic kernel functions and the application of the local linearization procedure to these functions. On the other hand, thorough investigations of various discrete-element types of paneling schemes are required. These amount to selecting a promising candidate from the DL scheme, the Constant Pressure Panel (CPP) scheme, and the Linear Pressure Panel (LPP) scheme, for a unified paneling scheme applicable throughout the regimes of subsonic, transonic, and supersonic flows. It is considered a challenging task, as no such unified paneling scheme has been found workable for unsteady flow calculations in the past. In later sections, it is demonstrated that our LPP scheme is indeed a unified method suitable for all linearized flow regimes. The success of this scheme really depends on the correct choice of the control point location. Then the local linearization procedure is combined with the LPP scheme to account for the nonuniformity of the steady mean flow (it is called 'nonlinear' flow hereafter; specifically, we refer to it as transonic/subsonic flow, transonic/supersonic flow, and nonlinear sonic flow).

To demonstrate the transonic LPP method, calculation examples are presented for pitching and flapping NACA64A006 airfoils in subsonic flow, for the pitching Guderley airfoil and parabolic-arc airfoils in sonic flow, and for the pitching wedges and parabolic-arc airfoils in supersonic flow. Both purely linearized flow results and nonlinear results were compared with those calculated by various methods. A MKF procedure was performed on a Guderley airfoil for the case of shockless smoothed sonic flow. Also, based on the proposed MKF concept, the oscillatory shock patching scheme was derived for the case of Eckhaus-Landahl's aileron buzz model. Finally, assessments of and recommendations for the present method are given.

SECTION 2

BASIC FORMULATION

The total time-dependent velocity potential $\bar{\Omega}(\bar{x},\bar{y},\bar{z},\bar{t})$ can be written as

$$\bar{\Omega} = U_\infty \bar{x} + \bar{\Phi}(\bar{x},\bar{y},\bar{z},\bar{t}) \tag{2.1}$$

where the barred symbols indicate the true physical quantities and U_∞ being the freestream velocity. The perturbed potential $\bar{\Phi}$ is normalized by $(U_\infty \bar{c})$ and is split into a steady and unsteady component, i.e.,

$$\bar{\Phi}/(U_\infty \bar{c}) \equiv \Phi(x,y,z,t) = \phi(x,y,z) + \hat{\varphi}(x,y,z,t) \tag{2.2}$$

where $(x,y,z,t) = (\bar{x}/\bar{c},\ \bar{y}/\bar{c},\ \bar{z}/\bar{c},\ \bar{t}U_\infty/\bar{c})$ and $\bar{c}$ is the physical chord length. For transonic flow, the first term, ϕ, is governed by the steady-flow nonlinear small disturbance equation (e.g., Reference 20) and the second term, $\hat{\varphi}$, is governed by the oscillating flow equation (e.g., Reference 21).

$$\Box\varphi = \nu_\infty(\phi_x\varphi_x)_x \tag{2.3}$$

where

$$\begin{cases} \Box = \Delta + \dfrac{\partial^2}{\partial y^2} + \dfrac{\partial^2}{\partial z^2} \\ \Delta = (1 - M_\infty^2)\dfrac{\partial^2}{\partial x^2} - 2ikM_\infty^2\dfrac{\partial}{\partial x} + k^2M_\infty^2 \\ \varphi = \hat{\varphi}e^{-ikt} \end{cases} \tag{2.4}$$

[illegible]

Mach number, the [illegible]

(defined as [illegible]

frequency of oscillation.

Transonic acceleration potential [illegible]

The acceleration potential, [illegible]

[illegible]

where [illegible] is some function of time. [illegible]

can be written in terms of the [illegible]

[illegible]

Substituting Equations (2.5) and (2.7) into Equations [illegible] and keeping terms of comparable order to those in Equation [illegible]

[illegible]

The acceleration potential can be split into two components, i.e.,

[illegible]

where

[illegible]

and $()_x \equiv \frac{\partial}{\partial x}$ and $\nu_\infty \equiv (\gamma + 1)M_\infty^2$. The parameters M_∞, γ, and k are the freestream Mach number, the specific heat ratio of the gas, and the reduced frequency (defined as $k = \omega\bar{c}/(2U_\infty)$, where $\bar{c}$ is the chord length, and ω is the circular frequency of oscillation).

2.1 Transonic Acceleration Potential

The acceleration potential, Ψ, is related to the fluid pressure and density as

$$\Psi = -\int \frac{dp}{\rho} + F(t) \tag{2.5}$$

where F(t) is some function of time. According to Bernoulli's equation, Ψ can be written in terms of the total potential, $\Omega(= \bar{\Omega}/(U_\infty\bar{c}))$, i.e.,

$$\Psi = \Omega_t + (\nabla\Omega \cdot \nabla\Omega - 1)/2 \tag{2.6}$$

Substituting Equations (2.1) and (2.2) into Equations (2.5) and (2.6) and keeping terms of comparable order to those in Equation (2.3), we obtain

$$\Psi \simeq \phi_x + [\hat{\phi}_t + (1 + \phi_x)\hat{\phi}_x] \tag{2.7}$$

The acceleration potential can be split into two components, i.e.,

$$\Psi = \psi_o + \psi e^{ikt} \tag{2.8}$$

where

$$\begin{cases} \psi_o = \Lambda_o\phi \quad , \quad \Lambda_o \equiv \dfrac{\partial}{\partial x} \\ \psi = \Lambda\varphi \quad , \quad \Lambda = ik + (1 + \phi_x)\dfrac{\partial}{\partial x} \end{cases}$$

It is seen that the transonic acceleration potential, ψ, contains an additional term, ϕ_x, to the one commonly used by the purely subsonic and supersonic flow analysis.

2.2 The Transonic Acceleration Potential Equations

Applying operator Λ to Equation (2.3), making use of Equation (2.8), and keeping only the lowest order terms result in

$$\Box\psi = \nu_\infty[(\phi_x\psi_x)_x + (\phi_{xx}\varphi_x)_x + ik(\phi_x\varphi_x)_x] + \varphi_x \cdot \Box\phi_x \tag{2.9}$$

Furthermore, if we assume that ϕ_x is a one-dimensional function depending only on x, the last term in Equation (2.9) becomes $\varphi_x\Delta\phi_x$. After some rearranging, Equation (2.9) can be further simplified to the following form, i.e.,

$$\beta_o^2\psi_{xx} + \psi_{yy} + \psi_{zz} + A\psi_x + B\psi = -ik\varphi \cdot F \tag{2.10}$$

where

$$\begin{cases} \beta_o^2 = 1 - M_\infty^2 - \lambda \\ A = -2\Gamma - ik(2M_\infty^2 + \lambda) \\ B = k^3[M_\infty^2 - (\gamma + 2)\lambda_o] - \mu_o + 2ik\Gamma_o \\ F = \mu_o + k^2(\gamma + 2)\lambda_o - 2ik\Gamma_o \end{cases} \tag{2.11}$$

Parameters λ, λ_o, Γ, Γ_o, μ, and μ_o are all steady mean-flow coefficients defined as

$$\begin{cases} \lambda = \nu_\infty\phi_x = (\gamma + 1)\lambda_o \\ \Gamma = \nu_\infty\phi_{xx} = (\gamma + 1)\Gamma_o \\ \mu = \nu_\infty\phi_{xxx} = \nu_\infty\mu_o/(\gamma M_\infty^2 + 1) \end{cases} \tag{2.12}$$

It is seen that Equation (2.10) contains two dependent variables, ψ and φ, as related by Equation (2.8). Hence, Equation (2.10) is in essence an integro-differential equation in terms of ψ only. To simplify the equation, we assume the mean flow is accelerated at a fairly slow rate such that $\Gamma_o \sim O(k)$ and $\mu \sim O(k^2)$, the right-hand side of Equation (2.11) can thus be ignored up to the third order in k, i.e.,

$$\beta_o^2 \psi_{xx} + \psi_{yy} + \psi_{zz} + A\psi_x + B\psi = 0 \tag{2.13}$$

In the Addendum to this report, Landahl derived a transonic acceleration potential equation (Equation (L.1)) with a more general approach in which he also recognized the acceleration potential obtained in Equation (2.8). Starting out with the full potential equation, he arrived at a slightly different low-frequency oscillatory equation from ours (Equations (2.13) and (2.11)). It turns out that the difference lies only in the coefficients A and B; Landahl's expressions read

$$\begin{cases} A = -2\Gamma - ik[2M_\infty^2 - (\frac{2}{\gamma + 1})\lambda] + 2\beta_\infty^2(\gamma - 1)\Gamma_o \\ \\ B = k^2 M_\infty^2 - \mu - 2ik\gamma\Gamma_o \end{cases} \tag{2.14}$$

When Equation (2.14) is compared with Equation (2.11), it is seen that the difference is insignificant between the coefficients 'A', but there is some disagreement between Landahl's and our coefficient 'B'. The latter difference could be a result of our approximation in starting with the small disturbance equation. However, further investigations on this issue are needed.

Next, let us examine the coefficients, A and B, represented by other theories. Previous work in References 14, 15, and 21 all suggested replacing the freestream Mach number by a local Mach number in the DL method, the pressure-mode method or the sonic box method. We caution that such a replacement only partially recovers the mean-flow nonuniformity, and that some terms were left out. If one consistently ignores the $O(\phi_x^2)$ term in the approximations, the expressions in the previous work then differ from Equation (2.11)

by a complex coefficient $2\Gamma - ik\lambda$ in A and a complex coefficient $k^2(2\lambda + \lambda_0) + \sigma_0 - 2ik\Gamma_0$ in B. This implies that a part of the mean-flow damping mechanism was ignored. In our earlier work (Reference 16) and that of Dowell (Reference 23), both proposed to employ the velocity potential equation (Equation (2.3)) as the governing equation for ψ. In this case, the differences from Equations (2.11) are a complex coefficient, $\Gamma + ik\lambda$ in A and a complex coefficient $k^2(\lambda + \lambda_0) + \mu_0 - 2ik\Gamma$ in B. With reference to Equation (8a) of our AGARD paper (Reference 17), it is seen that the coefficient A remains unchanged but the coefficient B differs by a complex coefficient, $k^2\lambda_0 + \mu_0 - \mu + 2ik\Gamma$. Clearly, the additional terms are generated as a result of introducing the transonic acceleration potential.

In the subsequent calculation scheme, we have set up a completely general input for the coefficients A and B, so that one can easily assess various degrees of approximation by judging from the numerical results as well. Other than Equation (2.11), we often used, in the latter calculation, the following two sets of coefficients for expedient calculations. The first set is the AGARD paper formulation in which only purely linearized acceleration potential operator was used, resulting

$$\begin{cases} A = -2(\Gamma + ikM_\infty^2) - ik\lambda \\ B = k^2M_\infty^2 \end{cases} \tag{2.15}$$

The second set is the further simplification of the above, i.e.,

$$\begin{cases} A = -2(\Gamma + ikM_\infty^2) \\ B = k^2M_\infty^2 \end{cases} \tag{2.16}$$

Clearly, when Γ is a constant, Equation (2.16) is reduced to Oswatitsch and Maeder's parabolic approximation (References 24 and 25).

SECTION 3

DEVELOPMENT OF TRANSONIC KERNEL FUNCTION

To derive the kernel function, it is necessary to integrate Equation (2.8) along the mean flow direction. Hence, the integrated transonic velocity potential in the subsonic freestream can be expressed in terms of ψ as

$$\varphi = e^{-ikf(x)} \int_{-\infty}^{X} \frac{\psi}{1 + \phi_{x_o}} e^{ikf(x_o)} dx_o \tag{3.1}$$

where

$$f(x) = \int^{x} \frac{dx}{1 + \phi_x} \quad \text{and} \quad X = x - \xi$$

Establishing the kernel function by the above equation results in a rather complicated formulation. However, if we restrict the analysis in the low frequency range, namely $O(k^3, k^2\phi_x)$, Equation (3.1) can be approximated to yield the commonly-used kernel function, i.e.,

$$K_m(X,Y,0) = \left\{ \lim_{z \to o} \frac{\partial^2}{\partial z^2} \int_{-\infty}^{X} e^{ikx_o} \psi_m(x_o, Y, z) dx_o \right\} \cdot e^{-ikX} \tag{3.2}$$

where $X = x - \xi$, $Y = y - \eta$, and subscripts m = o, 1 and 2 representing the sonic, supersonic, and subsonic cases, respectively.

3.1 Basic Solutions

Basic solutions, ψ_m, should satisfy Equation (2.13). There are several ways to derive approximate solutions from Equation (2.13), depending on the

stage at which we apply the primary step of the local linearization procedure (Reference 26), that is, to assume the parameters λ, Γ, and μ to be constants. The simplest form can be obtained by assuming constant coefficients of Equation (2.13) as the start. The three-dimensional basic solutions have been derived previously in Reference 18 (see Equations (10a), (10b), and (10c)); they read

$$\psi_0 = \frac{C_0}{x} \cdot e^{-\left(A_0 x + \frac{Ar^2}{4x}\right)} \quad , X \geq 0, \tag{3.3}$$

for sonic flow; and

$$\psi_1 = C_1 e^{-A_1 x} \cosh(\sqrt{A_2} R)/R \quad , X \geq |\beta| r, \tag{3.4}$$

for transonic/supersonic flow; and

$$\psi_2 = C_2 e^{-A_1 x + A_2 R}/R \quad , \text{for all } X, \tag{3.5}$$

for transonic/subsonic flow,

where

$$\begin{cases} A_0 = B/A \\ A_1 = A/2\beta_0^2 \\ A_2 = -(A^2 - 4\beta_0^2 B)^{1/2}/2\beta_0^2 \\ R = (X^2 + \beta_0^2 r^2)^{1/2} \\ r^2 = \overline{Y}^2 + z^2 \end{cases} \tag{3.6}$$

and C_0, C_1, and C_2 are the associated constants. For the case of two-dimensional flow, which is the case considered, the basic solutions can be obtained from solving the two-dimensional version of Equation (2.13) or taking the integral transform of Equations (3.3) through (3.5) in the spanwise direction, i.e., the y-direction. These solutions read

$$\psi_0 = \frac{c_0}{\sqrt{x}} e^{-\left[A_0 x + \frac{Az^2}{4x}\right]} \quad , X \geq 0, \tag{3.7}$$

for sonic flow

$$\psi_1 = c_1 e^{i\alpha_0 x} J_0(\sigma R) \quad , X \geq Bz \tag{3.8}$$

$$= 0, \quad \text{otherwise,}$$

for transonic/supersonic flow

$$\psi_2 = c_2 e^{i\alpha_0 x} H_0^{(2)}(\sigma R) \quad , \text{for all } X, \tag{3.9}$$

for transonic/subsonic flow.

where J_0 and $H_0^{(2)}$ are the zeroth order Bessel function and the zeroth-order Hankel's function of the second kind, respectively; both functions contain complex arguments, namely the complex parameters, σ.

The complex arguments read

$$\alpha_0 = \frac{iA}{2\beta_0^2} = -\frac{iA}{2m_0^2}$$

$$m_0^2 = -\beta_0^2 \tag{3.10}$$

$$\begin{cases} \sigma = \dfrac{i\rho}{m_0} \\ \rho = -\dfrac{1}{2m_0}\sqrt{A^2 + 4m_0^2 B} \end{cases} , \tag{3.11}$$

for transonic/supersonic flow, and

$$\begin{cases} \sigma = \dfrac{\chi}{\beta_0} \\ \chi = \dfrac{1}{2\beta_0}\sqrt{4\beta_0^2 B - A^2} \end{cases} , \tag{3.12}$$

for transonic/subsonic flow; the constants c_0, c_1, and c_2 read

$$\begin{cases} c_0 = 2i\sqrt{\dfrac{\pi}{A}} \\ c_1 = \dfrac{2\pi}{m_0} \\ c_2 = -\dfrac{i\pi}{\beta_0} \end{cases} \tag{3.13}$$

It should be noted that the sonic solution Equation (3.7) can also be derived as a limiting case of the transonic/supersonic basic solution, Equation (3.8), and that of the transonic/subsonic basic solution, Equation (3.9). When we let β_0^2 or m_0^2 approach zero, and meanwhile keeping X nonvanishing in the latter equations, it can be shown that both expressions lead to the sonic solution by means of asymptotic expansions of the Bessel function and the Hankel function for the large argument σR. Also, we note that these basic

solutions (Equations (3.7) through (3.9)) contain the purely sonic/supersonic/subsonic basic solutions (i.e., the linear solutions) as special cases. Indeed, when the transonic parameters Γ, λ, and μ are put to zero, the sonic solution (Equation (3.7)) transonic/supersonic solution (Equation (3.8)) and the transonic/subsonic solution (Equation (3.9)) reduce to the purely linearized solutions of Rott (Reference 27), of Miles (Reference 28), and of Possio (Reference 29), as expected. Hence, it is appropriate to describe these basic transonic solutions as the 'transonic/supersonic' solution or the 'transonic/subsonic' solution, thus, implying that they are general enough to cover the transonic flow range as well as the linearized flow range.

3.2 Transonic Kernel Functions

The derivation of the transonic kernel functions, based on the previous basic solutions, is an essential step towards the MKF formulation. During the course of our study, the transonic/subsonic kernel function was first derived, followed by the transonic/supersonic kernel function, and lastly by the sonic kernel function. In the subsequent development, we will present these kernel functions in this study sequence.

- Transonic/Subsonic Kernel Function (m = 2)

Substituting Equation (3.9) into Equation (3.2), and making use of the governing equation (2.13) results in

$$K_2(X,z) = \lim_{z\to o} I_2 \cdot e^{-ikX} \tag{3.14}$$

where

$$I_2 \equiv \int_{-\infty}^{X} \frac{\partial^2}{\partial z^2} H_o^{(2)}(\sigma R) e^{ikx_o} dx_o$$

$$= c_2 \cdot \left\{ \left[\frac{\beta_o^2 \sigma x_o}{R} e^{i(\alpha_o + k)x_o} H_1^{(2)}(\sigma R) + i\beta_o^2(\alpha_o + k) H_o^{(2)}(\sigma R) \right]_{-\infty}^{X} \right.$$

$$\left. + [\beta_o^2(\alpha_o + k)^2 - \chi^2] \int_{-\infty}^{X} e^{i(\alpha_o + k)x_o} H_o^{(2)}(\sigma R) dx_o \right\}$$

and $H_1^{(2)}$ is the first-order Hankel function of the second kind. The last integral can be reduced to a simpler integral by means of Laplace transform. As the first two terms vanish in the far field, the I_2 expression is further simplified. Consequently, after the limiting process, we obtain the transonic/subsonic kernel functions, i.e.,

$$K_2(X,0) = c_2 \left\{ \left[\frac{\beta_0^2 \sigma X}{|X|} H_1^{(2)}(\sigma|X|) + i\beta_0^2(\alpha_0 + k) H_0^{(2)}(\sigma|X|) \right] e^{i(\alpha_0 + k)X} \right.$$

$$+ [\beta_0^2(\alpha_0 + k)^2 - \chi^2] \cdot \left[\left(-\frac{2}{i\pi s} \right) \ell n \left(\frac{S}{\sigma^*} \right) \right.$$

$$\left. \left. + \int_0^X e^{i(\alpha_0 + k)x_0} H_0^{(2)}(\sigma|x_0|) dx_0 \right] \right\} \cdot e^{-ikX} \qquad (3.15)$$

where

$$\begin{cases} \sigma^* = i\sigma \\ s = i\sqrt{(\alpha_0 + k)^2 - \sigma^2} \\ S = i(\alpha_0 + k) + s \end{cases} \qquad (3.16)$$

Several special cases can be reduced from Equation (3.15). In the case of parabolic approximation (Reference 24) where $\lambda = \mu = 0$, the steady kernel function can be obtained by setting k approach zero. Thus, the kernal functions read

$$K_2(X,0) = \left(\frac{2c_2 i}{\pi} \right) \Gamma e^{\frac{\Gamma}{\beta_\infty^2} X} \cdot \left\{ Sgn(X) \cdot K_1\left(\frac{\Gamma}{\beta_\infty^2} |X| \right) + K_0\left(\frac{\Gamma}{\beta_\infty^2} |X| \right) \right\} \qquad (3.17)$$

where K_1 and K_0 are modified Bessel functions of the first and the zeroth order, respectively. Furthermore, letting Γ approach zero results

$$K_2(X,0) = \frac{\beta_\infty}{2X} \tag{3.18}$$

This is exactly the purely-subsonic steady kernel function.

In the case of unsteady purely-subsonic kernel function, we take the limit in Γ approaching zero for Equation (3.14). The result reads

$$K_2(X,0) = -\frac{k\pi}{\beta_\infty} \cdot \left\{ e^{\frac{ikx_0}{\beta_\infty^2}} \cdot \left[iM_\infty \mathrm{Sgn}(X) H_1^{(2)}(\kappa|X|) - H_0^{(2)}(\kappa|X|) \right] + \frac{2i\beta_\infty}{\pi} \ln\left(\frac{1+\beta_\infty}{M_\infty}\right) + ik\int_0^X H_0^{(2)}(\kappa|x_0|) e^{\frac{ikx_0}{\beta_\infty^2}} dx_0 \right\} \cdot e^{-ikX} \tag{3.19}$$

where $\kappa = \lambda/\beta_\infty$, and $\mathrm{Sgn}(X) = 1$ if $X > 0$ and $\mathrm{Sgn}(X) = -1$ if $X < 0$.

This is precisely the expression of Possio's integral equation, which was derived by Watkins, Runyan, and Woolston starting from a three-dimensional kernel function (Reference 30, Equation (B.18)).

- Transonic/Supersonic Kernel Function (m = 1)

Based on the nature of the supersonic wave propagation, the domain of interest for the transonic/supersonic kernel function is confined to (mz,X) rather than (-∞,X). Hence, the kernel function reads

$$K_1(X,0) = \lim_{z \to 0} I_1 \cdot e^{-ikX} \tag{3.20}$$

where

$$I_1 \equiv \frac{\partial^2}{\partial z^2} \int_{mz}^{X} e^{ikx_o} \cdot \psi_1 \, dx_o$$

$$= \frac{\partial^2}{\partial z^2} \int_{mz}^{X} c_1 e^{i(\alpha_o + k)x_o} J_o(\sigma R) H(x_o - mz) dx_o \qquad (3.21)$$

Applying the differentiation, making use of Equation (3.2), and finally taking the limiting process yields

$$K_1(X,0) = c_1 m_o^2 \left\{ e^{-i\left(k + \frac{k_o}{m_o^2}\right)X} \left[\delta(X) + \frac{ik_o}{m_o^2} H(X) J_o(\sigma X) - \sigma H(X) J_1(\sigma X) \right] \right.$$

$$\left. - \left(\frac{\rho^2}{m_o^2} + \frac{k_o^2}{m_o^4} \right) e^{-ikX} \int_o^X H(x_o) e^{\frac{-ik_o x}{m_o^2}} J_o(\sigma x_o) dx_o \right\} \qquad (3.22)$$

where

$k_o / m_o^2 \equiv -(\alpha_o + k)$

$\delta(X)$ is Dirac's delta function

$H(X)$ is the Unit Step function.

Various special cases of Equation (3.22) will be discussed here. For parabolic approximation, $\lambda = \mu = 0$, the steady kernel function in this case reads

$$K_1(X,0) = c_1 m_\infty^2 \cdot \left\{ \delta(X) + \frac{i\Gamma}{m_\infty^2} H(X) \cdot J_1\left(\frac{-i\Gamma}{m_\infty^2} X \right) \right\} \qquad (3.23)$$

where $m_\infty^2 = M_\infty^2 - 1$.

As Γ approaches zero, the above becomes

$$K_1(X,0) = c_1 m_\infty^2 \cdot \delta(X)$$

On the other hand, for purely supersonic flow case, where $\Gamma = \lambda = \mu = 0$, the unsteady kernel function Equation (3.22) reduces to

$$K_1(X,0) = c_1 m_\infty^2 \left\{ e^{\frac{-ikM_\infty^2}{m_\infty^2} X} \cdot \left[\delta(X) + \frac{ik}{m_\infty^2} H(X) J_0(\kappa X) - \frac{kM_\infty}{m_\infty^2} H(X) J_1(\kappa X) \right] + \frac{k^2}{m_\infty^2} e^{-ikX} \int_0^X H(x_0) e^{\frac{-ikx_0}{m_\infty^2}} J_0(\kappa x_0) dx_0 \right\} \qquad (3.24)$$

where $\kappa = \frac{kM_\infty}{m_\infty^2}$ and $c_1 = \frac{2\pi}{m_\infty}$

The above equation checks identically with Watkins and Berman's supersonic kernel function (Equation (49), Reference 31).

- Sonic Kernel Function (m = 0)

The Sonic Kernel function derived here is meant to be the transonic kernel function, for $\beta_0 = 0$ (or M = 1.0), thus including the transonic thickness effect. Inserting the basic solution Equation (3.9) into Equation (3.2) and making use of the governing sonic equation, Equation (2.13) yields

$$K_0(X,0) = c_0 A \left| \frac{e^{\tilde{\alpha}_0 X}}{\sqrt{X}} - 2\tilde{\alpha}_0 \int_0^{\sqrt{X}} e^{\tilde{\alpha}_0 \lambda^2} d\lambda \right| e^{-ikX} \qquad (3.25)$$

where

$$\begin{cases} c_o = 2i\sqrt{\frac{\pi}{A}} \\ \\ \tilde{\alpha}_o = ik - \frac{B}{A} \end{cases}$$

The sonic kernel function can be derived from either Equation (3.15) or Equation (3.22). It can be shown that Equation (3.24), in fact, is the sonic limiting case of these subsonic and supersonic kernel functions. The limiting procedures depend primarily on the validity of the asymptotic expansion of the Hankel function and the Bessel function, provided that the domain of 'X' (of the argument σX) be excluded from zero.

For the case of purely sonic flow, we let $\Gamma = \lambda = \mu = 0$, and let $M_\infty = 1.0$, Equation (3.25) then is reduced to the same form as the equation itself except that the coefficients, c_o and $\tilde{\alpha}_o$, are simplified to

$$\begin{cases} c_o = 4\sqrt{\frac{\pi i k}{2}} \\ \\ \tilde{\alpha}_o = \frac{ik}{2} \end{cases} \qquad (3.26)$$

The purely sonic kernel function here checks identically with that derived by Watkins, et al., (Equation (B.23), Reference 30).

SECTION 4

PANEL METHODS FOR PRESSURE EVALUATION

The objective of the present formulation is to make use of the kernel function approach for solving the downwash integral equation, i.e.,

$$W(x) = \frac{1}{2\pi} \int_0^{\ell} K_m(X,0)p(\xi)d\xi \qquad (4.1)$$

where ℓ is the total normalized chord length (normalized by half-chord length, i.e., $\ell = 2$) and the pressure function is the solution sought, defined as

$$p(\xi) = \left| p_{lower}(\xi) - p_{upper}(\xi) \right| \Big/ \left(\frac{1}{2} \rho_\infty U_\infty^2 \right) \qquad (4.2)$$

Given the downwash function W(x), one is required to solve for $p(\xi)$. The solution techniques for pressure in the kernel function approach can be broadly categorized in two classes, namely, the pressure-mode method (e.g., References 11 and 12) and the panel method or the discrete element method, e.g., References 10, 13, and 14. The general approach is to prescribe an approximate solution $p(\xi)$ in the following form, i.e.,

$$p(\xi) = \sum_{i=1}^{N} p_i f_i(\xi) \qquad (4.3)$$

where ξ and the subscript 'i' represent the sending point and the sending panel. In the pressure-mode method, further knowledge of f_i is needed, a priori. For the panel methods, f_i can be expressed more freely in various ways, depending on the sophistication of the paneling scheme as one desires.

There are several panel methods now being widely used. The simplest method is the doublet lattice (DL) method (e.g., Reference 13). It is a commonly-used tool for flutter analyses. But the method is restricted to the

subsonic flow regime due to its inherent elliptical characteristic of the collocation scheme adopted. The constant pressure panel (CPP) method was first proposed by Woodward (Reference 32) and was extended to cope with the unified unsteady, purely subsonic/supersonic three-dimensional flow calculations by Winther (Reference 33). While the unsteady part of the subsonic calculation worked out successfully, the unsteady part of the supersonic flow calculation did not. This then led us to investigate the applicability of the Linear Pressure Panel (LPP) method for a unified unsteady, subsonic/transonic/supersonic flow calculations. The LPP method, also known as the elementary vortex distribution (EVD) method, was first proposed by Shen, et al., (Reference 34) for incompressible steady flow calculation for lifting wings with jet-augmented flaps. Apart from the unsteady subsonic work by Fromme, et al., (Reference 35), no attempt was made to unify such an approach to the supersonic flow regime. In what follows, we shall discuss the DL, the CPP, and the LPP paneling schemes, with special emphasis on the development of the LPP method for unified unsteady transonic flow calculations.

4.1 DOWNWASH MATRIX EQUATION AND PRESSURE FUNCTIONS

The downwash integral equation (4.1) in combination with Equation (4.3) can be written in terms of the panels scheme as

$$W(x) = \frac{1}{2\pi} \sum_{i=1}^{N} \left[\int_{\xi_{i-1}}^{\xi_{i+1}} K(x - \xi) f_i(\xi) d\xi \right] \cdot p_i \qquad (4.4)$$

where

N = total number of panels

p_i = pressure at the sending point ξ_i(DL), or pressure magnitude on the panel (CPP), or pressure at the leading edge of the ith panel (LPP)

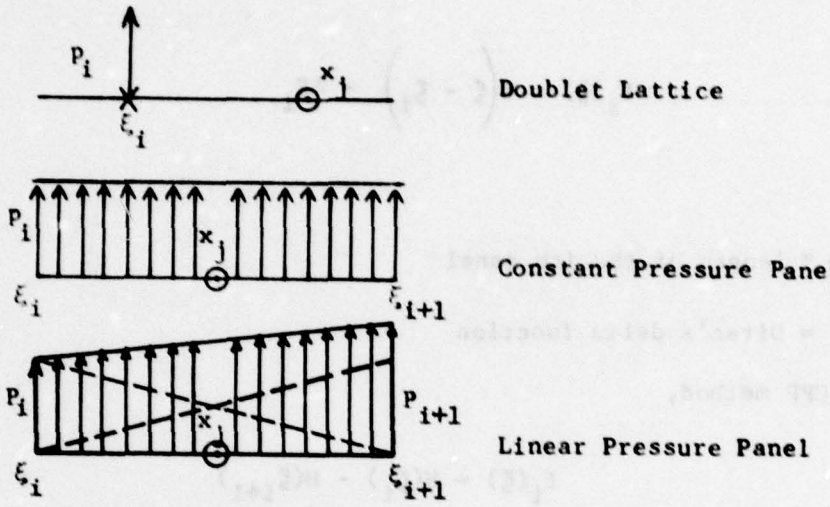

Figure 2. Sending and Receiving Points (or Panels) for DL, CPP, and LPP Methods

Now, let $W_j \equiv W(x_j)$ where x_j, is the location of the receiving point (or called the control-point) associated with the jth panel. In terms of the matrix element form, Equation (4.4) reads

$$W_j = D_{ji} \cdot p_i \tag{4.5}$$

where

$$D_{ji} = \frac{1}{2\pi} \int_{\xi_{i-1}}^{\xi_{i+1}} K(x_j - \xi) f_i(\xi) d\xi \tag{4.6}$$

and

$i = 1, \ldots, N$

$j = 1, \ldots, N$

N being some positive integer

In the ith panel, the pressure fuction $f_i(\xi)$ is prescribed by various models according to the panel schemes used.

For the DL method,

$$f_i(\xi) = \delta\left(\xi - \xi_i\right) \cdot \Delta\xi_i \tag{4.7}$$

where

$\Delta\xi_i$ = length of the ith panel

$\delta(\xi)$ = Dirac's delta function

For the CPP method,

$$f_i(\xi) = H(\xi_i) - H(\xi_{i+1}) \tag{4.8}$$

where

$H(\xi)$ = the unit step function

For the LPP method, the ith regular panel element has the pressure function

$$f_i(\xi) = \begin{cases} (\xi_{i+1} - \xi)/(\xi_{i+1} - \xi_i) & , \quad \xi_i \le \xi \le \xi_{i+1} \\ (\xi - \xi_{i-1})/(\xi_i - \xi_{i-1}) & , \quad \xi_{i-1} \le \xi \le \xi_i \end{cases} \tag{4.9}$$

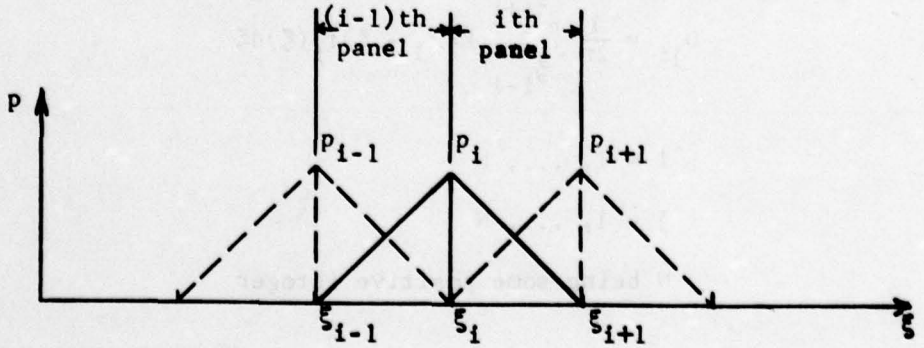

Figure 3a. Regular LPP Elements

4.2 The Kernel Matrix Element D_{ji}

Accordingly, the kernel matrix element D_{ji}, Equation (4.5) can be expressed, in terms of Equations (4.7) through (4.9), as follows.

For the DL method

$$D_{ji} = \frac{1}{2\pi} K_s(x_j - \xi_i)\Delta\xi_i \tag{4.10}$$

$$i = 1, \ldots, N$$

$$j = 1, \ldots, N$$

For the CPP method

$$D_{ji} = \frac{1}{2\pi} \int_{\xi_i}^{\xi_{i+1}} K_m(x_j - \xi)d\xi \tag{4.11}$$

For the LPP method

$$D_{ji} = \frac{1}{2\pi} \int_{\xi_{i-1}}^{\xi_{i+1}} K_m(x_j - \xi)f_i(\xi)d\xi \tag{4.12}$$

Notice that the domain of integration for the ith panel is $[\xi_i, \xi_{i+1}]$ for the CPP method and is $[\xi_{i-1}, \xi_{i+1}]$ for the LPP method. Clearly, these three methods differ from each other in their ease of application.

The DL method requires no integration for obtaining D_{ji}, hence is the simplest, whereas the CPP and the LPP method require the integration procedure. In fact, in terms of the integration scheme, the LPP method is no more than a 'higher-moment' integral of the CPP method; hence the integration procedure of the LPP method is slightly more complicated. On the other hand, it is this 'higher-moment' characteristic of the LPP method that provides a linear distribution of the calculated pressure, which is a definite refinement of the CPP method. The common characteristics of the CPP and the LPP methods are

that the edge behaviors (including leading edge singularities, trailing edge behaviors and hinge-point singularities, Reference 36) and the shock-jump behaviors (e.g., References 37 and 38) to a large extent, can be incorporated into their kernel matrix formulation, whereas the DL method does not have this advantage. However, these edge behaviors must be derived from analytical means. Such types of edge behavior and shock-jump behavior have not yet been formally derived for airfoils in the unsteady transonic regime (now with the exception of Reference 38). For this reason, in the subsequent calculation, we use either the known purely subsonic leading edge singularity or, for the most part, set up the calculation scheme without the incorporation of the edge behaviors. In the following paragraphs, however, pressure-function models are set up at various elements in different flow regimes. These pressure models, when properly assigned, indeed provide correct edge behaviors. This can be observed from the computed numerical results (see Section 5 and figures). However, one is cautioned that the 'singularity-like' leading edge (for subsonic or sonic flow) or the hinge point behaviors obtained are really not singular, if one takes up the present element modeling for $f_i(\xi)$ in paragraph 4.3. We achieve these 'singularity-like' edge behaviors by refining the element size in the neighborhood of these edges. The usual practice in our computation scheme is to distribute about five to ten elements within five percent chord length in the edge neighborhood. In so doing, one obtains more enhanced singularity-like behavior. What really happens in this outcome is the following. Although the $f_i(\xi)$'s are not singular, and the correct $f_i(\xi)$'s should be singular (but are integrable singularities), D_{ji} always remains regular in either case. Also, the value of D_{ji} would amount to the same order of magnitude locally for both cases. This then in turn assures the singularity-like behavior in the pressure function at these edges.

In what follows, we will restrict our considerations to the LPP method, as it constitutes the main body of the present MKF calculation procedure.

4.3 The Transonic LPP Model of $f_i(\xi)$

The success of the LPP method depends mainly on the correct modeling of the pressure function, hence $f_i(\xi)$. Here, regular elements and the irregular elements will be described. The regular elements consist of the usual regular panel element, the leading-edge element, and the hinge-point elements. The irregular elements consist of trailing-edge elements and the shock-point element. The last element will not be included in the following description.

- Regular Element

  The typical regular element is shown in Figure 3a and the pressure function is defined as Equation (4.9).

- Leading-Edge Element

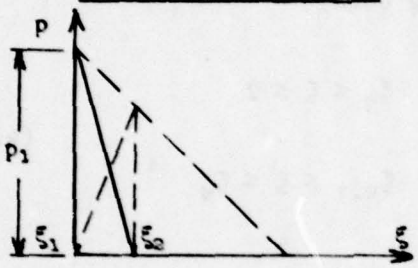

Figure 3b. Leading-Edge Element

$$\xi_1 = 0 \qquad \text{(i.e., the leading edge)}$$

$$\begin{cases} f_1(\xi) = \dfrac{\xi_2 - \xi}{\xi_2} & 0 \le \xi \le \xi_2 \\ f_1(0) = 1 \end{cases} \qquad (4.13)$$

As mentioned earlier, it is seen that the present modeling of $f_1(\xi)$ does not provide the leading-edge singularity.

- Hinge-Point Element

The pressure function behind the hinge point of the oscillating flap assumes the same pressure function as that of the leading-edge element, i.e., Equation (4.13), except that ξ is now the hinge-point location. Ahead of the hinge point ξ_1, the pressure function then assumes a mirror image of $f_1(\xi)$ along the hinge line $\xi = \xi_1$. It should be remarked that although the strength of the edge singularities varies, depending on the location (at the leading edge or at the hinge point), the local Mach number, and airfoil geometry, they are usually integrable singularities, even for the cases in oscillatory flow. Consequently, the kernel matrix D_{ji} here remains regular regardless of the edge behavior.

The trailing-edge elements are considered as irregular elements because they behave differently when the flow regime changes.

- Subsonic Trailing-Edge Element

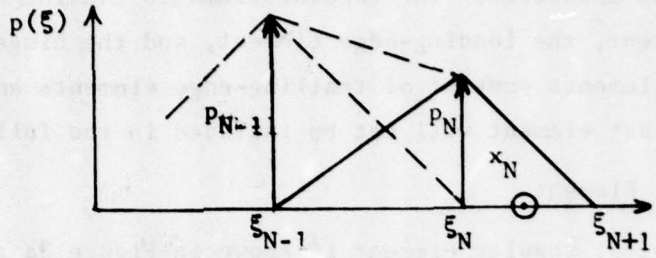

Figure 3c. Subsonic Trailing-Edge Element

$$\xi_{N+1} = 2 \qquad \text{(i.e., the trailing edge)}$$

$$f_N(\xi) = \begin{cases} (2 - \xi)/(2 - \xi_N) & , \quad \xi_N \le \xi \le 2 \\ (\xi - \xi_{N-1})/(\xi_N - \xi_{N-1}) & , \quad \xi_{N-1} \le \xi \le \xi_N \end{cases} \tag{4.14}$$

- Sonic Trailing-Edge Element

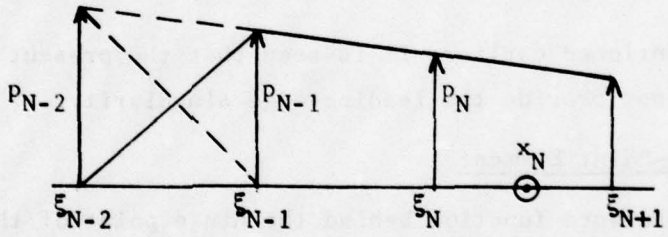

Figure 3d. Sonic Trailing-Edge Element

$$\xi_{N+1} = 2 \qquad \text{(i.e., the trailing edge)}$$

$$f_{N-1}(\xi) = \begin{cases} (\xi_N - \xi)/(\xi_N - \xi_{N-1}) & , \quad \xi_{N-1} \le \xi \le 2 \\ (\xi - \xi_{N-2})/(\xi_{N-1} - \xi_{N-2}) & , \quad \xi_{N-2} \le \xi \le \xi_{N-1} \end{cases} \tag{4.15}$$

$$f_N(\xi) = (\xi - \xi_{N-1})/(\xi_N - \xi_{N-1}) \quad , \quad \xi_{N-1} \le \xi \le 2$$

- Supersonic Trailing-Edge Element

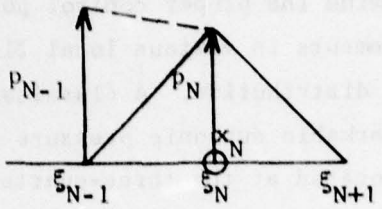

Figure 3e. Supersonic Trailing-Edge Element

$$\xi_N = 2 \qquad \text{(i.e., the trailing edge)}$$

$$f_N(\xi) = \begin{cases} (\xi_{N+1} - \xi)/(\xi_{N+1} - 2) & 2 \le \xi \le \xi_{N+1} \\ (\xi - \xi_{N-1})/(2 - \xi_{N-1}) & \xi_{N-1} \le \xi \le 2 \end{cases} \qquad (4.16)$$

It is necessary to clearly define the regular subsonic, sonic and supersonic elements at this stage. Given the mean flow pressure (or local Mach number), we can measure the local value of β_o^2 at the mid chord of the element. The panel element is then defined as the subsonic element, supersonic element, or sonic element depending on whether β_o is positive, negative, or zero, respectively. For the case of mixed flow (e.g., Figure 3f), two extra types of panel elements are added. First, the panel elements are tailored to fit the sonic point location; this results in two adjacent panel elements, one on the upstream side of the sonic point, the other on the downstream side. Thus, these adjacent elements are defined as the subsonic/sonic element and the sonic/supersonic element (Figure 3f).

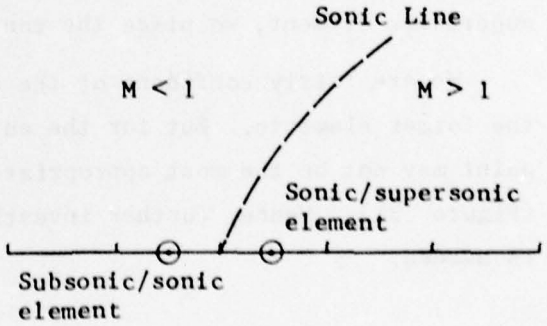

Figure 3f. Adjacent Elements in Mixed Flow

4.4 The Control Point x_j

It is crucial to determine the proper control point (or receiving point, x_j) location for the LPP elements in various local flow regimes in order to obtain the correct pressure distribution. A classical case is the Doublet Lattice method in which remarkable subsonic pressure distributions result when the control point is located at the three-quarter chord of each element (References 13 and 39).

As a result of our investigation, we found that the control-point location of each LPP element is not entirely independent of the local flow conditions. For regular elements and irregular trailing-edge elements, the control-point locations are determined by the following

$$x_j = \begin{cases} (\xi_j + \xi_{j+1})/2 & \text{for subsonic elements and sonic elements} \\ \xi_j & \text{for supersonic elements} \end{cases} \tag{4.17}$$

This is to say that the proper location of the control point should be placed at the midchord of the subsonic and the sonic elements, whereas it should be placed at the leading edge of the supersonic element. In the mixed-flow case, the adjacent subsonic/sonic element assumes the same control point location as that of the subsonic element. For the adjacent sonic/supersonic element, we place the control point at the midchord.

We are fairly confident of the choice of the control-point locations for the former elements. But for the adjacent element, our choice of the control point may not be the most appropriate, as shown in the sonic flow calculation (Figure 31). Hence, further investigation on the mixed flow panel elements is needed.

4.5 Evaluation of Kernel Matrix Element D_{ji}

To evaluate the D_{ji} integral (Equation 4.6)

$$D_{ji} = \frac{1}{2\pi} \int_{\xi_{i-1}}^{\xi_{i+1}} K_m(x_j - \xi) f_i(\xi) d\xi$$

it is necessary to assess the singular behavior of the transonic kernel function $K_m(X)$. In the previous section, we have shown that while the subsonic and the sonic kernels are singular, $K_2(X) \sim 1/X$ and $K_0(X) \sim 1/\sqrt{X}$, the supersonic kernel $K_1(X) \sim \delta(X)$ as $|X|$ approaches zero. Consequently, regular functions F_m $(m = 0,1,2)$ are introduced for the purpose of D_{ji} evaluation.

For convenience, let us first define the element integral operator in Equation (4.6) as

$$I_i\{ \cdot \} \equiv \frac{1}{2\pi} \int_{\xi_{i-1}}^{\xi_{i+1}} \{ \cdot \} d\xi \qquad (4.18)$$

Thus,

- Subsonic Element $(m = 2)$

$$D_{ji} = I_i \left\{ \frac{F_2(x_j - \xi)}{x_j - \xi} \cdot f_i(\xi) \right\}$$

$$F_2(x_j - \xi) = (x_j - \xi) K_2(x_j - \xi) \qquad (4.19)$$

- Supersonic Element $(m = 1)$

$$D_{ji} = \begin{cases} I_i\{F_1(x_j - \xi) \cdot f_i(\xi)\} + \frac{m_0}{4} \delta(x_j - \xi_i) & , x_j > \xi_{i-1} \\ 0 & , x_j \le \xi_{i-1} \end{cases} \qquad (4.20)$$

$$F_1(x_j - \xi) = \begin{cases} K_1(x_j - \xi) - \frac{\pi m_0}{2}\,\delta(x_j - \xi) & , x_j \geq \xi \\ 0 & , x_j < \xi \end{cases}$$

Sonic Element (m = 0)

$$D_{ji} = \begin{cases} I_i\left\{\dfrac{F_0(x_j - \xi)}{\sqrt{x_j - \xi}} \cdot f_i(\xi)\right\} & , x_j > \xi_{i-1} \\ 0 & , x_j < \xi_{i-1} \end{cases} \qquad (4.21)$$

$$F_0(x_j - \xi) = \begin{cases} \sqrt{x_j - \xi} \cdot K_0(x_j - \xi) & , x_j \geq \xi \\ 0 & , x_j < \xi \end{cases}$$

Now, since $F_m(X)$'s are analytic everywhere over the domain of interest in x_j and ξ, the singularities in D_{ji} involving cases of m = 2 and 0 are removed. Thus, the functions $F_m(X)$ are subject to the parabolic curve fit scheme. The values of $F_m(X)$ are obtained at three points of each element, namely, the leading edge, the midchord and the trailing edge. In the case of sonic and sonic/supersonic elements (with control point located at the midchord), we simplify the curve fit scheme by a linear fit in letting $F_m(X)$ go through the leading-edge point and the midchord.

As an example, we shall demonstrate the evaluation scheme for a regular subsonic element, using Equation (4.9) and Equation (4.19). First, let us write the curve-fit formula, i.e.,

$$F_2(x_j - \xi) = (x_j - \xi)K_2(x_j - \xi) \qquad 0 \leq x_j \leq 2$$

$$\simeq \bar{A}(x_j - \xi)^2 + \bar{B}(x_j - \xi) + \bar{C} \qquad (4.22)$$

where $\bar{A}$, $\bar{B}$, and $\bar{C}$ are determined by the parabola fit. Now, according to Equation (4.9) and $F_2(X)$ given above, D_{ji} can be integrated, for the ith or the (i+1)th element (denoted as ΔD_{ji}), to yield (refer to Figure 3a)

$$\Delta D_{ji} = \frac{\theta_i}{4\pi}\left\{\bar{A}\delta_i^2\left(\bar{x} - \frac{1}{3}\right) + \bar{B}\delta_i + 2\bar{C}\left[1 + (\bar{x} - 1)\ln\left|\frac{\bar{x} - 1}{\bar{x}}\right|\right]\right\} \tag{4.23}$$

where

$$\bar{x} = (x_j - \xi_i)/\delta_i \tag{4.24}$$

$$\delta_i = \begin{cases} -(\xi_i - \xi_{i-1}) & , \xi_{i-1} \le \xi \le \xi_i \\ \xi_{i+1} - \xi_i & , \xi_i \le \xi \le \xi_{i+1} \end{cases}$$

$$\theta_i = \begin{cases} 1 & , \xi_{i-1} \le \xi \le \xi_i \\ -1 & , \xi_i \le \xi \le \xi_{i+1} \end{cases}$$

Notice that now ΔD_{ji} is a regular function as a result of the proper arrangement of $F_2(X)$. For the evaluated formulas of ΔD_{ji} for the sonic and the supersonic elements, we refer them to Appendix A.

SECTION 5

RESULTS AND DISCUSSION

In this section, numerical results for all flow regimes are presented and followed by brief discussions. Figures 4 through 13 present all the transonic/subsonic results for thin airfoils (flat plates) and for a pitching or flapping NACA64A006 airfoil, using either the Transonic Doublet Lattice method (TDL2D code) or the Transonic Linear Pressure Panel method (TLP2D code). Based on the unified formulations in the previous section, we shall demonstrate further that the LPP method is equally applicable to the sonic and supersonic cases, whereas the DL method is not. Figures 14 through 22 present transonic/supersonic results for pitching thin airfoils (flat plates), wedges, and parabolic-arc airfoils. Sonic flow results are shown in Figures 24 through 31, for pitching thin airfoils, Guderley airfoils, and parabolic-arc airfoils. In particular, Figure 23 illustrates the divergence of the purely subsonic and purely supersonic kernel calculations, and Figure 31 presents results of a study for the mixed kernel function procedure.

Notice that in all the figures, only the in-phase and out-of-phase pressure distributions, $\Delta Cp'$ and $\Delta Cp''$, or their magnitudes and phase angles, $|\Delta Cp|$ and Φ, are presented. The pressure coefficients are defined by Equation (4.2) as

$\Delta Cp'$ = Real part [p], the in-phase pressure and

$\Delta Cp''$ = Imaginary part [p], the out-of-phase pressure.

All the pressure coefficients are plotted against the chordwise coordinate, x. For convenience of presentation, the range of x and that of ξ is changed to (0,1), this amounts to changing the total chord length $\ell = 1$, instead of 2, as defined in Section 4. The percent thickness in all the plots is defined

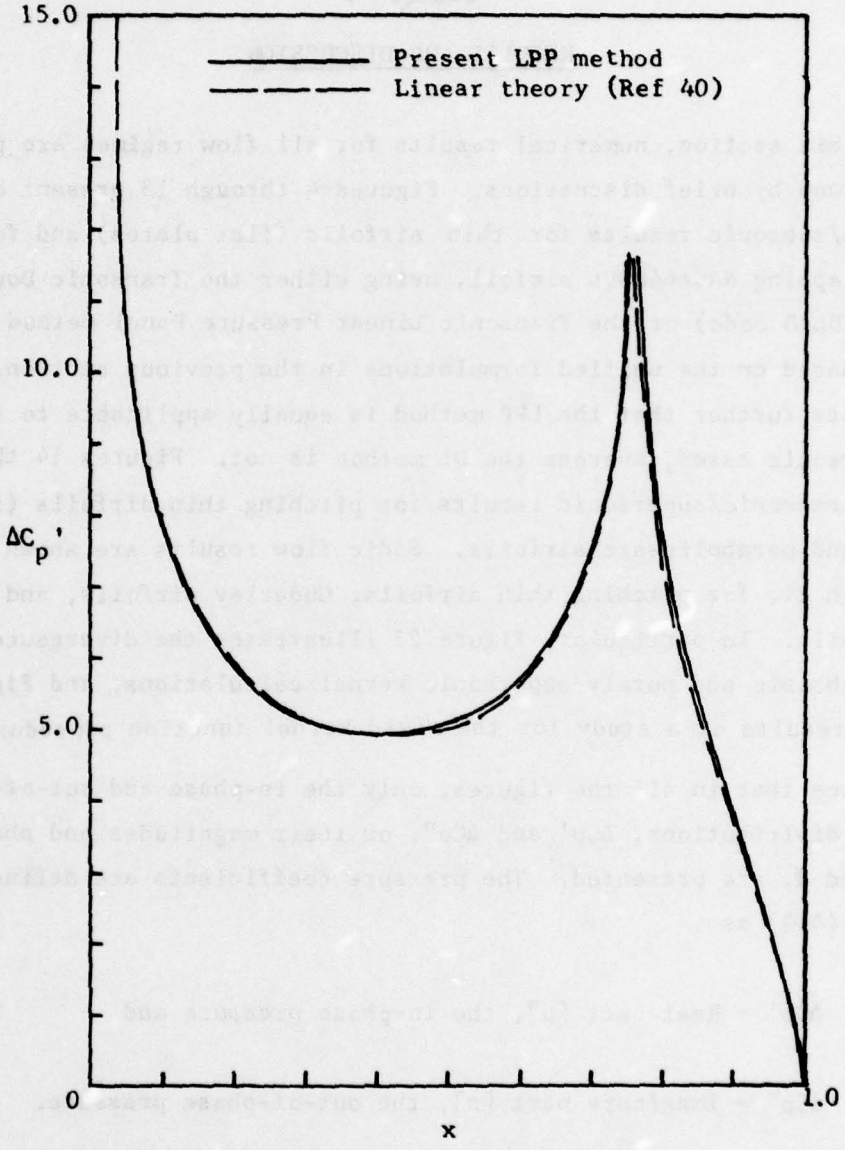

Figure 4. Flapping NACA64A006 Airfoil at $M_\infty = 0.825$ and $k = 0$ with Hinge Point at Three-Quarter Chord

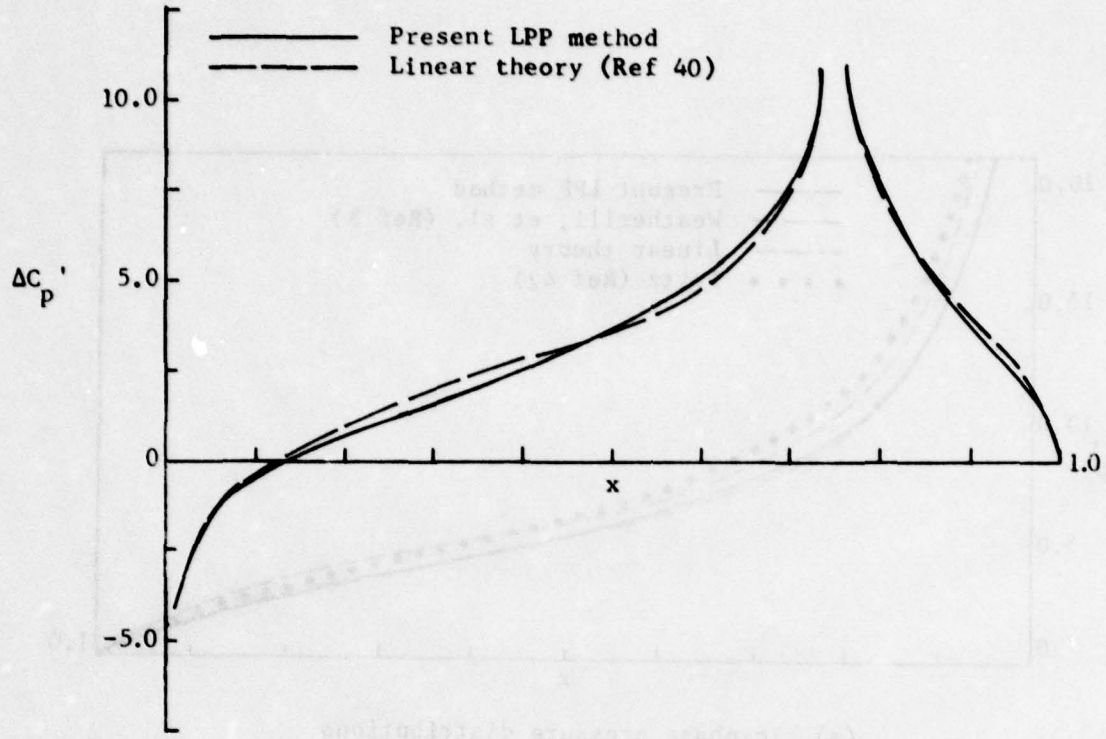

(a) In-phase pressure distributions

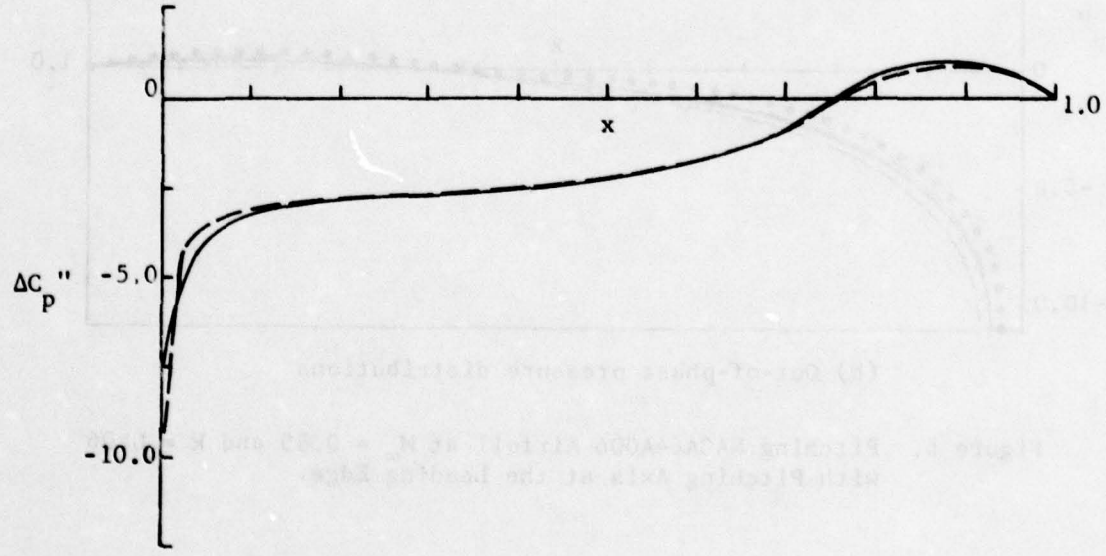

(b) Out-of-phase pressure distributions

Figure 5. Flapping NACA64A006 Airfoil at M_∞ = 0.825 and k = 0.062 with Hinge Point at Three-Quarter Chord

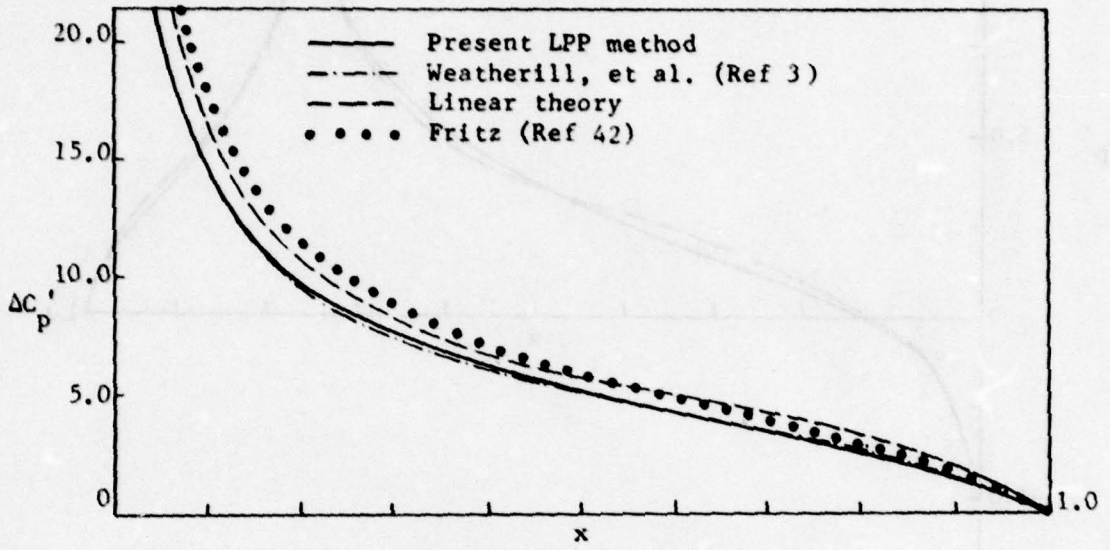

(a) In-phase pressure distributions

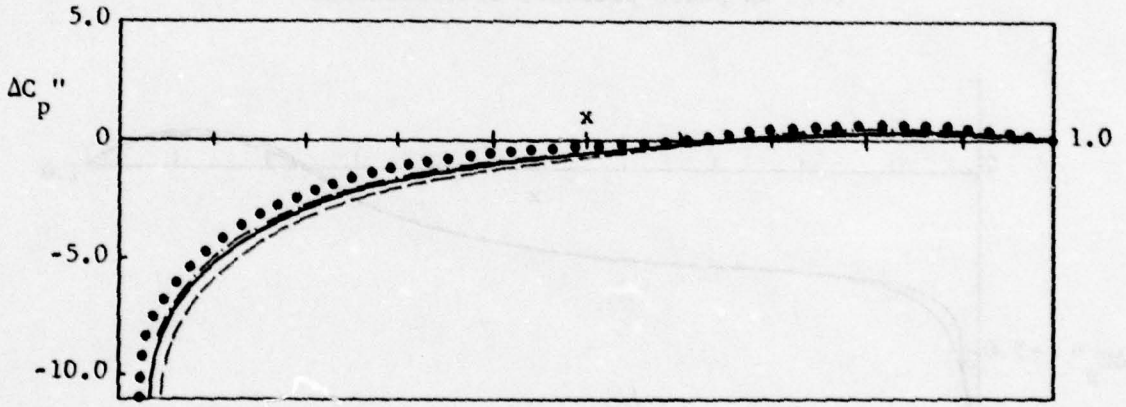

(b) Out-of-phase pressure distributions

Figure 6. Pitching NACA64A006 Airfoil at $M_\infty = 0.85$ and $k = 0.06$ with Pitching Axis at the Leading Edge

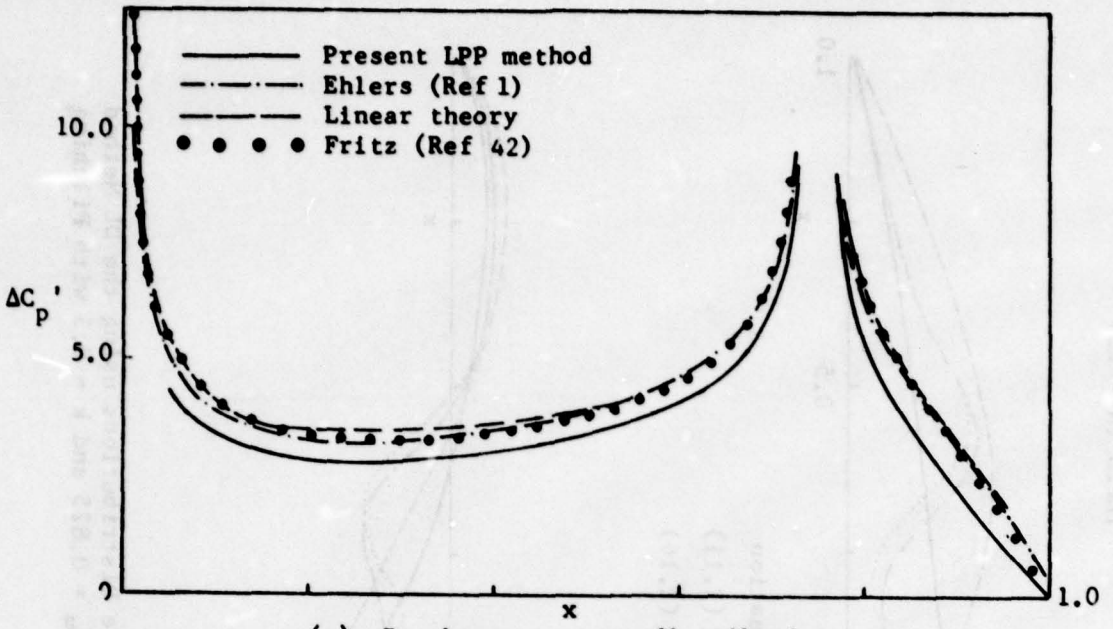

(a) In-phase pressure distributions

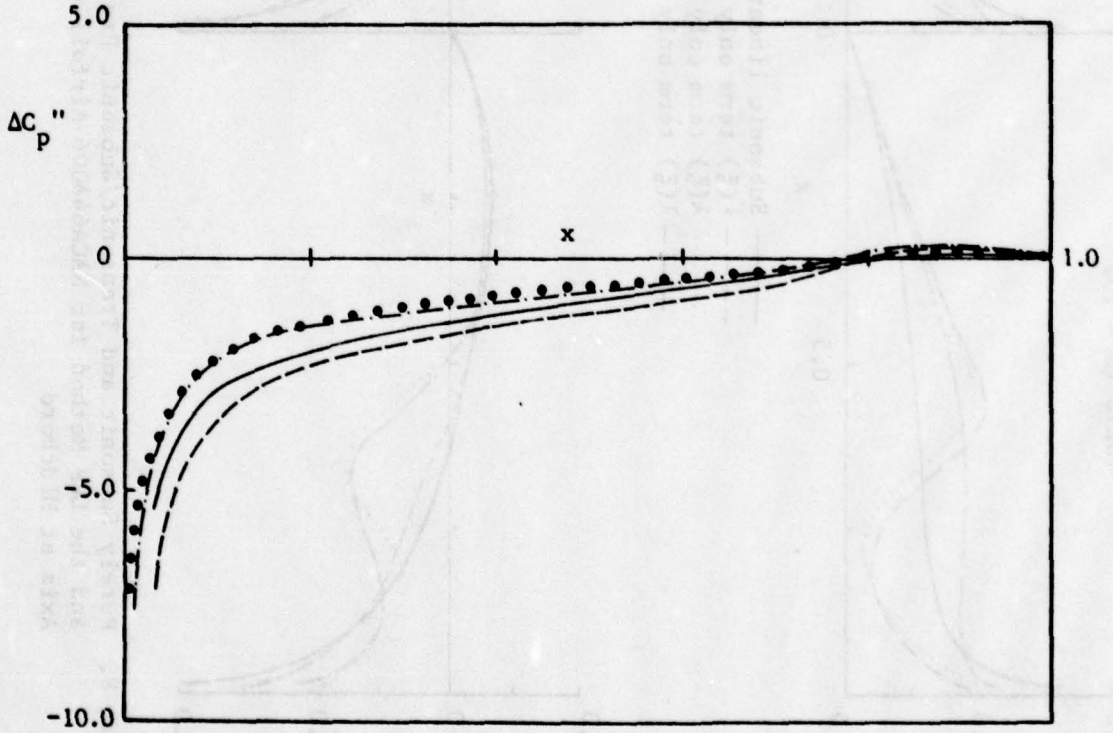

(b) Out-of-phase pressure distributions

Figure 7. Flapping NACA64A006 Airfoil at M_∞ = 0.85 and k = 0.06 with Hinge Point at Three-Quarter Chord

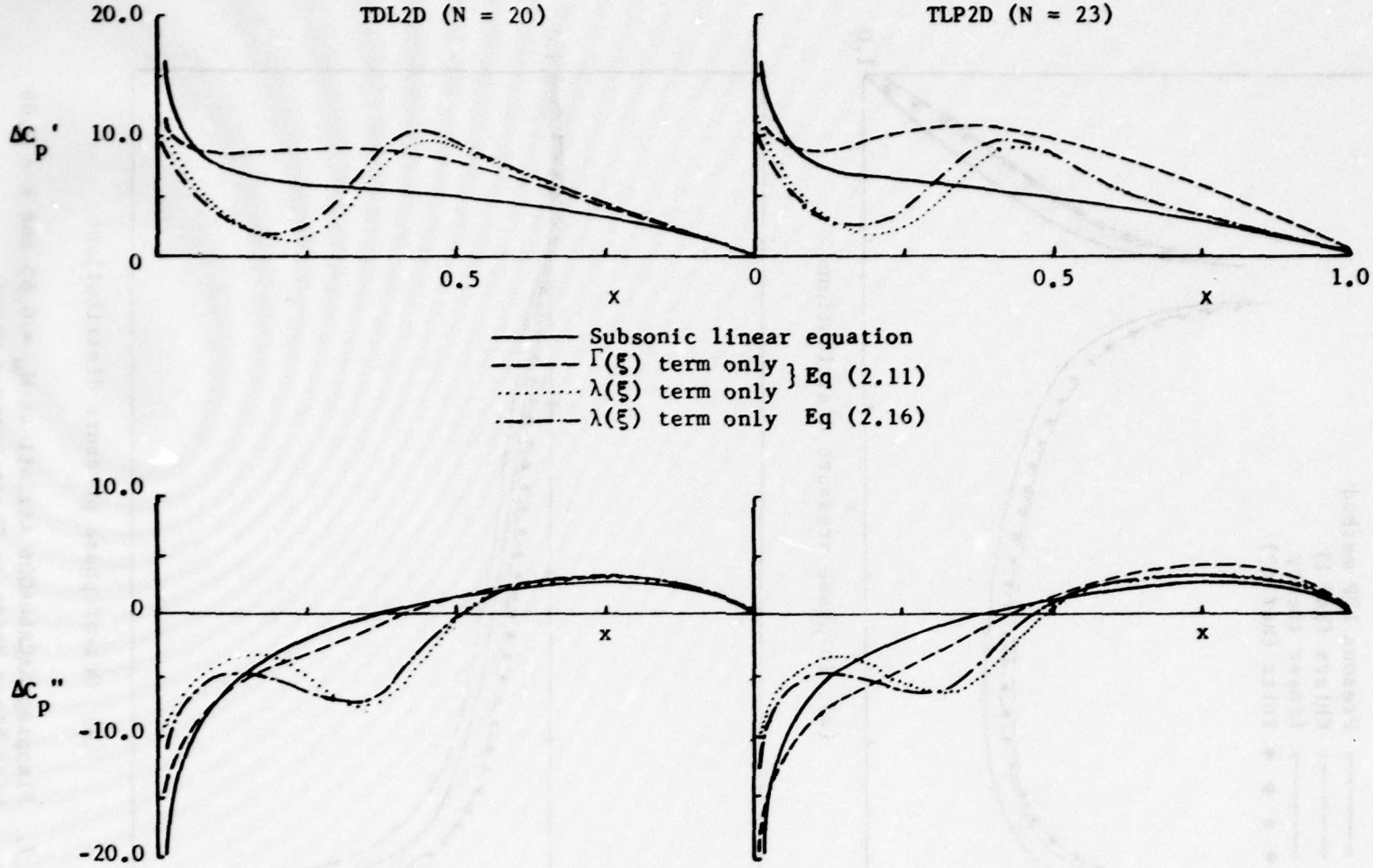

Figure 8. Purely Subsonic and Transonic/Subsonic Pressure Distributions using the DL Method and the LPP Method for NACA64A006 Airfoil at $M_\infty = 0.825$ and $k = 0.3$ with Pitching Axis at Midchord

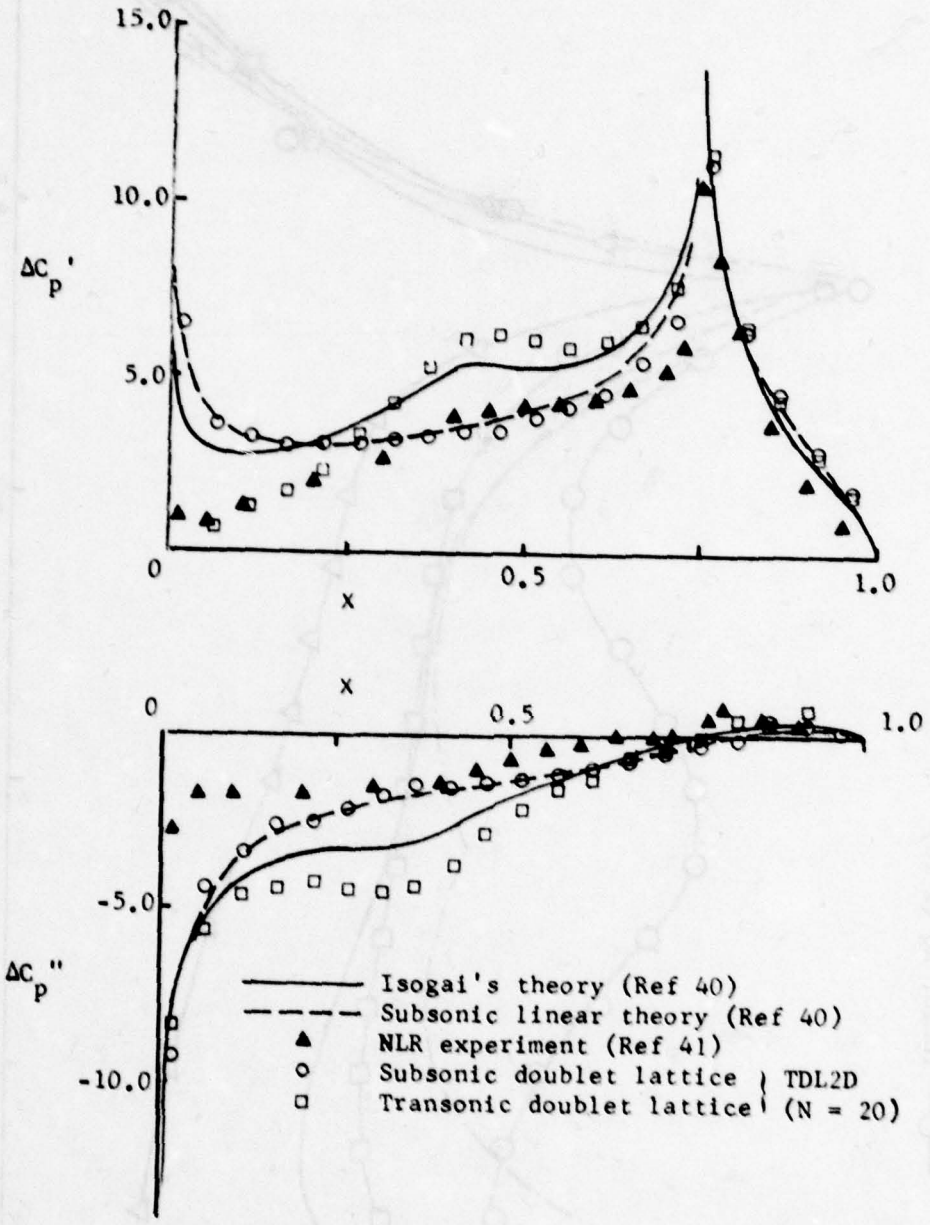

Figure 9. Flapping NACA64A006 Airfoil at $M_\infty = 0.825$ and $k = 0.062$ with Hinge Point at Three-Quarter Chord

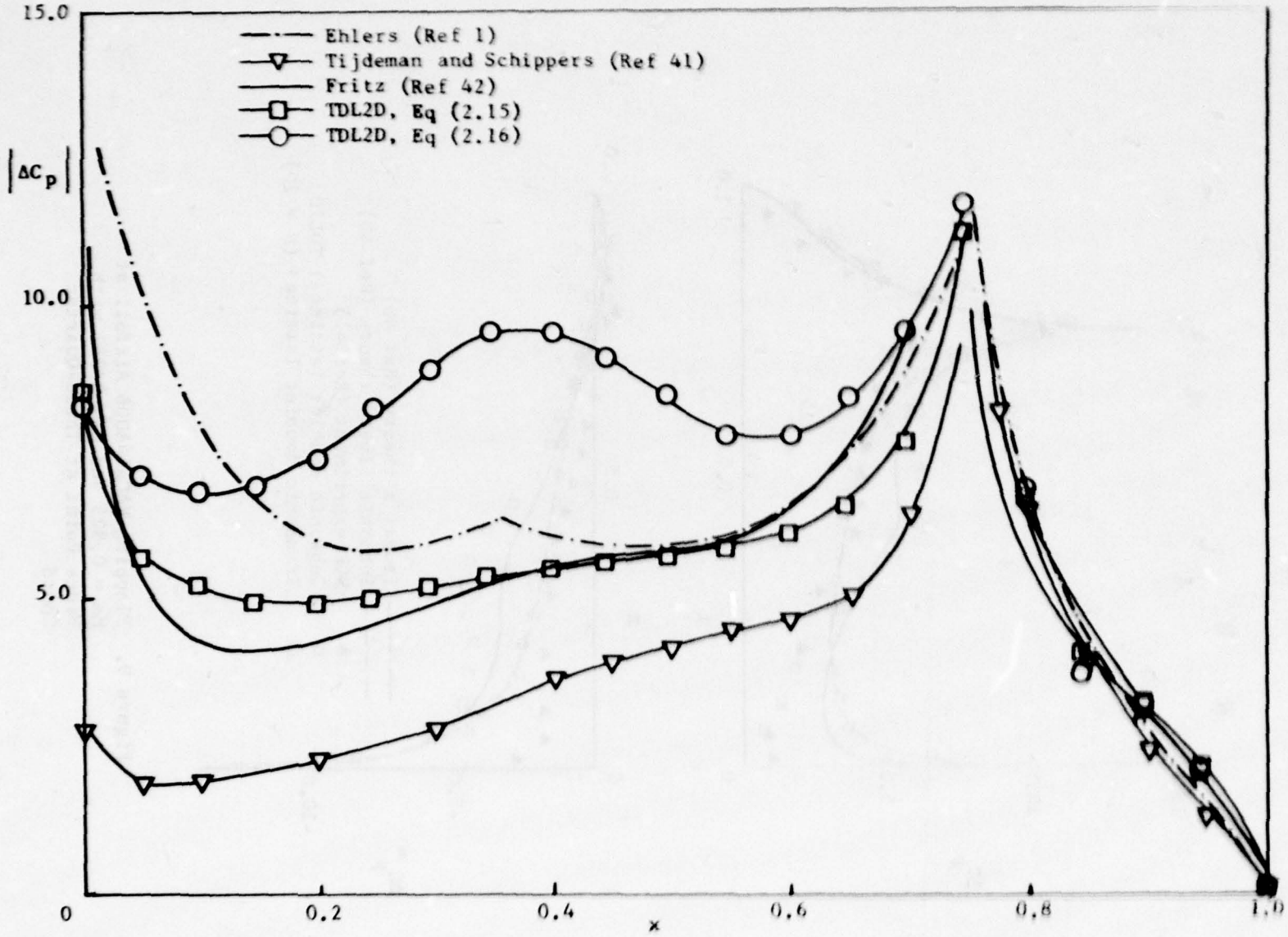

Figure 10. Pressure Magnitudes for a Flapping NACA64A006 Airfoil at $M_\infty = 0.8$ and $k = 0.253$ with Hinge Point at Three-Quarter Chord

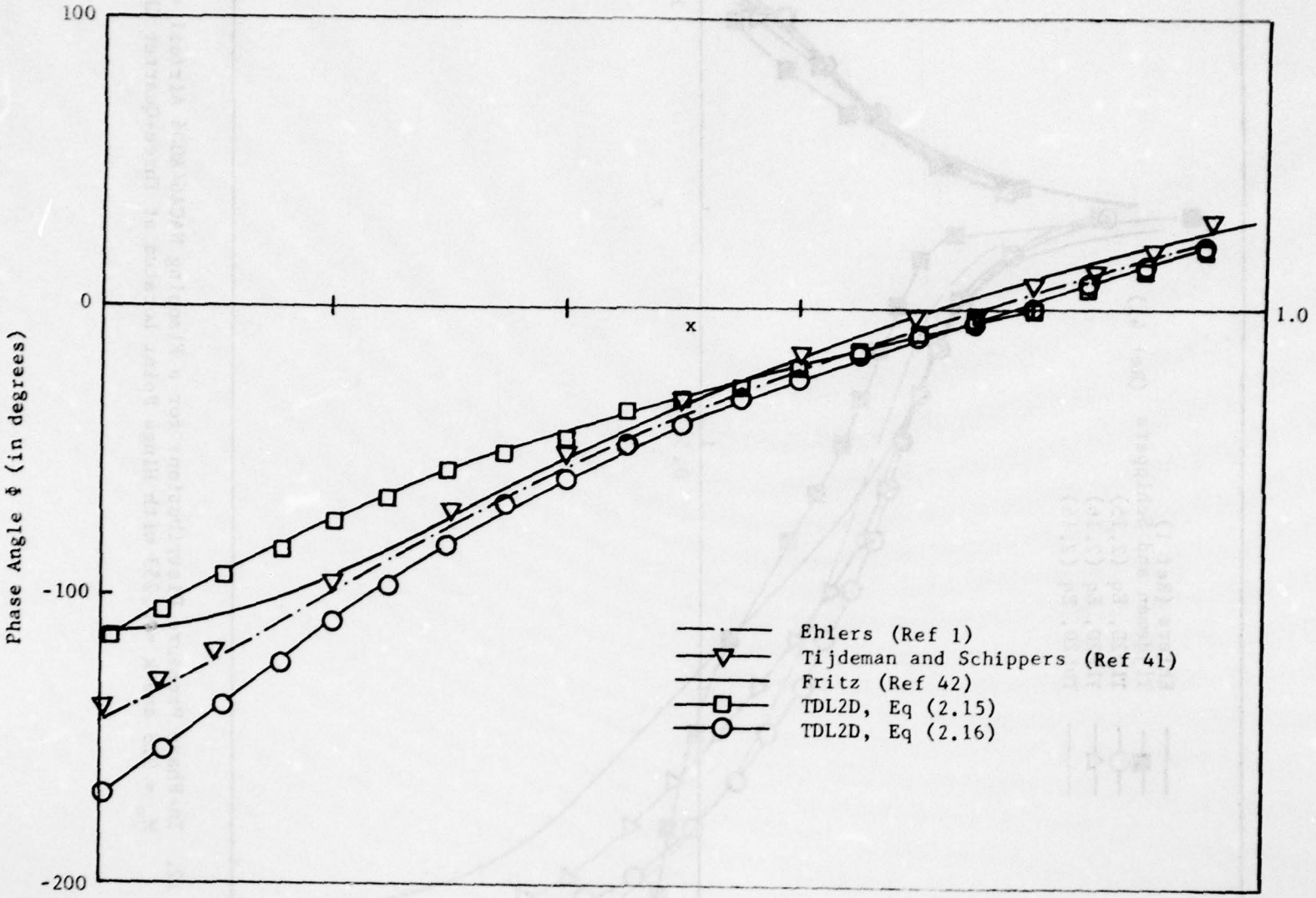

Figure 11. Phase Angles for a Flapping NACA64A006 Airfoil at M_∞ = 0.8 and k = 0.253 with Hinge Point Located at Three-Quarter Chord

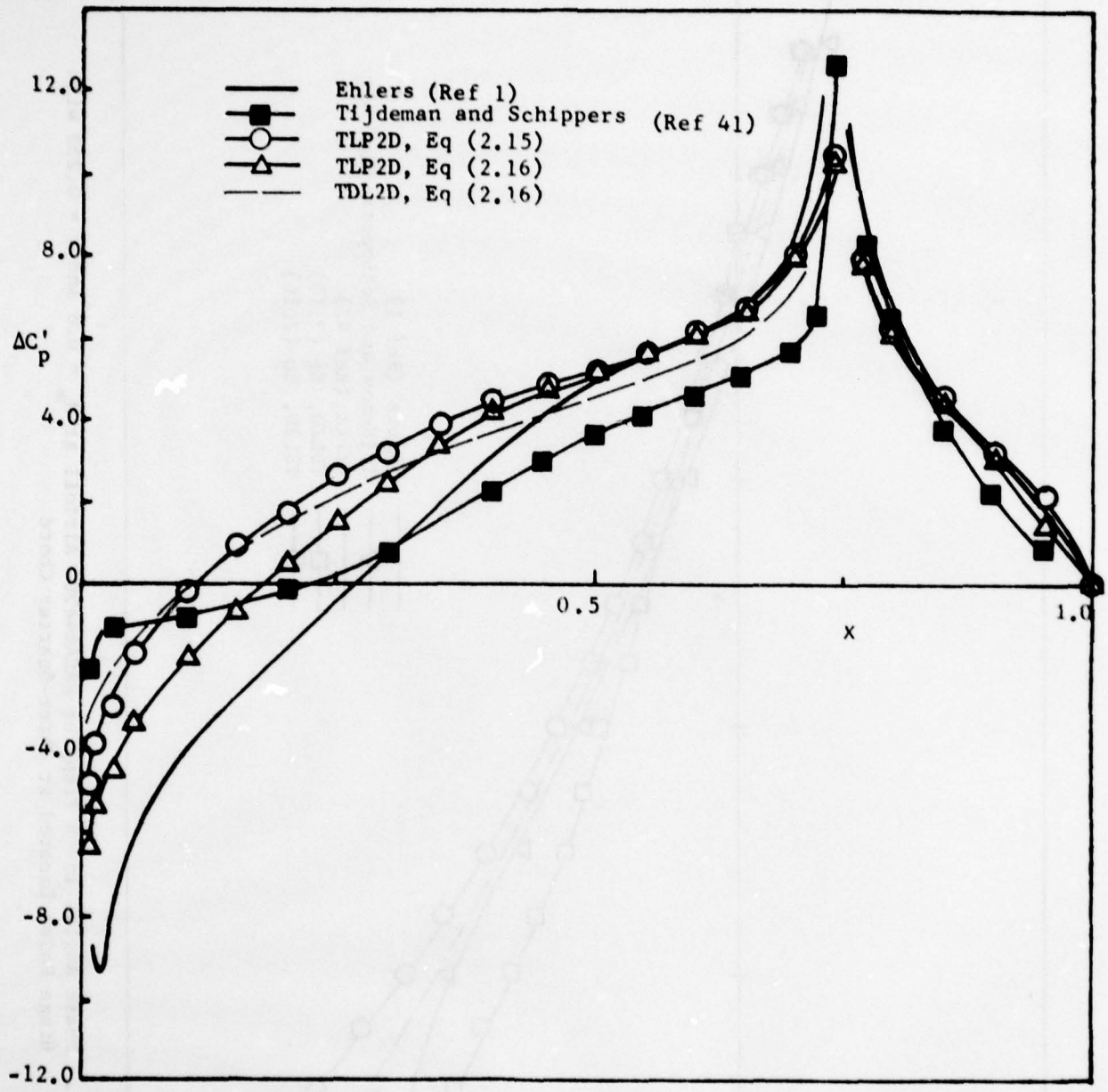

Figure 12. In-Phase Pressure Distributions for a Flapping NACA64A006 Airfoil at $M_\infty = 0.8$ and $k = 0.253$ with Hinge Point Located at Three-Quarter Chord

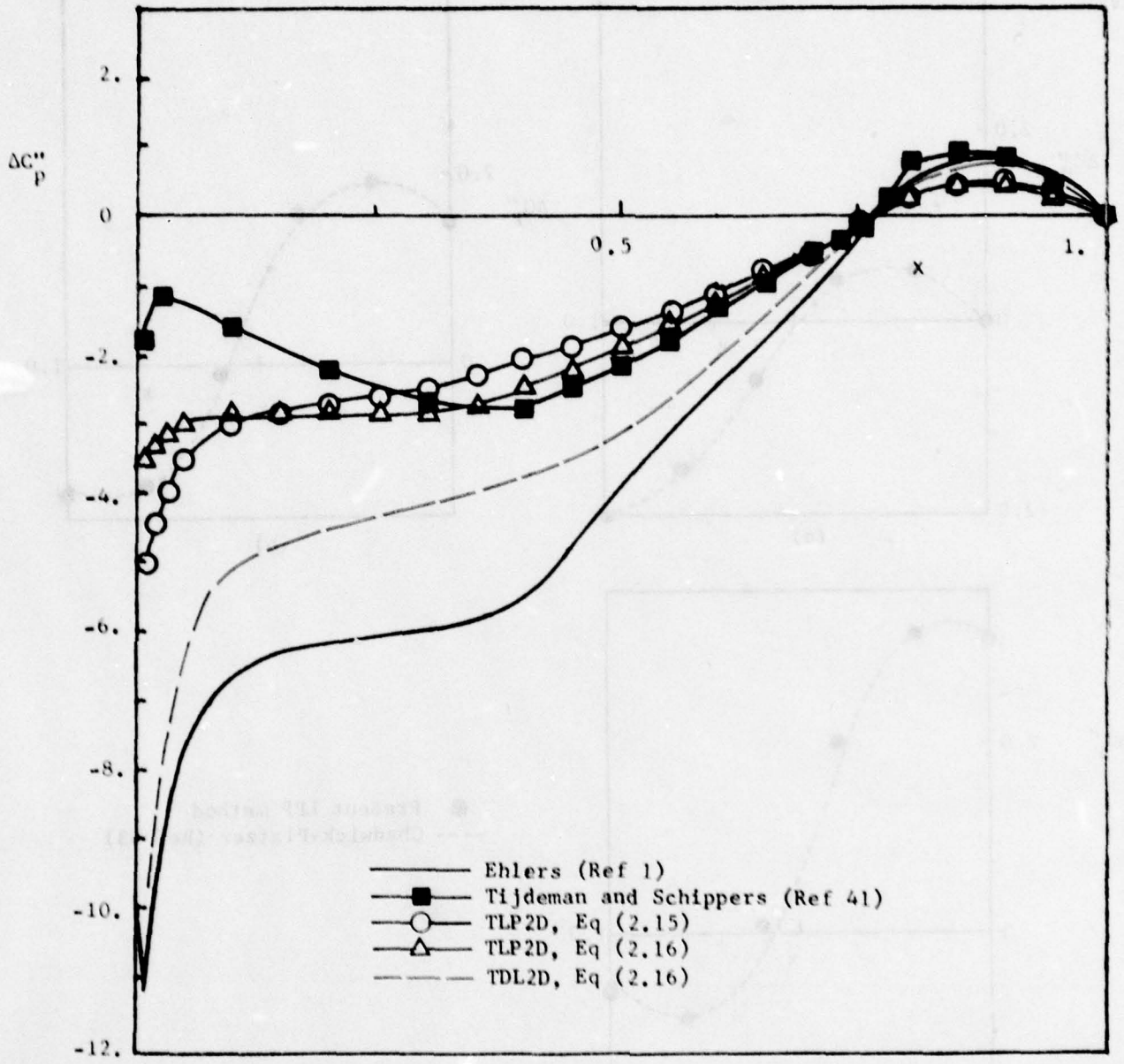

Figure 13. Out-of-Phase Pressure Distributions for a Flapping NACA64A006 Airfoil at $M_\infty = 0.8$ and $k = 0.253$ with Hinge Point at Three-Quarter Chord

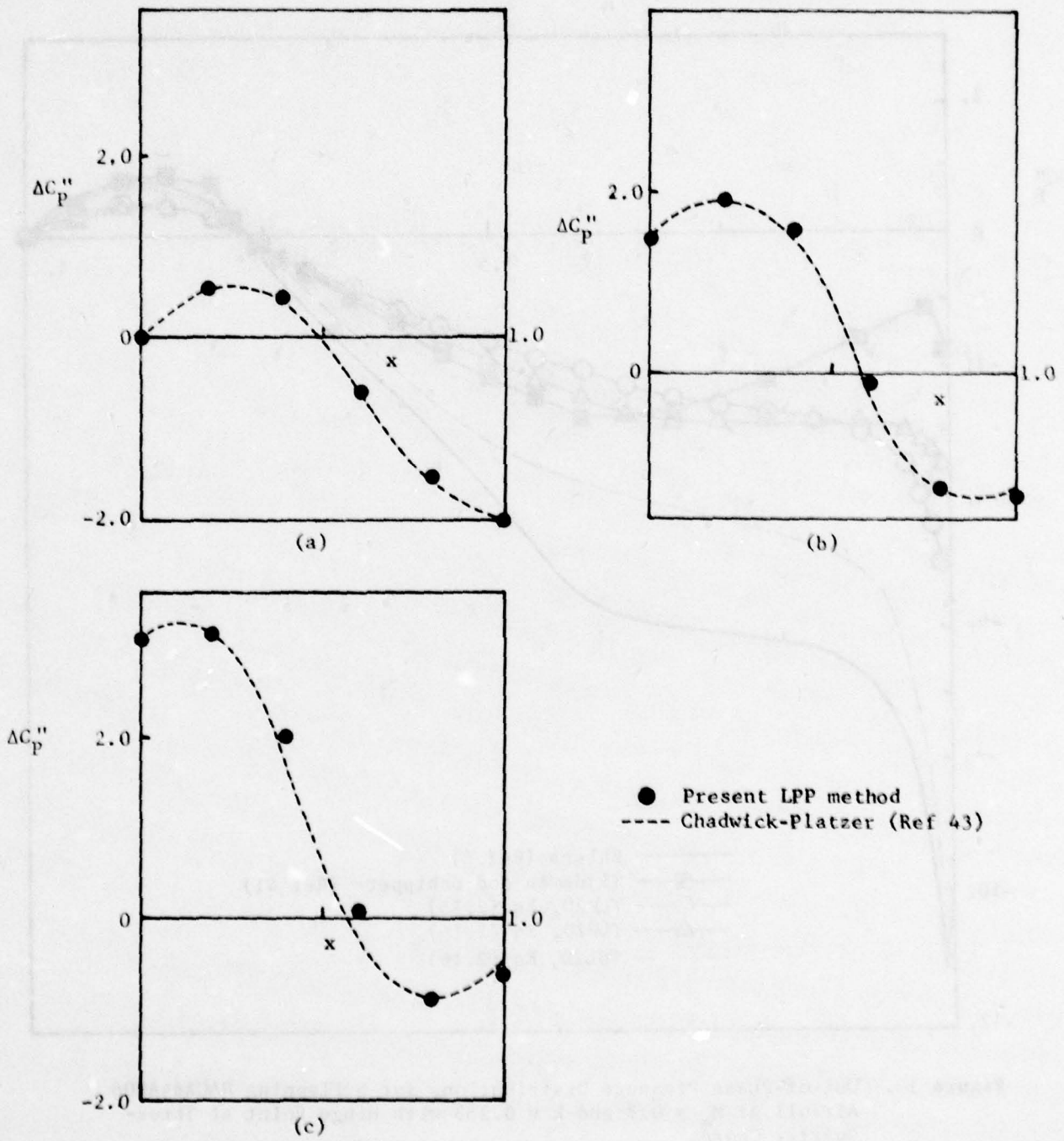

Figure 14. Pitching Thin Airfoil ($\tau = 0$) at $M_\infty = 1.2$ and Reduced Frequency $k = 1.0$ with Pitching Axes at (a) Leading Edge, (b) Midchord, and (c) Trailing Edge

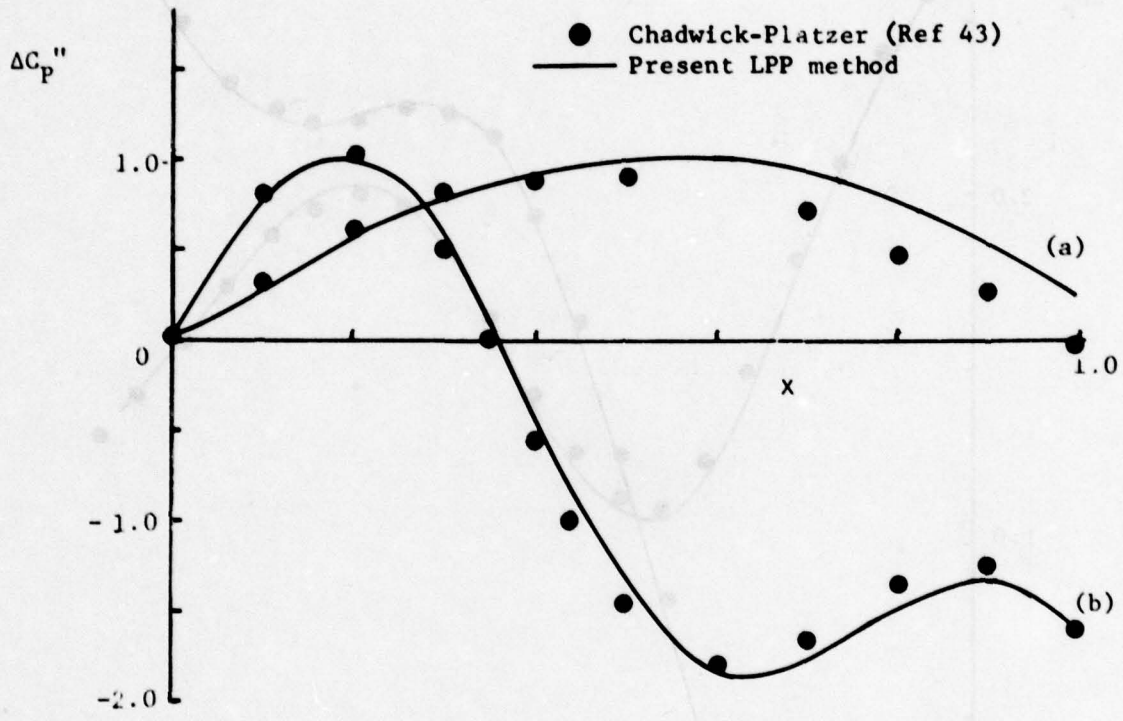

Figure 15. Pitching Thin Airfoil ($\tau = 0$) at $M_\infty = 1.15$ and Reduced Frequencies at (a) $k = 0.2$ and at (b) $k = 0.6$ with Pitching Axis at the Leading Edge

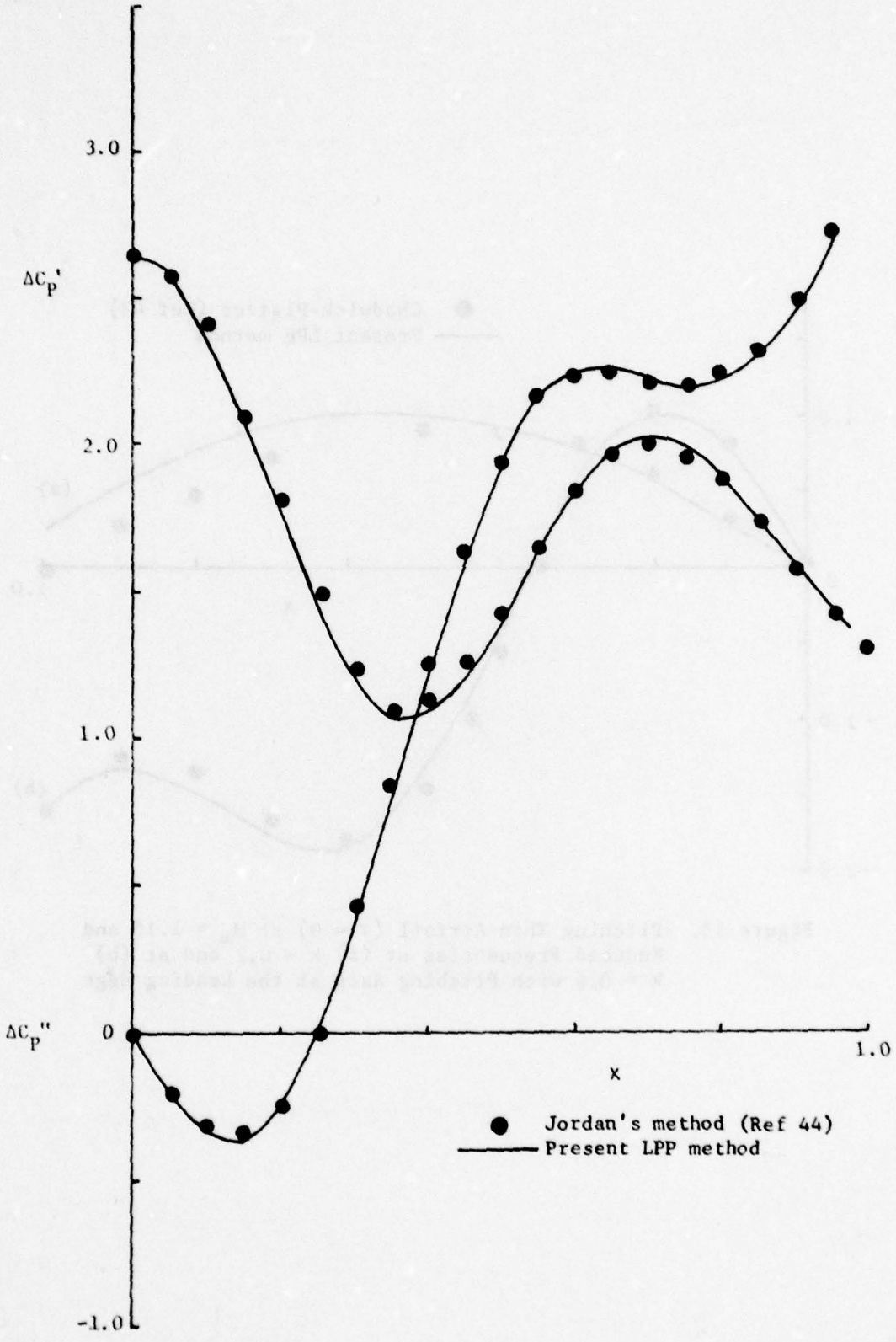

Figure 16. Pitching Thin Airfoil ($\tau = 0$) at $M_\infty = 1.25$ and Reduced Frequency $k = 1.0$ with Pitching Axis at the Leading Edge

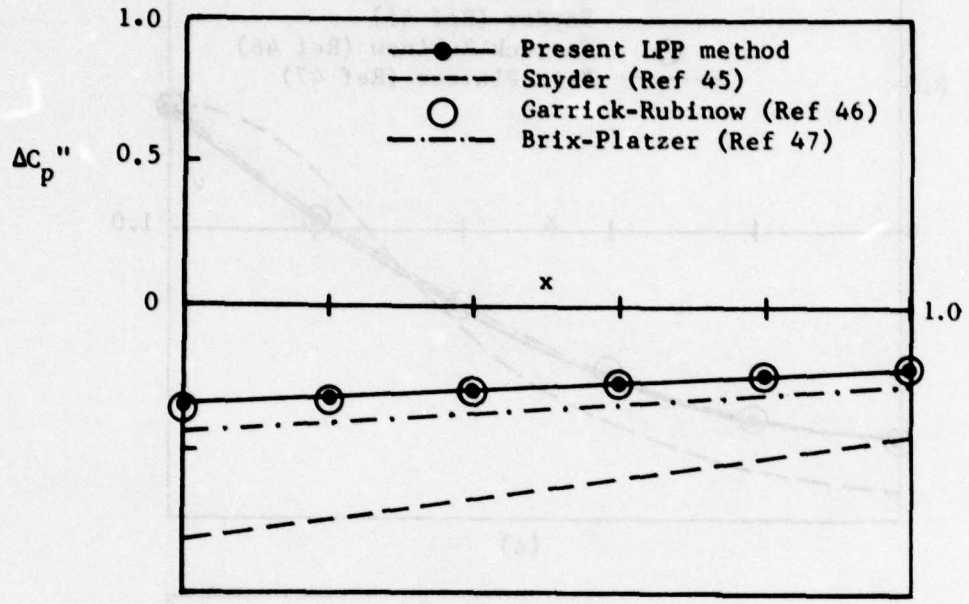

(a)

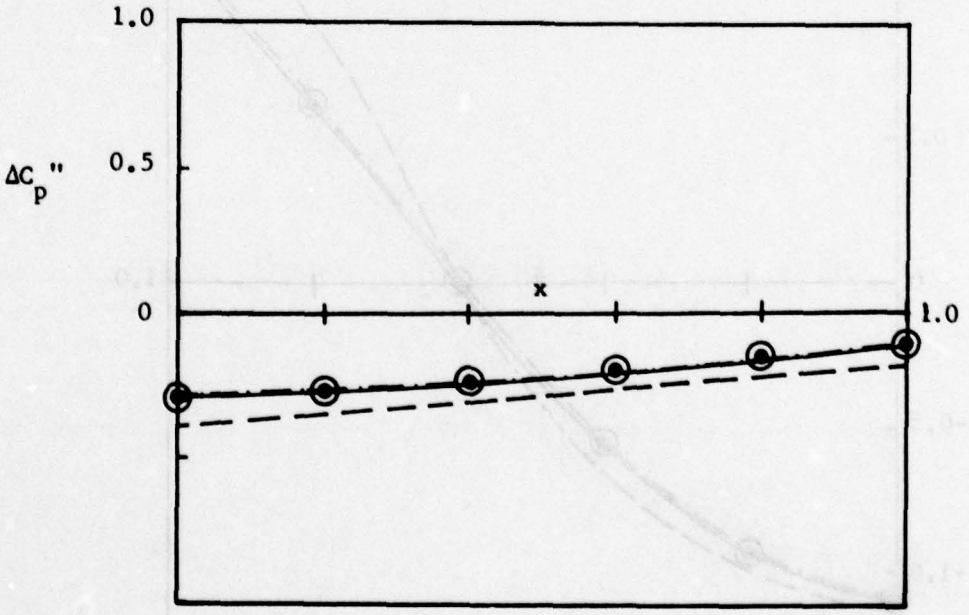

(b)

Figure 17. Pitching Thin Airfoil (τ = 0) at M_∞ = 1.5 and (a) k = 0.02, (b) k = 0.166 with Pitching Axis at Midchord

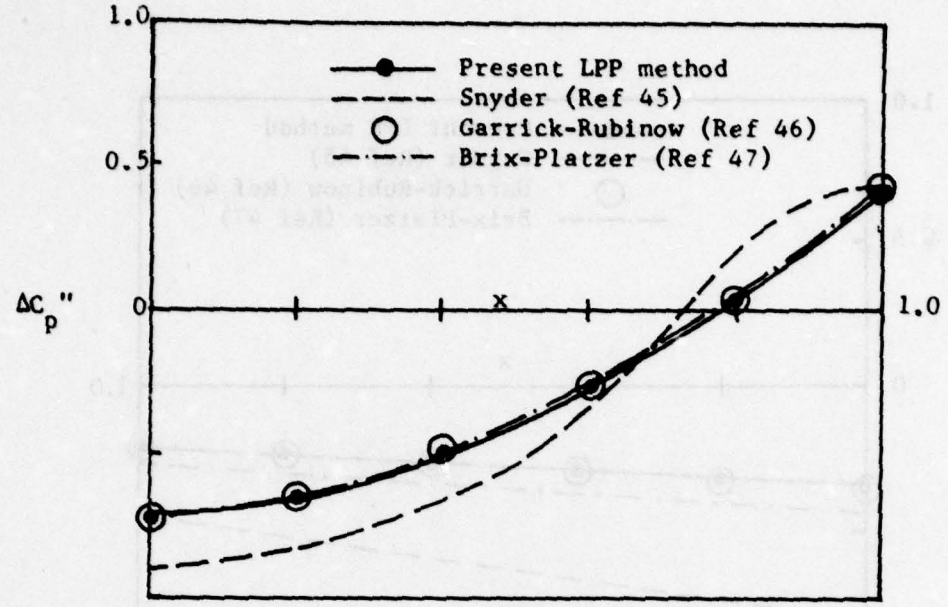

(a)

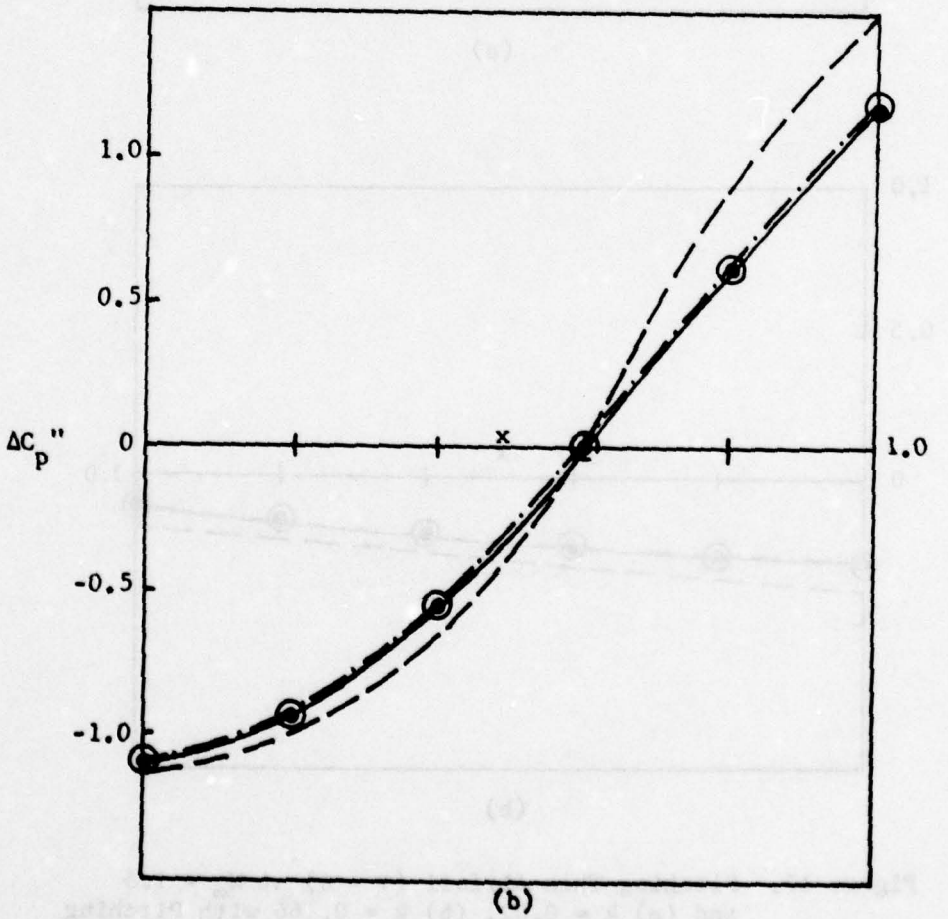

(b)

Figure 18. Pitching Thin Airfoil (τ = 0) at M_∞ = 1.5 and (a) k = 0.416, (b) k = 0.625 with Pitching Axis at Midchord

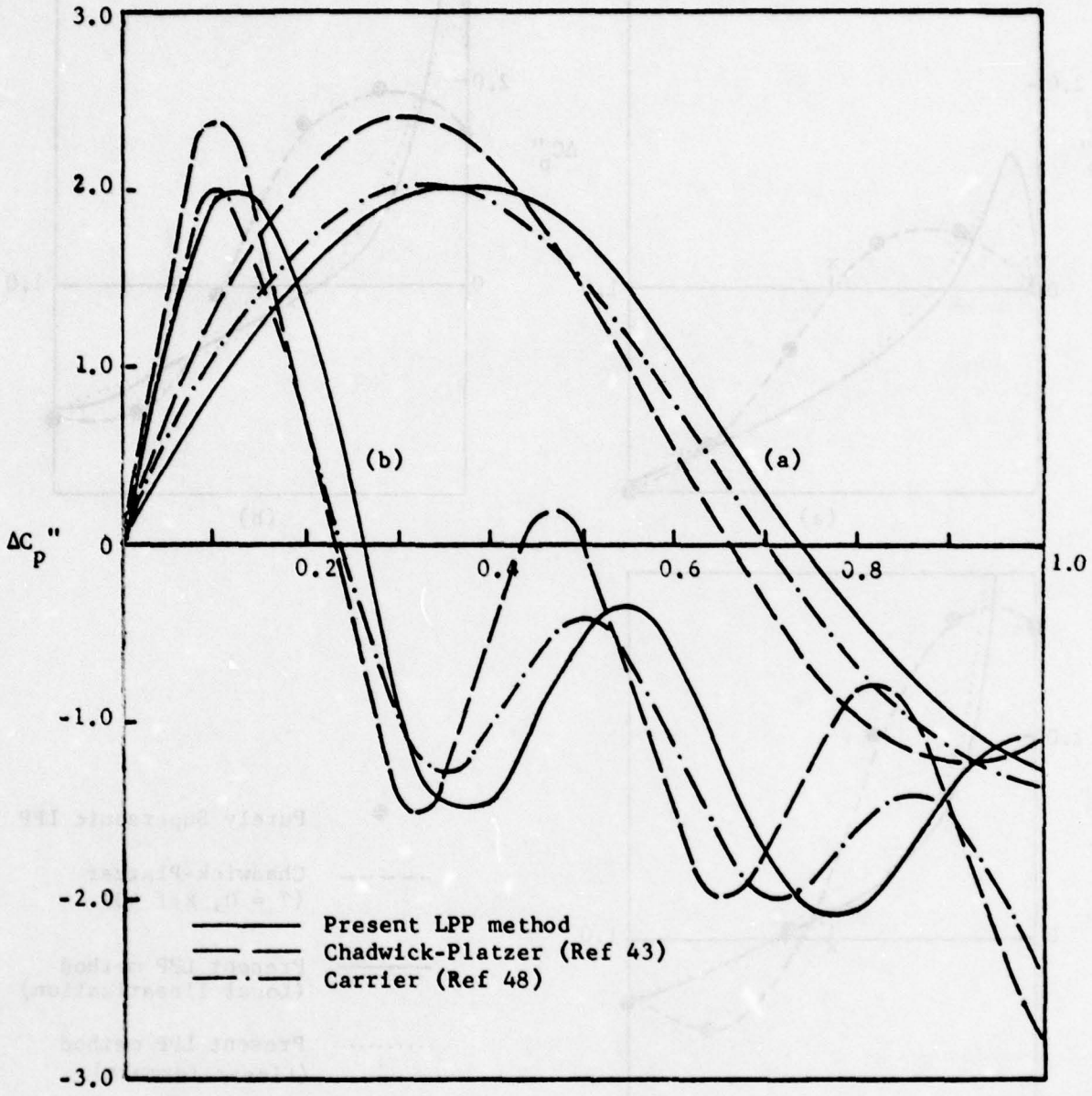

Figure 19. Transonic/Supersonic Out-of-Phase Pressure Distributions for 5% Thick Wedge at M_∞ = 1.15 and (a) k = 0.2, (b) k = 0.6 with Pitching Axis at the Apex

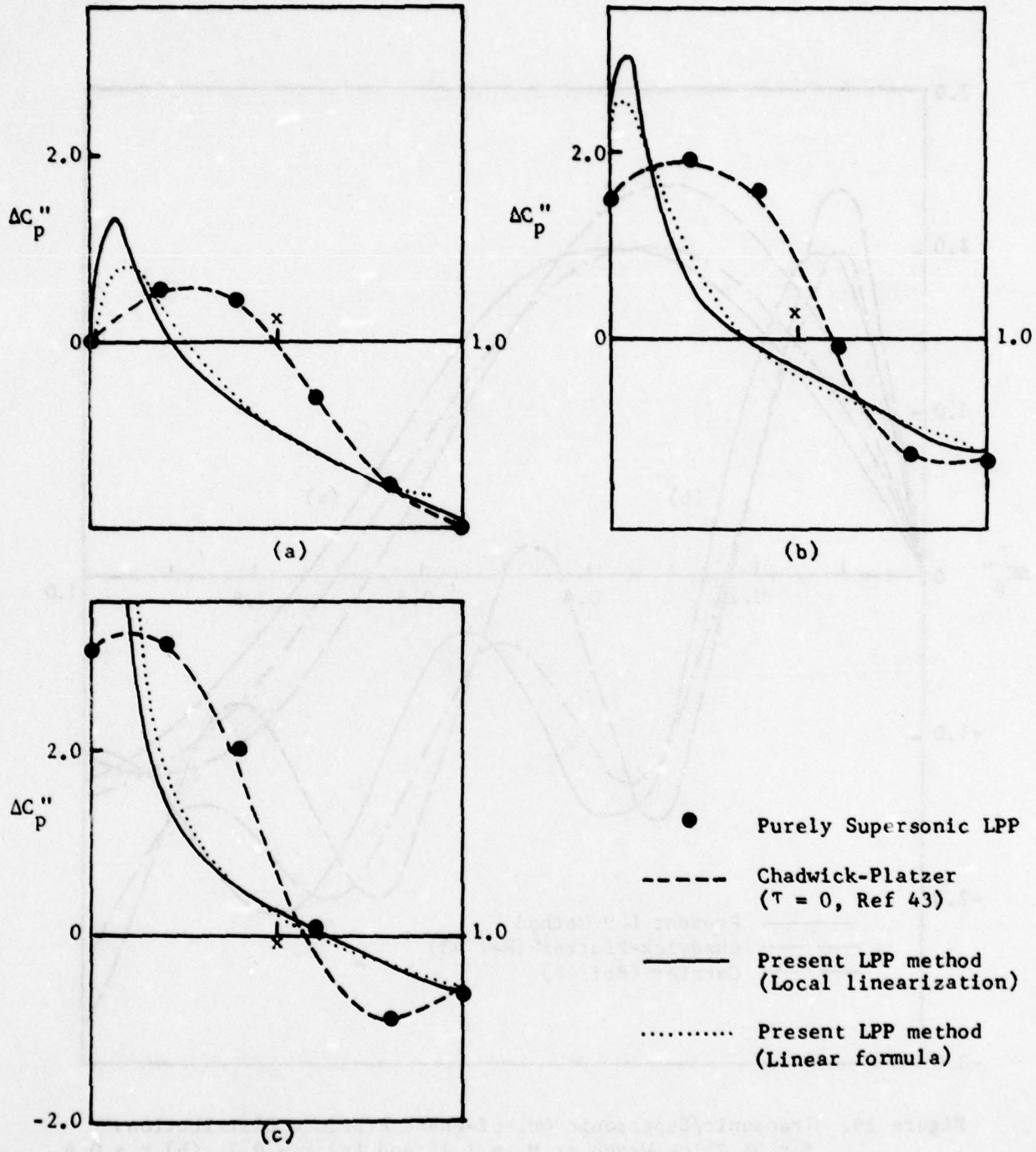

Figure 20. Transonic/Supersonic Pressure Distributions for a Parabolic-Arc Airfoil with Thickness $\tau = 0.0125$ at $M_\infty = 1.2$ and $k = 0.5$ with Pitching Axes at (a) Leading Edge, (b) Midchord, and (c) Trailing Edge, using Linear Supersonic Steady Flow Input and Local Linearization Steady Flow Input

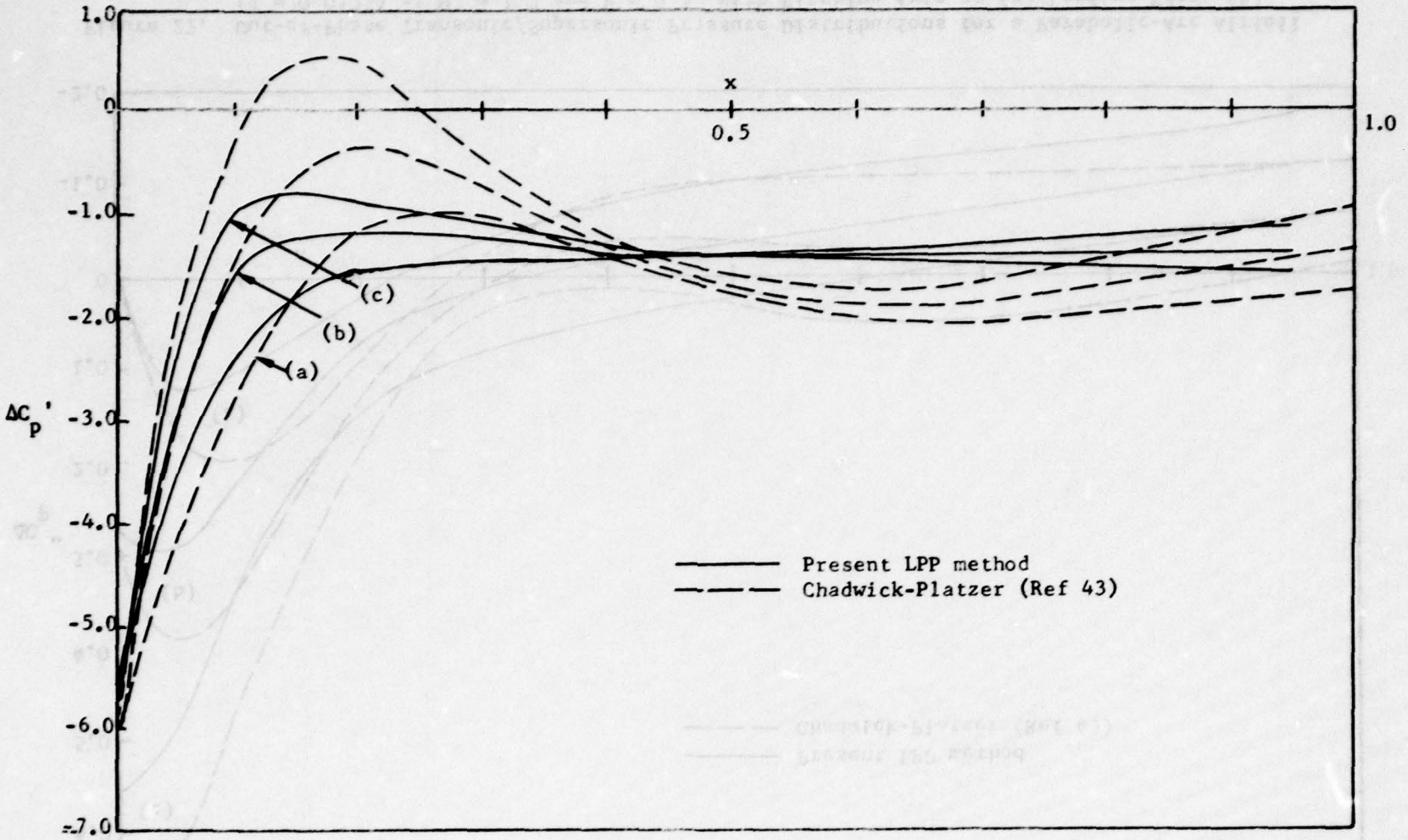

Figure 21. In-Phase Transonic/Supersonic Pressure Distributions for a Parabolic-Arc Airfoil (τ = 0.0125) at M_∞ = 1.2 and k = 0.5, with Pitching Axis at (a) Leading Edge, (b) Midchord, and (c) Trailing Edge, using Spreiter's Local Linearization Input (Eq 15, Ref 49)

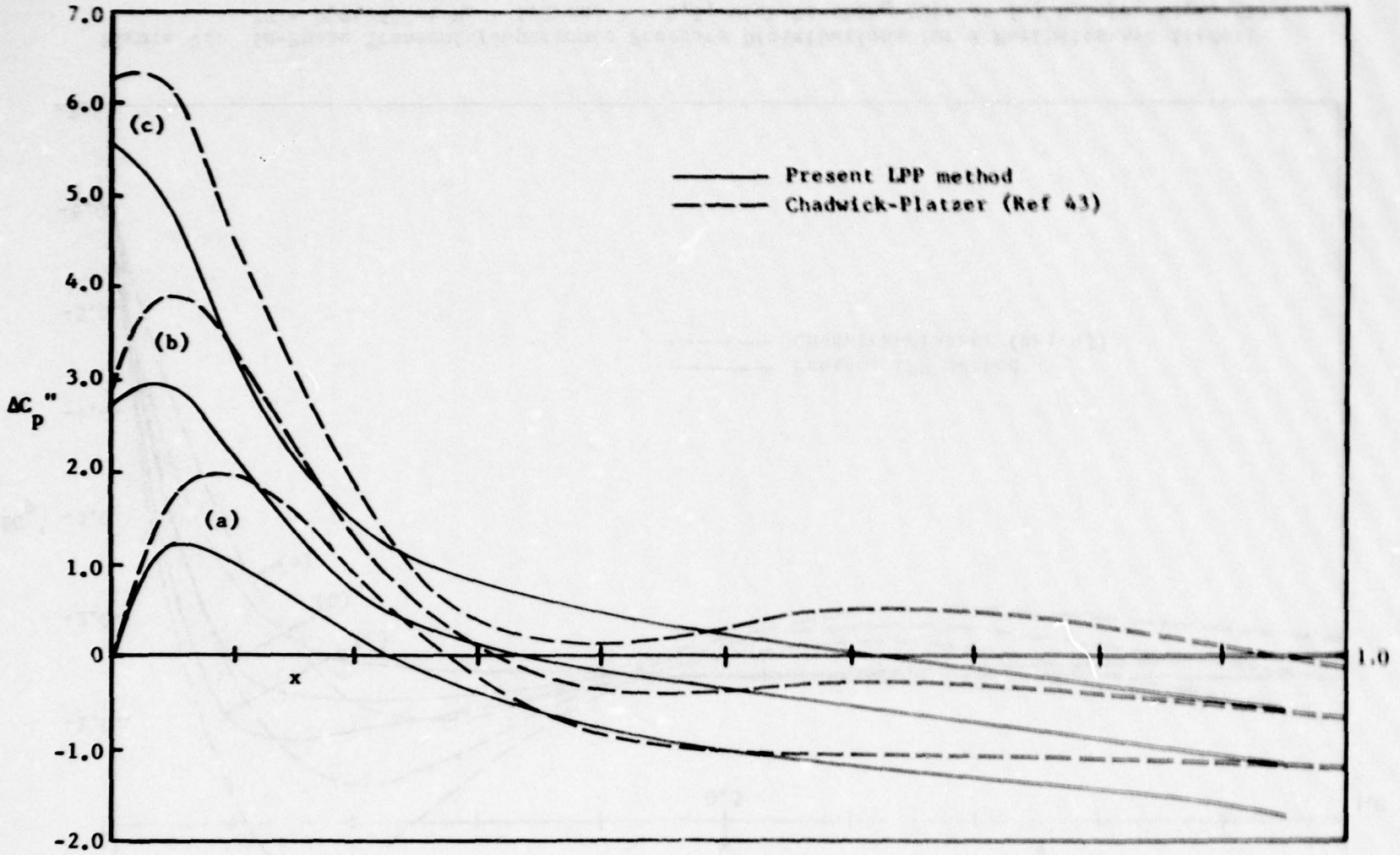

Figure 22. Out-of-Phase Transonic/Supersonic Pressure Distributions for a Parabolic-Arc Airfoil ($\tau = 0.0125$) at $M_\infty = 1.2$ and $k = 0.5$, with Pitching Axis at (a) Leading Edge, (b) Midchord, and (c) Trailing Edge, Using Spreiter's Local Linearization Input (Eq 15, Ref 49)

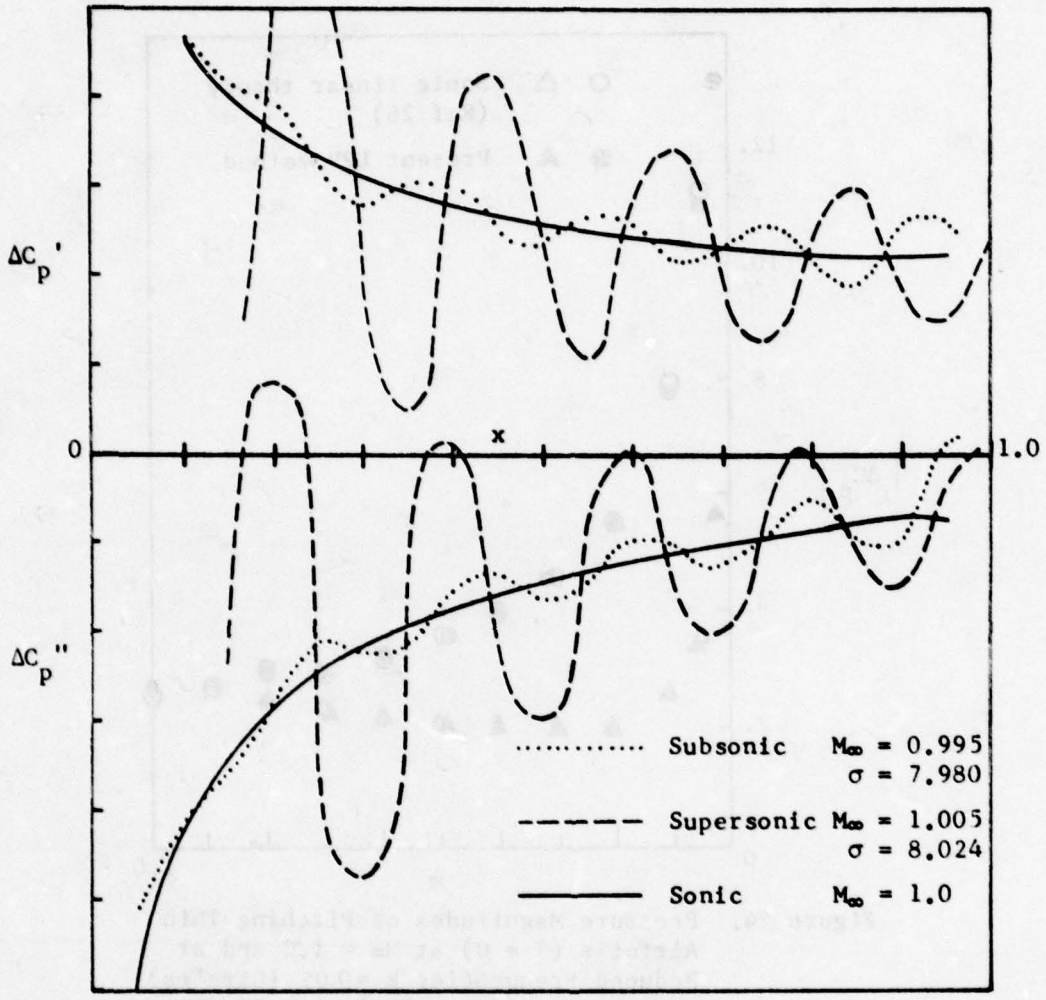

Figure 23. Oscillatory Pressure Distributions on a Pitching Airfoil ($\tau = 0$, $k = 0.08$) as M_∞ Approaches Sonic, all using Purely Linearized Flow Solutions ($\Gamma = \lambda = \mu = 0$)

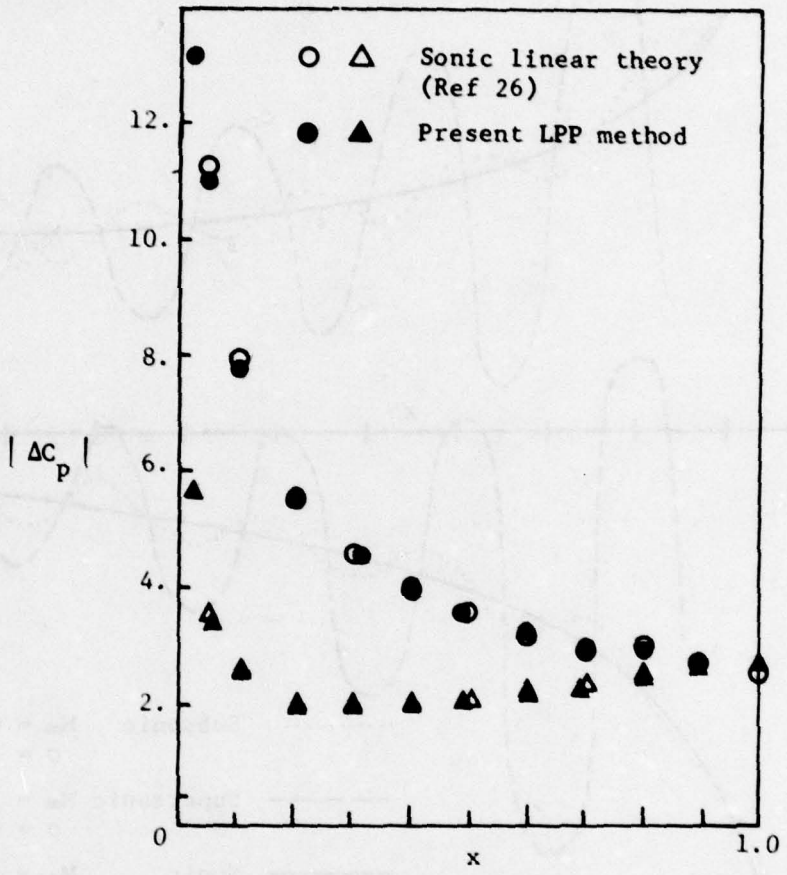

Figure 24. Pressure Magnitudes of Pitching Thin Airfoils ($\tau = 0$) at $M_\infty = 1.0$ and at Reduced Frequencies k =0.05 (Circles) and k = 0.5 (Triangles) with Pitching Axis at the Leading Edge

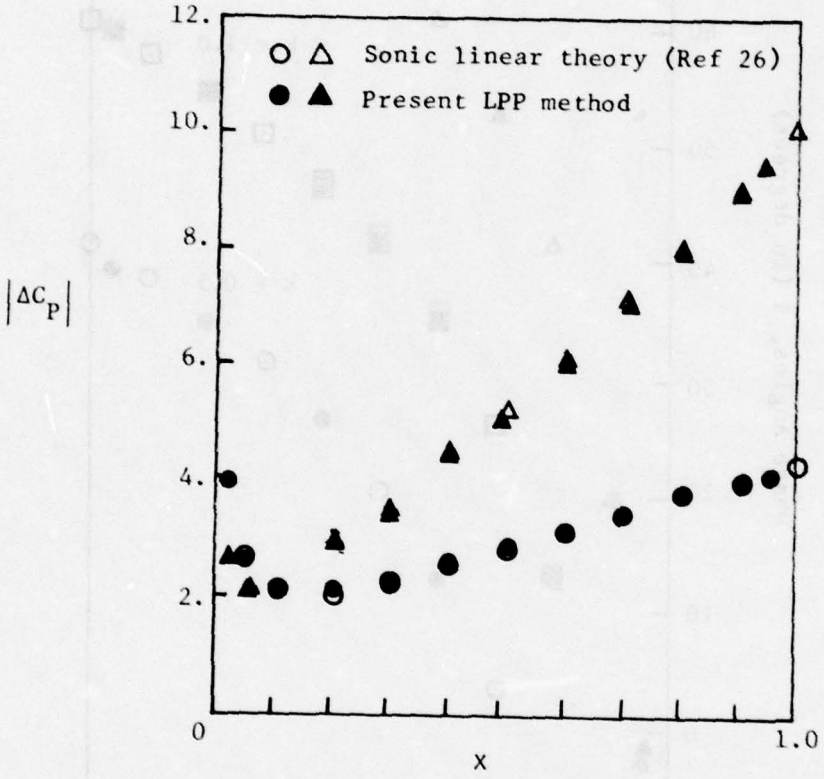

Figure 25. Pressure Magnitudes of Pitching Thin Airfoils ($\tau = 0$) at $M_\infty = 1.0$ and at Reduced Frequencies $k = 1.0$ (Circles) and $k = 2.5$ (Triangles) with Pitching Center at the Leading Edge

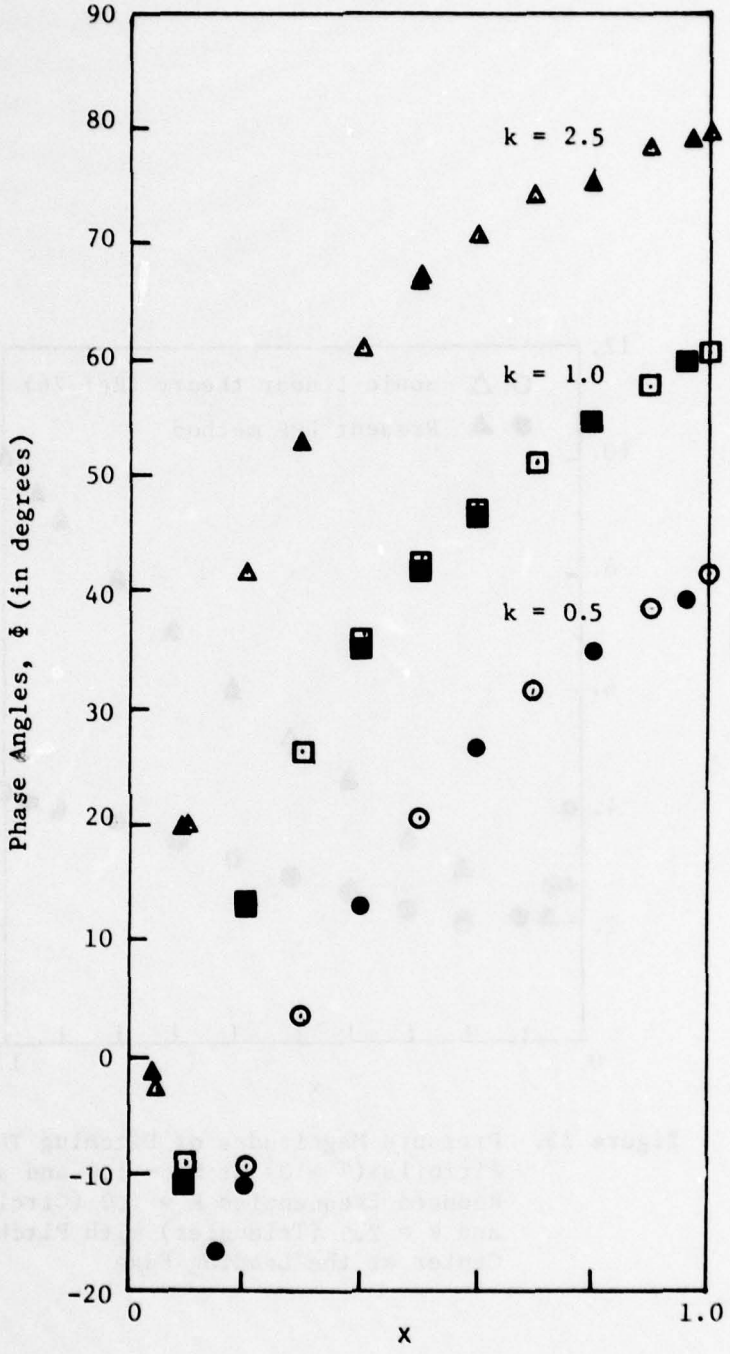

Figure 26. Phase Angles of Pitching Thin Airfoils ($\tau = 0$) at $M_\infty = 1.0$, with Pitching Axis at the Leading Edge, using the Sonic Linear Theory (Ref 26, open symbols) and the Present LPP Method (solid symbols)

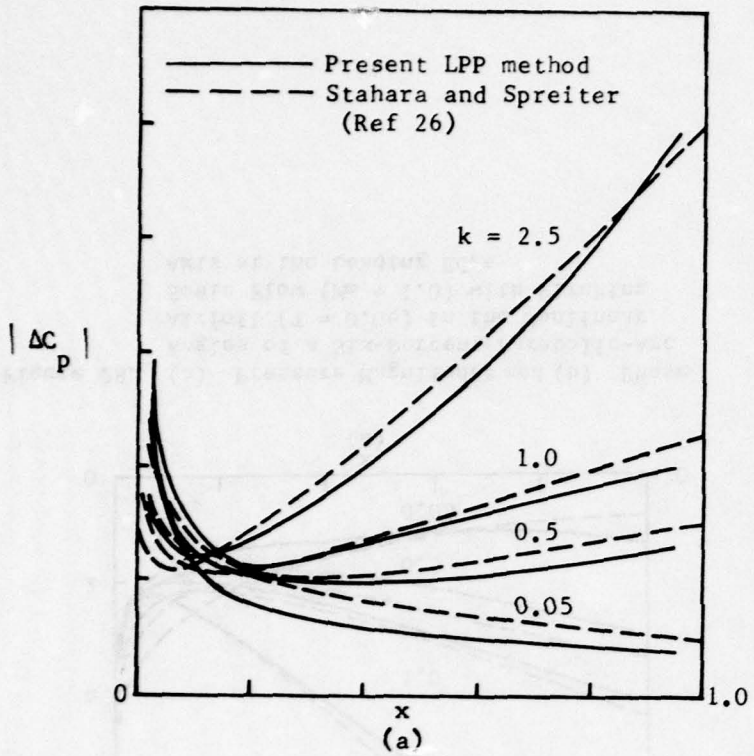

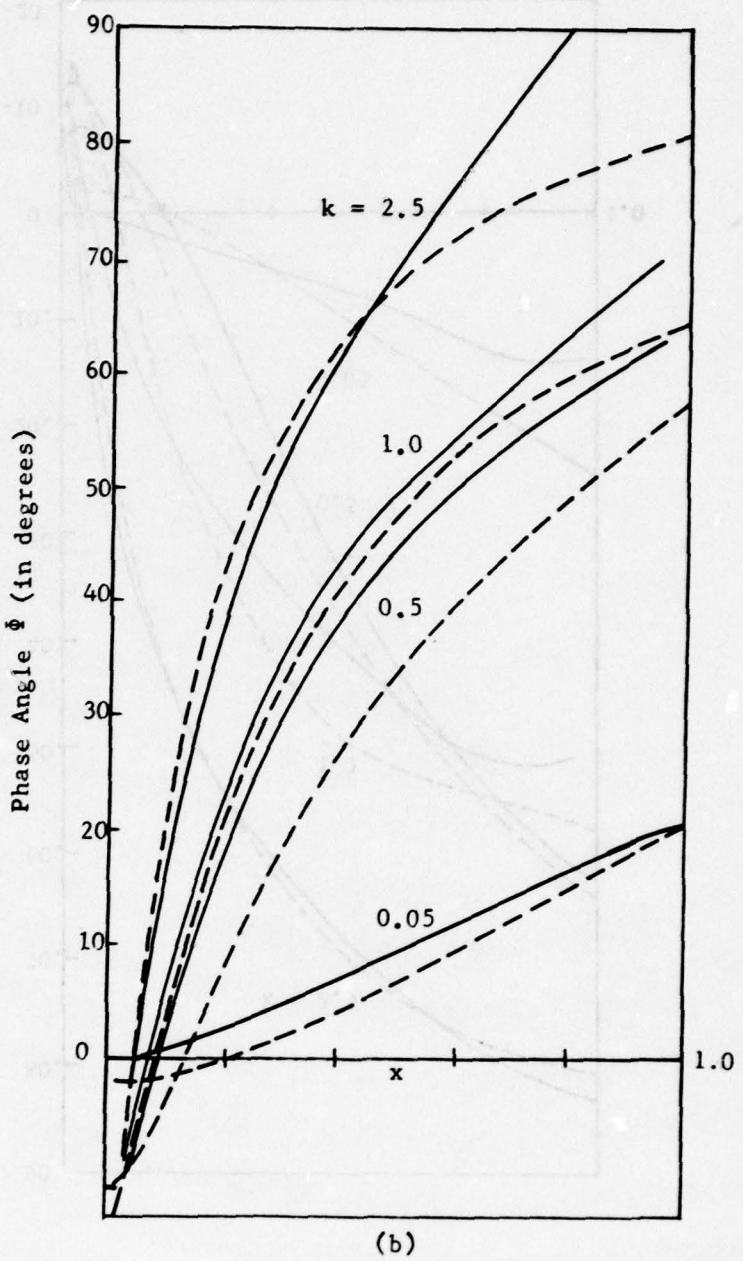

Figure 27. (a) Pressure Magnitudes and (b) Phase Angles of a Six-Percent Pitching Guderley Airfoil ($\tau = 0.06$) in the Nonlinear Sonic Flow ($M_\infty = 1.0$) with Pitching Axis at the Leading Edge

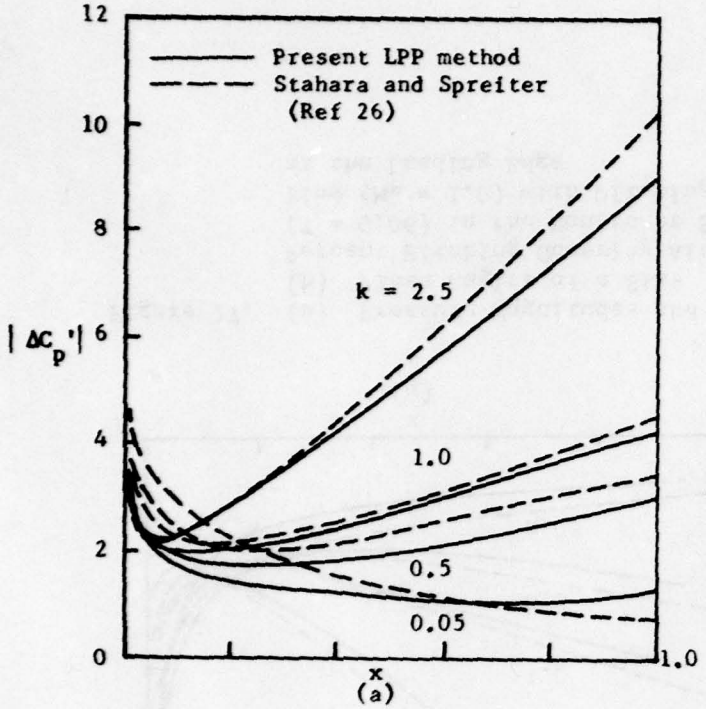

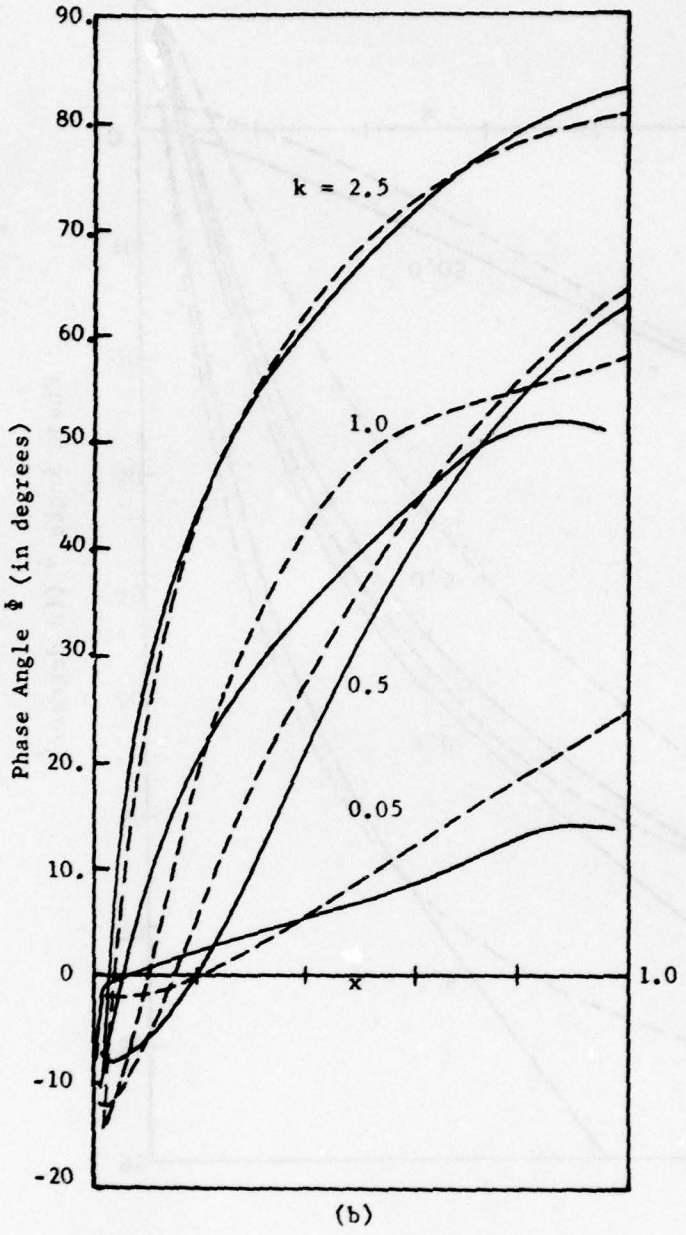

Figure 28. (a) Pressure Magnitudes and (b) Phase Angles of a Six-Percent Parabolic-Arc Airfoil ($\tau = 0.06$) in the Nonlinear Sonic Flow ($M_\infty = 1.0$) with Pitching Axis at the Leading Edge

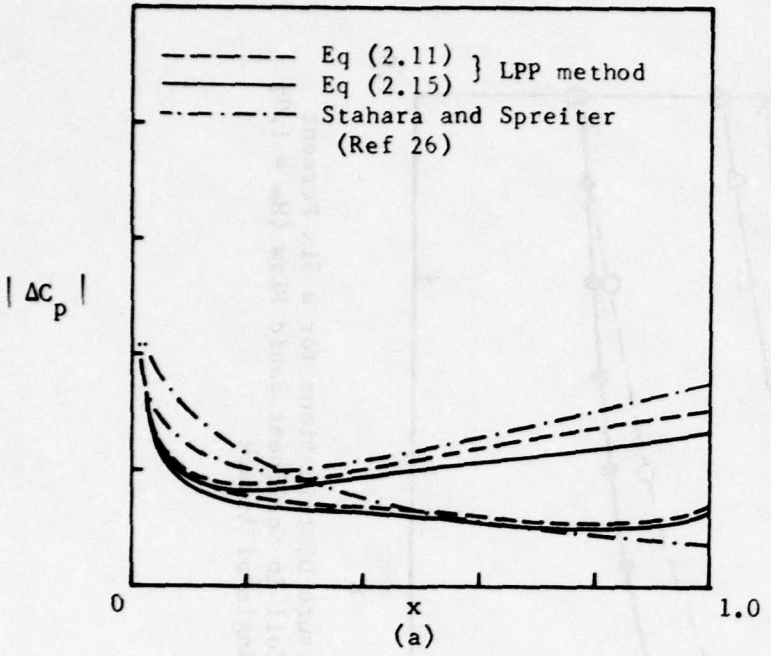

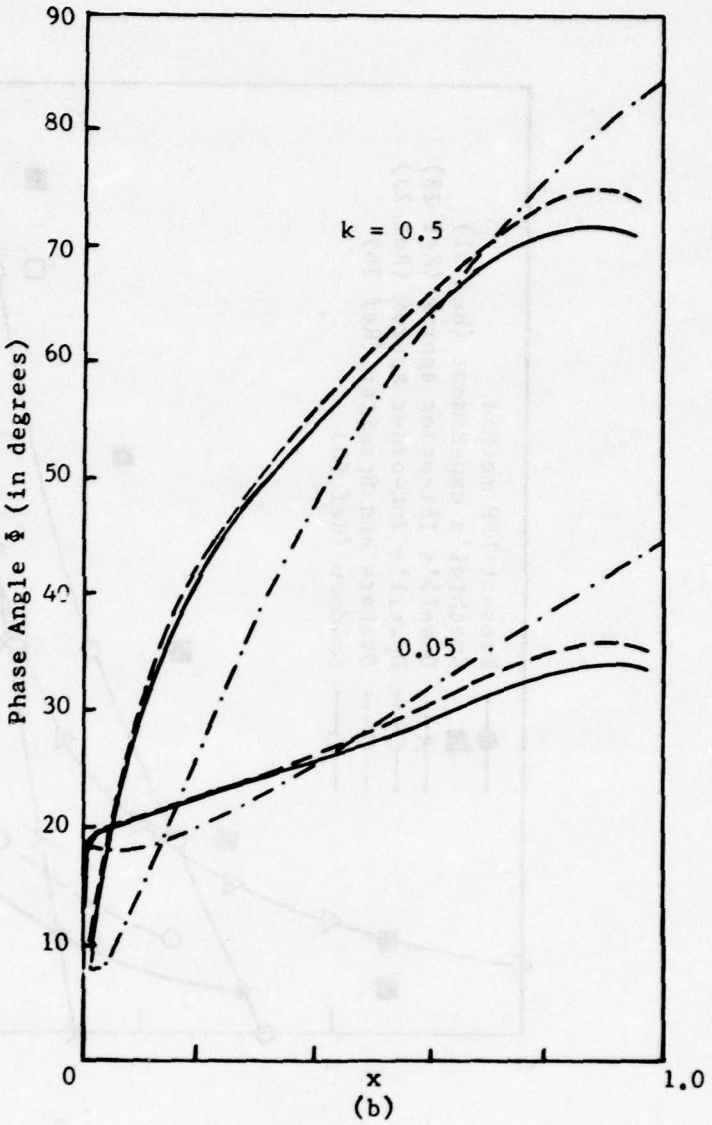

Figure 29. Comparison of (a) Pressure Magnitudes and (b) Phase Angles for a Six-Percent Pitching Parabolic-Arc Airfoil (τ = 0.06) in Nonlinear Sonic Flow (M_∞ = 1.0) using Various Approximations

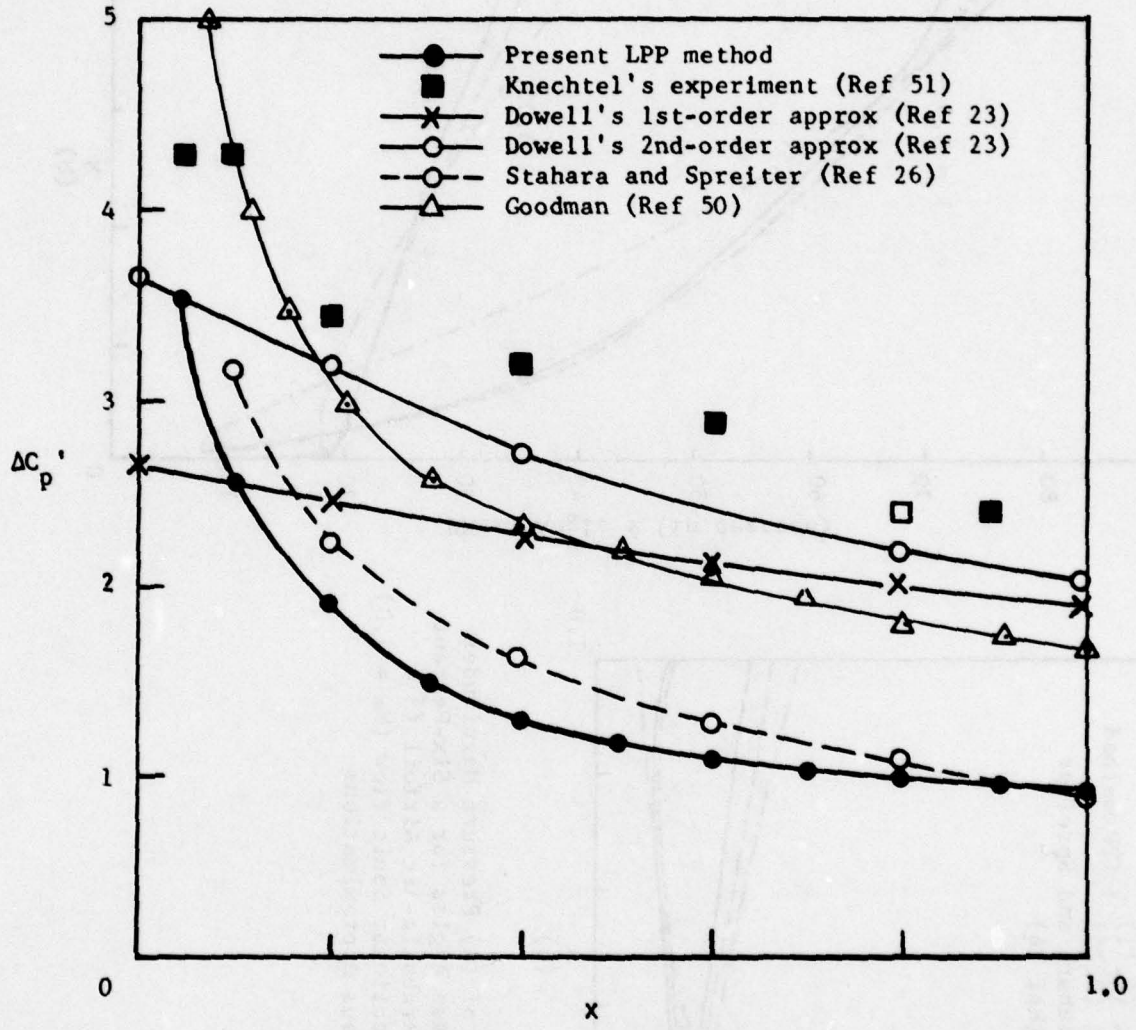

Figure 30. Comparison of Pressure Distributions for a Six Percent Parabolic-Arc Airfoil in Nonlinear Sonic Flow ($M_\infty = 1.0$; $k = 0$) at Steady Angle of Attack

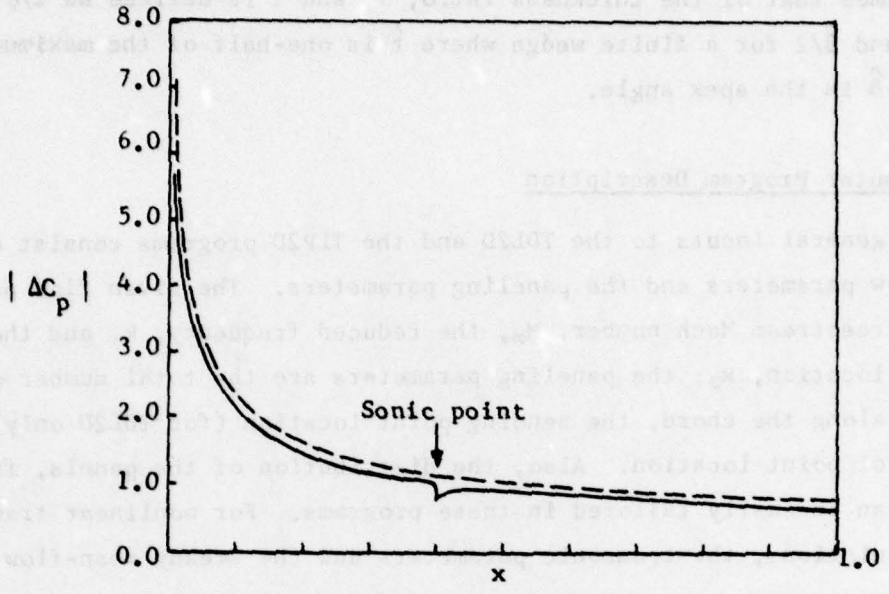

(a) Pressure magnitudes

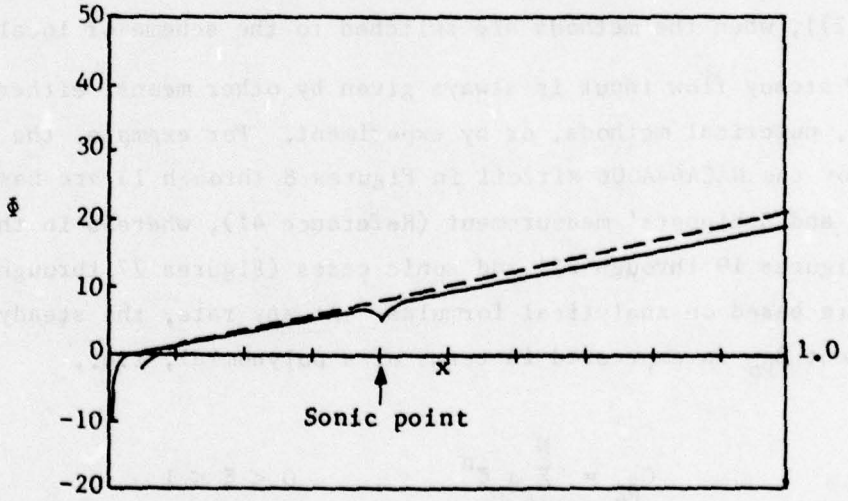

(b) Phase angles (in degrees)

Figure 31. Comparison of the Pressure Distributions of a Six-Percent Pitching Guderley Airfoil in Nonlinear Sonic Flow ($M_\infty = 1.0$) at $k = 0.05$, using the Sonic Kernel Function (broken lines) and the Mixed Kernel Function Methods (Solid Lines)

as two times that of the thickness ratio, τ, and τ is defined as $\hat{t}/\bar{c}$ for an airfoil and $\hat{\theta}/2$ for a finite wedge where $\hat{t}$ is one-half of the maximum thickness and $\hat{\theta}$ is the apex angle.

5.1 Computer Program Description

The general inputs to the TDL2D and the TLP2D programs consist of the given flow parameters and the paneling parameters. The given flow parameters are the freestream Mach number, M_∞, the reduced frequency, k, and the pitching axis location, x_o; the paneling parameters are the total number of panels assigned along the chord, the sending point location (for TDL2D only), and the control point location. Also, the distribution of the panels, fine or coarse, can be easily tailored in these programs. For nonlinear transonic flow calculations, the transonic parameters and the steady mean-flow input must be considered. The coefficients A and B are built in with options of using Equation (2.11), (2.15), or (2.16); the transonic parameters, λ, Γ, and μ can also be assumed different values, or put to zero individually. These parameters become functions of the steady mean-flow pressure (see Equation (5.2)), when the methods are switched to the scheme of local linearization.

The steady flow input is always given by other means, either by other theories, numerical methods, or by experiment. For example, the steady flow inputs for the NACA64A006 airfoil in Figures 8 through 13 are based on Tijdeman and Schippers' measurement (Reference 41), whereas in the supersonic cases (Figures 19 through 22) and sonic cases (Figures 27 through 31), the inputs are based on analytical formulas. At any rate, the steady pressure coefficient C_{p_o} is expressed in terms of a polynomial, i.e.,

$$C_{p_o} = \sum_{n=0}^{N} a_n \xi^n \quad , \qquad 0 < \xi < 1 \tag{5.1}$$

where ξ is the 'sending-point' coordinate, N is an integer up to N = 9. Of course, a_n's are obtained by applying the curve-fit scheme to the given data. The C_{p_o}'s used for all figures are listed in Appendix C. Thus, the transonic parameters read

$$\begin{cases} \lambda = \dfrac{-v_\infty}{2} C_{p_o}(\xi) \\ \Gamma = \dfrac{-v_\infty}{2} C_{p_o}'(\xi) \\ \mu = \dfrac{-v_\infty}{2} C_p''(\xi) \end{cases} \tag{5.2}$$

In the TLP2D code, the parameter β_o^2, rather than M, is used as an indicator of the type of the local flow characteristics, and hence the type of panel element that should be applied. Given C_{p_o}, Equation (5.1), the calculation scheme is switched to subsonic, sonic, or supersonic type according to wherever β_o^2 is less than, equal to, or greater than zero, measured at the midchord (usually the control point) of each element. Such a local-flow indicator is specially designed for the case of mixed flow, hence the mixed kernel function procedure. More will be discussed in the sonic flow section.

5.2 Transonic/Subsonic Results

The in-phase and the out-of-phase pressure distributions (i.e., $\Delta C_p'$ and $\Delta C_p''$) for flapping and pitching NACA64A006 airfoils in purely subsonic flow are presented in Figures 4, 5, 6, and 7. The purpose here is to check out the TDL2D and the TLP2D codes against the linear theory. It is seen that the present results are in good agreement with the linear theory and those by the finite-difference method (References 3, and 42). It should be remarked that in all these cases, the results obtained using the TDL2D code are indistinguishable from those in Figures 4 through 7 using the TLP2D code.

Figures 8 through 13 present the transonic/subsonic calculations in the subcritical regime for NACA64A006 airfoils in pitching and flapping motions. In these cases, the steady mean-flow inputs, C_{p_o}'s, are given by Tijdeman and Schippers (Reference 41), and are curve-fitted as polynomials (see Appendix C). Figure 8 compares the linear and the nonlinear results calculated by TDL2D

and TLP2D codes for a pitching airfoil. Figures 9 through 13 show the nonlinear results based on TDL2D or TLP2D codes for flapping airfoils. It can be observed that all theoretical methods produce pressure magnitudes generally larger than the experimental data (Reference 41). Such a difference could be due to neglecting the boundary layer effects in the analysis. For detailed discussion on this issue, one is referred to References 14, 19, and 53. In Figure 11, the present results in phase angles are seen to have some deviation from the finite-difference results (References 1 and 42) from the leading edge to midchord. In Figures 12 and 13, various results in pressure magnitudes and phase angles are plotted using the TDL2D code, TLP2D code, and Ehler's finite-difference method. Again, it is seen that there is some disagreement between the present results and the experimental data behind the leading edge. Although the TDL2D result checks well with the TLP2D result in $\Delta C_p'$, considerable difference is seen in the $\Delta C_p''$ results. The cause of this difference is not clear and will be subject to future investigation.

Some remarks are in order with regard to our experience in using the developed codes. First, as pointed out earlier, our results exhibit some discrepancies in the transonic/subsonic calculations, particularly near the leading edge. Our experience shows that these are caused mainly by the leading edge singularity of the steady mean-flow. This type of singularity actually results from the ill-formulation of the small disturbance theory in the leading edge region, be it linear or nonlinear, due to the incompatibility of the equation and the linearized boundary condition. In other words, the singularities may vary in their 'strengths' in different flow regimes, but once they are adopted as the steady mean-flow inputs for our transonic parameters (Equation (5.2)), discrepancies, or even numerical instabilities may occur. (In particular, the most sensitive parameter of all is the acceleration parameter, Γ, which is often very large in the neighborhood of the leading edge.)

To attain a stable computation procedure, one is required to keep the value of Γ constant and let it be no greater than order of one in the first few panels. Then Γ resumes its local values at the panel where the true value of Γ is indeed below one. Strictly speaking, this procedure is not altogether legitimate. In the Addendum, Professor Landahl's general formulation of the phase correction method (Equation L.4) may circumvent such a procedure. In his formulation, the Γ-term can be integrated out altogether as a result of a further delay step of the local linearization application. For this reason, it is felt that some serious attention must be given to Landahl's phase-correction method.

Next, we need to describe the ease of application of the TDL2D code and the TLP2D code. In all the calculations using the TDL2D code, we only require equal spacing panels; normally we set N = 20, regardless of pitching or flapping motion. In the cases of using TLP2D code, more refined panels are required in the neighborhood of the leading edge and the hinge points, the panel numbers ranges N = 23 to N = 33. As the LPP method is a higher moment method than the DL method (see Section 4), the total CPU time for the same case required using TLP2D code runs usually more than twice of that using TDL2D code.

5.3 Transonic/Supersonic Results

To check out the LPP method in the supersonic regime, calculations using the TLP2D code are first performed for several purely supersonic examples (Figures 14 through 18). Computed results for pitching flat plates using TLP2D are compared with Chadwick-Platzer's result using the linearized method of characteristics (MOC) (Reference 43) in Figures 14 and 15; also, computed results are compared with Jordon's theoretical result (Reference 44) for in-phase and out-of-phase pressure distributions in Figure 16. In these fairly high frequency ranges (k = 0.5 and 0.6), it is seen that the present results are in good agreement with the other results. Figures 17 and 18 again show the comparisons of the out-of-phase pressure distributions of the present method with those obtained by the classical method of Garrick and Rubinow

(Reference 46), by Brix-Platzer's linearized MOC (Reference 47) and by Snyder's finite difference method (Reference 45). Our results are in excellent agreement with the results calculated according to Garrick and Rubinow. Figures 19 through 22 show the transonic/supersonic calculations in the nonlinear supersonic (or low-supersonic) regime for wedges and for parabolic-arc airfoils. Using the linear formula (Equation (4.26), Reference 54) for a wedge ($\tau = 0.05$) as steady mean-flow input (see Appendix C), we obtained the out-of-phase pressures at two different frequencies. The comparisons in Figure 19 show that our result is in better agreement with Carrier's exact theory than Chadwick-Platzer's MOC method. Notice that the present calculation scheme for the wedge case makes no approximations, as the transonic parameter, λ, is constant and Γ and μ are identically zero. Figure 20 shows the nonlinear results quite substantially, particularly near the leading edge. The C_{p_o}'s used are based on the linear formula Reference 54) and a modified linear-fit of Spreiter's nonlinear formula (Equation (15), Reference 49); again, all the C_{p_o} coefficients can be found in Appendix C. In Figures 21 and 22, in-phase and out-of-phase pressure distributions for the same given conditions (as Figure 20) are compared with those obtained using Chadwick-Platzer's MOC method. Observing from the results in Figures 19, 21, and 22, we found that, unlike the transonic/subsonic results, our TLP2D code produces generally lower in pressure magnitudes than those of Chadwick-Platzer's. However, in their computation procedure, the steady mean-flow results and the oscillatory flow results are all self-generated and the former result is truly nonlinear (based on Teipel, Reference 55). It would be interesting, therefore, to check against these results by using Teipel's mean-flow input in the TLP2D program.

5.4 Sonic Results

In Section 3, it was shown that the sonic kernel function (Equation (3.25)) is a limiting case of the transonic subsonic kernel function (Equation (3.15)) and of the transonic/supersonic kernel function (Equation (3.22)). Here,

a numerical study was performed to check out the sonic limit for these kernel functions. Figure 23 shows that although the kernel functions are continuous throughout the sonic limit, the LPP method (N = 23 for all cases) produces oscillatory pressure distributions as M_∞ approaches one (the parmeter σ approaches infinity). Such outcomes were found by Jordan (Reference 44), using the pressure-mode method, and was subsequently discussed, in terms of the wave mechanism, by Landahl (Reference 21). This then led Jordan to be in favor of the sonic kernel function when the freestream speed is in the neighborhood of the sonic regime. However, the objective here is a rather different one. We attempt to establish a proper mixed kernel function procedure by starting out with a case of sonic flow without shock wave (Figure 31). Nevertheless, in so doing, one must check out the sonic kernel function procedure together with the LPP method. This then constitutes the following calculation results using the sonic-flow kernel functions (Figures 24 through 30).

Thus, the linear sonic flow calculations are first performed for a pitching thin airfoil (flat plate) in order to check out the application of the TDL code at $M_\infty = 1.0$. Calculated pressure magnitudes and phase angles are compared with those obtained by Stahara and Spreiter (Reference 26) in Figures 24, 25, and 26. Excellent agreement can be seen for all cases considered. Figures 27 and 28 present our calculated results for a pitching Guderley airfoil and a pitching parabolic-arc airfoil; the steady mean-flow C_{p_o} for both cases are taken from Reference 26 and are curve-fitted in Appendix C. It is seen that the present results in pressure magnitudes are generally lower than those by Reference 26 (similar to the finding of our supersonic pressure magnitude to the MOC method). Also, considerable differences in phase angle exist at various reduced frequencies between both cases. We believe that these differences could be caused by two factors in the method of approach. First, the unsteady local linearization method by Stahara and Spreiter really did not include the edge condition. Since their formulation is based on the velocity potential, to cope with such a condition would require the Schwartzchild iterative procedure. Second, in their analysis

(Reference 26), the transonic parameters appeared in the kernel potential are all expressed in terms of 'receiving point' x rather than the 'source-point' ξ. This amounts to ignoring the higher-order flow influences due to the panels upstream. Figure 29 shows the comparison of the results between using the full equation (2.11), and using the approximate equation, (2.15). It is seen that the deviation in pressure distribution is slight when the reduced frequency is low. Figure 30 exhibits a comparison of all previous sonic methods with the present LPP method for a pitching parabolic-arc airfoil ($\tau = 0.06$) at a constant angle of attack. Instead of using the steady mean-flow C_{p_o} given in Appendix C, we adopted Dowell's value ($a_o = 0.45$ and $b_o = 0.585$, Reference 23), which amounts to $\lambda = 0.585$ and $\Gamma = 0.45$ for our inputs. Consequently, the lifting pressure plot shows that, once again, our value is of the lowest magnitude, but it follows the same behavior of Goodman's theoretical distribution.

Finally, in Figure 31, the mixed kernel function procedure is tested, using a nonlinear sonic flow example. For simplicity, the Guderley airfoil is chosen, in which the sonic point is located exactly at 40 percent chord. Altogether, 33 panel elements are employed, with 15 equal-space elements (5 percent chord each), four compact elements (occupying 5 percent chord) at the leading edge and 14 compact elements (occupying 10 percent chord) in the neighborhood of the sonic point. In fact, the panel width is based on the criterion that each panel width be restricted by $\Delta x \leq \pi/4 \, |\sigma|$. While the transonic/subsonic kernel function (Equation (3.15)) is applied to the elements throughout the whole airfoil, the transonic/supersonic kernel function (Equation (3.22)) is applied only to those downstream of the sonic point. At the sonic point, which is situated between subsonic and supersonic panels, the nonlinear sonic kernel function (Equation (3.25)) is used. The calculated result is not altogether satisfactory. It is seen that MKF results follow closely to the ones by the sonic kernel function method, but that cusps occur in these results at the sonic point. At this stage of the MKF development, it is not clear whether the sonic cusp is due to an erroneous kernel function evaluation or due to an inappropriate paneling scheme in the neighborhood of the sonic point. Future investigation on this problem is mandatory for the development of the MKF method.

SECTION 6

CONCLUSIONS

A transonic kernel function method for unsteady flow calculations has been developed. The basic formulation of the transonic acceleration potential equation was derived and its basic solutions in two- and three-dimensional subsonic/transonic/supersonic flow regimes were obtained. Hence, the two-dimensional transonic/subsonic, transonic/supersonic, and sonic kernel functions were then established. To solve for the downwash integral equation, two discrete element methods were introduced; these are the Doublet Lattice method and the Linear Pressure Panel method. We realized that the former method is only restricted to the transonic/subsonic (or subcritical and purely subsonic) flow regime, while the latter method has the unified feature, if the control point is properly chosen, for subsonic/transonic/supersonic flow calculations, although the calculation scheme is more time-consuming than the former.

To demonstrate the transonic LPP method, numerical examples were presented for simple airfoil geometries in pitching motions for all flow regimes. For thin airfoil cases (i.e., for purely subsonic/sonic/supersonic cases), excellent agreements were found with the analytical results based on previous classical theories. For transonic/subsonic cases, the pressure magnitude is found to be generally larger than other results, while for transonic/supersonic and nonlinear sonic cases, it is found to be lower than the results of other theories. Numerical studies revealed that discrepancies and sometimes even numerical divergence in the present transonic/subsonic calculation (e.g., Figures 10 and 11) are largely attributed to the drastic variation of the transonic acceleration parameters β_0 and Γ in the neighborhood of the leading edge. Such discrepancies, in principle, can be greatly improved, however, if one adopts Landahl's general formulation of phase correction method (see Equations (L.1) and (L.4) of the Addendum). Phase angles can thus be corrected

accordingly; however, this would amount to developing a scheme in acoustic ray tracing. Lastly, the proposed MKF procedure is applied to a nonlinear sonic flow case. Close agreements are seen in comparing the MKF results with the nonlinear sonic kernel function results except at the sonic point. It is not clear that what causes the undesirable cusp at the sonic point and how to smooth it out at this time.

The present study leads to the following concluding remarks.

1. We have demonstrated that the combination of the transonic kernel function method with a properly chosen discrete element method such as the LPP method is a suitable method for unified treatment of unsteady transonic flow calculations.
2. Our calculations among other unsteady flow methods assure the distinctive departure of the nonlinear results from the linear ones in all transonic flow regimes (not to mention the supercritical regime).
3. The present study indeed paves the road for the MKF method development in the supercritical regime. It also opens up ways for the future development of a three-dimensional LPP method.

In view of the encouraging results obtained by the present transonic LPP method, we recommend the following projects for further development and extension of the present work.

1. Improve the LPP method algorithm so that the TLP2D code can be made equally cost-effective as the TDL2D code.
2. Generalize the TLP2D code to include three degrees of freedom, i.e., pitching, plunging, and flapping in all flow regimes.
3. Incorporate Landahl's general formulation with phase corrections into our TLP2D code.
4. Improve the MKF procedure for smoothed sonic flow cases and develop the MKF method so that the TLP2D code can cope with supercritical flow regime, as this can be considered as the most important step in the MKF method. In this regard, two steps are suggested.

a. Computation of the Eckhaus-Landahl flow model (see Appendix B).

b. Computation of the oscillatory supercritical flow with embedded shock waves.

ADDENDUM

KERNEL-FUNCTION METHOD FOR TRANSONIC UNSTEADY FLOW

by

M.T. Landahl

The basic differential equation for the acceleration potential, ψ, reads (corrected and valid for low frequencies only, two-dimensional case considered)

$$\beta_o^2 \psi_{xx} + \psi_{zz} + A\psi_x + B\psi = 0 \qquad \text{(L.1)}$$

where

$$\begin{cases} \beta_o^2 = \beta_\infty^2 - M_\infty^2(\gamma + 1)\phi_x \\ A = -2ikM_\infty^2(1 + \underline{\phi_x}) - 2M_\infty^2[(\gamma + 1) - \underline{\beta_\infty^2(\gamma - 1)}]\phi_{xx} \\ B = \underline{M_\infty^2[k^2 - (\gamma + 1)\phi_{xxx} - 2ik\gamma\phi_{xx}]} \\ \beta_\infty^2 = 1 - M_\infty^2 \end{cases}$$

For M_∞ close to unity and for low frequencies, the terms underlined may be neglected. Thus, the differences between this result and the earlier one by D. Liu are unimportant.

To find an approximate solution valid for the receding wave portion we set

$$\psi = \psi_1 e^{\alpha(x)} \qquad \text{(L.2)}$$

and choose $\alpha(x)$ such that the equation for ψ has only 0(1) coefficients. One finds the following equation for ψ_1:

$$\beta_o^2 \psi_{1xx} + \psi_{1zz} + A_1 \psi_{1x} + B_1 \psi_1 = 0 \qquad \text{(L.3)}$$

where

$$\begin{cases} A_1 = A + 2\beta_o^2 \alpha' \\ B_1 = B + \beta_o^2 \alpha'' + \beta_o^2 (\alpha')^2 + A\alpha' \end{cases}$$

and the prime superscript is defined as a total differentiation, i.e., $(\cdot)' \equiv \frac{d}{dx}(\cdot)$.

We set $f = \beta_0^2\alpha$. Then, with $\beta_0^2 = \beta_\infty^2 - M^2(\gamma + 1)_x$, we have

$$\begin{cases} A_1 = -2ikM_\infty^2 + 2(\beta_0^2)' + 2f \\ B_1 = M_\infty^2[k^2 - (\gamma + 1)\phi_{xxx} - 2ik\gamma\phi_{xx}] + \dfrac{f}{\beta_0^2}[-2ikM_\infty^2 + 2(\beta_0^2)'] \\ \qquad + \beta_0^2\left(\dfrac{f}{\beta_0^2}\right)' + \dfrac{f^2}{\beta_0^2} \end{cases}$$

For the receding wave, we anticipate that $\alpha' = 0(\beta_0^{-2})$, i.e., that $f = 0(1)$. Hence, in order for the coefficient B_1 to be finite in the limit $\beta_0^2 \to 0$ we must have

$$-2ikM_\infty^2 + (\beta_0^2)' + f = 0$$

or

$$\alpha = -\ell n(\beta_0^2) + \int \frac{2ikM_\infty^2}{\beta_0^2}\,dx$$

With this substitution we may set

$$\psi = \psi_1 \beta_0^{-2} e^{\int \frac{2ikM_\infty^2}{\beta_0^2}\,dx} \tag{L.4}$$

where ψ_1 is one solution of the equation

$$\beta_0^2\psi_{1xx} + 2ikM_\infty^2\psi_{1x} + \psi_{1zz} + M_\infty^2[k^2 - 2ik\gamma\phi_{xx}]\psi_1 = 0 \tag{L.5}$$

The solution of this equation may be expected to exhibit slow variations with respect to x, since the shortwave component should be described by the phase factor $\exp\{\int(2ikM_\infty^2/\beta_0^2)dx\}$. Therefore, the first term may be

neglected. Also, in the last term, $2ik\gamma\phi_{xx}$ could be neglected compared to k^2 (for low frequencies, both k^2 and $2ik\gamma\phi_{xx}$ may be neglected). Note the plus sign in front of the ψ_{1x}-term. Compare this with Landahl's result in Symposium Transsonicuum I (Reference 56). The result for ψ thus obtained is only valid for the receding-wave portion. For the advancing-wave portion, there should be no factor β_o^{-2}.

We shall now consider a recipe for constructing a uniformly valid approximation for the pressure kernel starting from the local linearization result, i.e., the solution obtained by assuming a uniform flow of Mach number equal to the value at the sonic point. Denote this solution by superscript L. The kernel function is obtained from the doublet solution ψ_d, and from the above, one can prepare the following approximation:

$$\psi_d = \frac{c_{no}(\nu)}{c_n(\nu)} \psi_d^{(L)} e^{i(\theta - \theta^{(L)})}$$

where c_n is the group velocity of acoustic waves having wave front at an angle, ν, to the x-axis (see Figure L1), c_{no}, the value at the source point, θ, the phase angle of the acoustic waves along a particular ray connecting source and field points, and $\theta^{(L)}$, the phase of the local solution.

This approximate is consistent with the acoustic ray theory (see Landahl's article in Symposium Transsonicuum II, Reference 53).

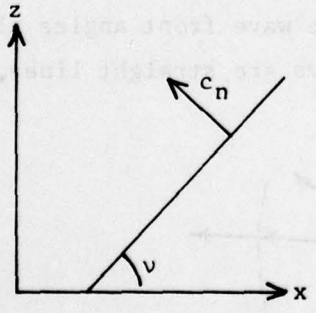

Figure L1. Group Velocity of Acoustic Waves

$$\vec{C} = a \cdot \vec{n} + \vec{U}$$

$$\vec{U} = (1 + \phi_x)\vec{i} + \phi_z\vec{j}$$

$$c_n = \vec{C} \cdot \vec{n} = a - (1 + \phi_x)\sin\nu + \phi_z \cos\nu$$

where a is the speed of sound.

For the two-dimensional case, only the angles $\nu = \pi/2$ and $-\pi/2$ appear, so for the receding wave

$$c_n = a - (1 + \phi_x) \simeq M_\infty^{-1} - 1 - M_\infty^2(\gamma + 1)\phi_x$$

(Note: $\beta_0^2 = 1 - M^2 \equiv 1 - (1+\phi_x)^2/a^2 \simeq \beta_\infty^2 - M_\infty^2(\gamma + 1)\phi_x$)

hence

$$a - (1 + \phi_x) = a^2(a + 1 + \phi_x)^{-1}[\beta_\infty^2 - M_\infty^2(\gamma + 1)\phi_x]$$

$$\simeq \frac{1}{2}[\beta_\infty^2 - M_\infty^2(\gamma + 1)\phi_x] \equiv \frac{1}{2}\beta_0^2$$

The phase angle may easily be calculated in the two-dimensional case. During the time 'dt' the acoustic wave propagates a distance $dx = c_n dt$ and hence

$$\theta = k\int_x^{xo} \frac{d\xi}{c_n(\xi)} \simeq k\int_x^{xo} \frac{2d\xi}{\beta_0^2}$$

is the phase shift between the source point, x_0, and a field point, x.

In the three-dimensional case, the calculation of the phase shift becomes more complicated. It will then be necessary to trace the acoustic rays emanating from each source point, and the wave front angles along the way. In the ordinary linearized case, the rays are straight lines, but in

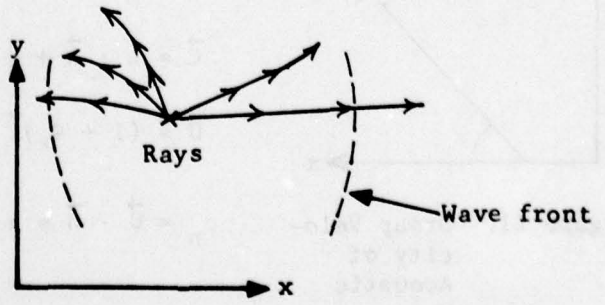

Figure L2. Rays and Wave Fronts

the transonic case they would be curved, particularly for the receding wave portions. I suggest that a ray tracing program be worked out so that one can see how rays will behave for a particular three-dimensional wing case. Possibly, the ray curvature may be small so that one could approximate the ray path by a straight line between the source and the field point, in which case the determination of the phase angle simplifies considerably.

Going back to the two-dimensional case, the kernel is obtained from the integral

$$K = \lim_{z \to 0} \left\{ \int_{-\infty}^{x} e^{-ik(x - x_1)} \psi_{d_z}(x_1) dx_1 \right\}$$

$$\simeq \lim_{z \to 0} \left\{ \int_{-\infty}^{x} e^{-ik(x - x_1)} \frac{c_{n_o}}{c_n(x_1)} \psi_{d_z}{}^{(L)}(x_1) e^{i[\theta(x_1) - \theta^{(L)}(x_1)]} dx_1 \right\}$$

For small k, which is the main concern here, the main phase variation comes from the term $\exp(i\theta)$, the phase variation in the linear solution being cancelled by the term $\exp(-i\theta^{(L)})$. Now, from the receding-wave solution

$$\frac{\partial \theta}{\partial x} = 2k/\beta_o{}^2 = \frac{k}{c_n}$$

Hence, integration by parts of the above approximate kernel gives

$$K \simeq \lim_{z \to 0} \left\{ \frac{c_{n_o}}{ik} \psi_{d_z}{}^{(L)} e^{i(\theta - \theta^{(L)})} \right.$$

$$\left. - c_{n_o} \int_{-\infty}^{x} e^{-ik(x - x_1)} \psi_{d_z}{}^{(L)}(x_1) e^{i[\theta(x_1) - \theta^{(L)}(x_1)]} dx_1 \right\}$$

Of the two terms, the first one would be the most important one for low values of k. If we now compare with the kernel obtained for the purely linear case

$$K = \lim_{z \to 0} \left\{ \frac{c_{n_o}}{ik} \Psi_{d_z}^{(L)} - c_{n_o} \int_{-\infty}^{x} e^{-ik(x - x_1)} \Psi_{d_z}^{(L)} dx_1 \right\}$$

we find that a good approximation should be obtained by taking the local linearized kernel function for the local Mach number at the source point and correcting it for the phase angle. Thus,

$$K_{trans} = K^{(L)} e^{i(\theta - \theta^{(L)})}$$

where θ and $\theta^{(L)}$ refer to phase angles between source and field point locations. Hence, the correction involves only the computation of phase shifts using ray theory.

APPENDIX A

EVALUATIONS OF ΔD_{ji}

In order to carry out the integrations for D_{ji} (denoted by ΔD_{ji}) such as Equations (4.19), (4.20), and (4.21), it is necessary to first curve-fit the analytical function $F_m(x_j - \xi)(m = 0,1,2)$, as shown in Equations (4.22) and (4.23) for the subsonic case. Notice that all the coefficients used (i.e., $\overline{A}$, $\overline{B}$, and $\overline{C}$) in F_i are not those defined in Equations (2.11), (2.15), and (2.16) in the text; also, δ_i in the subsequent formulas should be distinguished from Dirac's delta function, δ.

As the subsonic flow expression was given in Equations (4.22) and (4.23), we shall only present the sonic-flow formula and the supersonic-flow formula for ΔD_{ji}.

- Sonic Elements

$$F_o(x_j - \xi) = \sqrt{x_j - \xi}\, K_o(x_j - \xi) \qquad , x_j \geq \xi$$

Fitting F_o as a parabola, we write

$$F_o(x_j - \xi) \cong \overline{A}(x_j - \xi)^2 + \overline{B}(x_j - \xi) + \overline{C}$$

$$\Delta D_{ji} = \frac{1}{105 \cdot \delta_i \pi} \left\{ -15\overline{A}(a^{7/2} - x_j^{7/2}) + 21(a\overline{A} - \overline{B})(a^{5/2} - x_j^{5/2}) \right.$$

$$\left. + 35(a\overline{B} - \overline{C})(a^{3/2} - x_j^{3/2}) + 105a\overline{C}(a^{1/2} - x_j^{1/2}) \right\} \qquad \text{(A.1)}$$

where

$$a = x_j - \xi_i - \delta_i$$

$$\delta_i = \begin{cases} -(\xi_i - \xi_{i-1}) & \xi_{i-1} \leq \xi \leq \xi_i,\ x_j \geq \xi_i \\ \text{for} & \\ \xi_{i+1} - \xi_i & \xi_i \leq \xi \leq \xi_{i+1},\ x_j \geq \xi_{i+1} \end{cases}$$

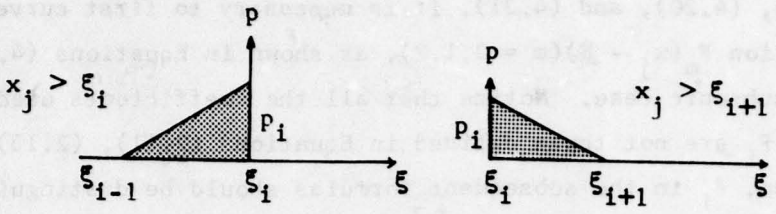

Figure A1. Sonic Element

For $x_j = 1/2(\xi_{i-1} + \xi_i) = x_{i-1}$,

$$\Delta D_{ii} = \frac{1}{15\pi} \sqrt{(\xi_i - \xi_{i-1})/2} \, [F_o(x_{i-1} - \xi_{i-1}) + 4F_o(0)] \qquad (A.2)$$

For $x_j = (\xi_i + \xi_{i+1})/2 = x_i$,

$$\Delta D_{ii} = \frac{2}{15\pi} \sqrt{(\xi_{i+1} - \xi_i)/2} \, [2F_o(x_i - \xi_i) + 3F_o(0)] \qquad (A.3)$$

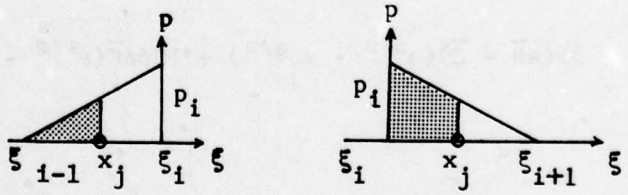

Figure A2. Sonic Elements Showing Receiving Points

- **Supersonic Elements**

$$F_1(x_j - \xi) = K_1(x_j - \xi) - \frac{\pi m_o}{2}\,\delta(x_j - \xi) \qquad x_j \geq \xi$$

here, δ is Dirac's delta function. For $x_j \geq \xi_i$,

$$\Delta D_{ji} = \frac{(\xi_i - \xi_{i-1})}{12\pi}\left[F_1(x_j - \xi_i) + 2F_1\left(x_j - \frac{\xi_i + \xi_{i-1}}{2}\right)\right] \qquad (A.4)$$

For $x_j \geq \xi_{i+1}$,

$$\Delta D_{ji} = \frac{(\xi_{i+1} - \xi_i)}{12\pi}\left[F_1(x_j - \xi_i) + 2F_1\left(x_j - \frac{\xi_i + \xi_{i+1}}{2}\right)\right] \qquad (A.5)$$

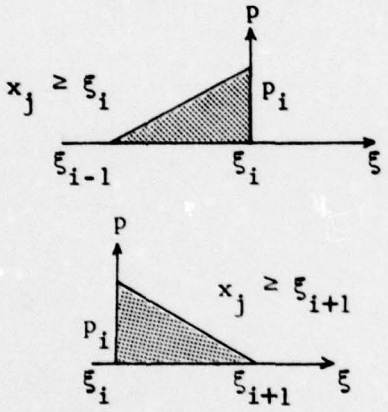

Figure A3. Supersonic Element

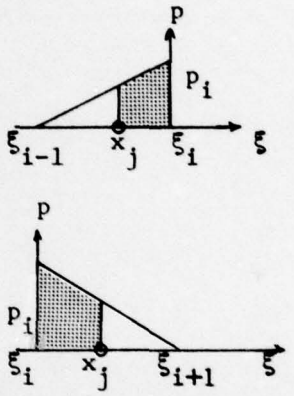

Figure A4. Supersonic Element Showing Receiving Points

For $x_j = (\xi_{i-1} + \xi_i)/2 = x_{i-1}$,

$$\Delta D_{ii} = \frac{(\xi_i - \xi_{i-1})}{48\pi}\left[F_1(x_{i-1} - \xi_{i-1}) + 2F_1(0)\right]$$

For $x_j = (\xi_i + \xi_{i+1})/2 = x_i$, (A.6)

$$\Delta D_{ii} = \frac{(\xi_{i+1} - \xi_i)}{48\pi}\left[5F_1(x_i - \xi_i) + 4F_1(0)\right] \qquad (A.7)$$

APPENDIX B

KERNEL FUNCTION FORMULATION ACCORDING TO ECKHAUS-LANDAHL'S SHOCK-JUMP MODEL

AD-A080 227 NORTHROP CORP HAWTHORNE CA AIRCRAFT GROUP F/G 20/4
TRANSONIC KERNEL FUNCTION METHOD FOR UNSTEADY FLOW CALCULATIONS--ETC(U)
MAY 79 D D LIU, W S PI, M T LANDAHL F33615-78-C-3202
UNCLASSIFIED NOR-79-52 AFFDL-TR-79-3085 NL

2 OF 2
AD A080227

END
DATE FILMED
3-80
DDC

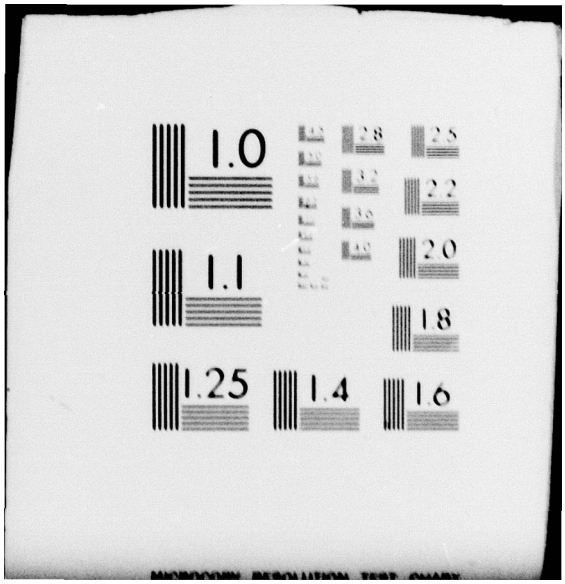
1.0
1.1
1.25
1.4
1.6
2.8
3.2
3.6
4.0
2.5
2.2
2.0
1.8

The oscillatory shock-jump relation based on Eckhaus-Landahl's one-dimensional model (Reference 21) can be written, in terms of the velocity potential, φ, as

$$\varphi_x^+ - i\alpha\varphi^+ = -\varphi_x^- - i\alpha\varphi^- \qquad \text{(B.1)}$$

where

$$\alpha = \frac{2kM_\infty^2}{1 - M^2(x_s^+)} \simeq \frac{kM_\infty^2}{1 - M(x_s^+)}$$

Notice that the LHS of Equation (B.1) represents the downstream condition immediately behind the shock wave, whereas the RHS represents the upstream condition immediately ahead of it. For simplicity, we let the local Mach numbers in Regions 1 and 2 be a uniform supersonic Mach number and a uniform subsonic Mach number. The mean shock jump is, of course, governed by the Prantdl shock relation. Let the shock point be x_s, and hence the control points in the panel '-' and '+' (see Figure B1) are denoted as x_s^- and x_s^+. Hence, $M_\infty = M_1$ and $M(x_s^+) = M_2$.

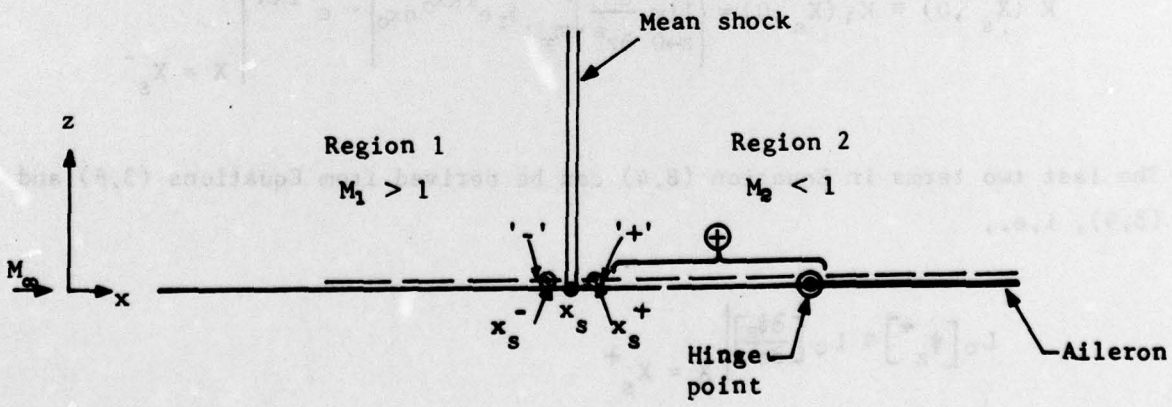

Figure B1. Eckhaus-Landahl Model Showing Notations

According to the usual linearized definition of acceleration potential (i.e., dropping the ϕ_x terms in Equation (2.8)), Equation (B.1) can be recast in the following form, after a differentation in the z-direction, i.e.,

$$\psi_z^+ - i(k + \alpha)\varphi_z^+ = -\psi_z^- + i(k - \alpha)\varphi_z^- \tag{B.2}$$

Now, if we define an operator L_o as

$$L_o[\cdot] \equiv e^{-kX} \cdot \lim_{z \to 0} \frac{\partial}{\partial z} [\cdot] \tag{B.3}$$

then L_o can be applied to Equation (B.2) and it yields

$$K^+ \equiv K^+(X_s^+,0) = \frac{1}{\alpha + k} \{(\alpha - k)K^-(X_s^-,0) - i(L_o[\psi_z^+] + L_o[\psi_z^-])\} \tag{B.4}$$

where

$$X_s^- = x_s^- - \xi \ , \ \xi \leq x_s^-$$

$$X_s^+ = x_s^+ - \xi \ , \ 1 > \xi > x_s$$

$$K^-(X_s^-,0) \equiv K_1(X_s^-,0) = \left\{ \lim_{z \to 0} \frac{\partial^2}{\partial z^2} \int_{m_\infty z}^{X} \psi_1 e^{ikx_o} dx_o \right\} \cdot e^{-ikX} \Bigg|_{X = X_s^-}$$

The last two terms in Equation (B.4) can be derived from Equations (3.8) and (3.9), i.e.,

$$L_o\left[\psi_z^+\right] \equiv L_o\left[\frac{\partial \psi_2}{\partial z}\right]\Bigg|_{X = X_s^+}$$

$$= -c_2 k M_2 e^{-i(\kappa_2 M_2 - k)X_s^+} \cdot H_1^{(2)}(\kappa_2 X_s^+)/X_s^+ \tag{B.5}$$

$$L_o[\psi_z^-] \equiv L_o\left[\frac{\partial \psi_1}{\partial z}\right]\Bigg|_{X = X_s^-} \tag{B.6}$$

$$= c_1 e^{-i(\kappa_1 M_1 + k)X_s^-} \cdot \left[H(X_s^-)kM_1 J_1(\kappa_1 X_s^-)/X_s^- - m^2 \delta'(X_s^-) J_o(\kappa_1 X_s^-)\right]$$

where

$$c_1 = \frac{2\pi}{m} \quad ; \quad m^2 = M_1^2 - 1$$

$$c_2 = -\frac{i\pi}{\beta} \quad ; \quad \beta^2 = 1 - M_2^2$$

$$\kappa_1 = kM_1/m_2$$

$$\kappa_2 = kM_2/\beta^2$$

Consequently, when the condition at $x = x_s^+$ is obtained, the integrated potential in Region 2 can be written as

$$\varphi_{\oplus}(X,z) = e^{-ikX} \cdot \left[\int_{X_s^+}^{X} e^{ikx_o} \psi dx_o + e^{ikX_s^+} \varphi(X_s^+, z)\right] \tag{B.7}$$

Next, let us introduce another operator, $L_o'[\cdot] \equiv \lim_{z \to 0} \frac{\partial^2}{\partial z^2}[\cdot]$, and apply this operator to Equation (B.7). After some rearrangement, we obtain the kernel function formula in Region 2, i.e.,

$$K_{\oplus}(X,0) = K_2(X,0) - \left[K_2(X_s^+,0) - K^+\right] \cdot e^{-ik(x - x_s^+)} \tag{B.8}$$

Notice that K_2 in Equation (B.8) is the usual subsonic kernel function in the absence of the shock wave.

For the application of the above kernel function formulation, we select the aileron-buzz model proposed by Eckhaus (Reference 52), see Figure B1. Thus, the shock wave is placed ahead of the hinge point. As we have assumed that the mean shock wave is one-dimensional, which is infinite in extent, the acoustic waves generated by the oscillating aileron cannot diffract toward Region 1 upstream. (Such a wave diffraction should be accounted for in the two-dimensional case, as it was shown by Tijdeman, Reference 14.) All the upstream influences on Region 2 from the supersonic side is taken care of by the shock-jump condition. Hence, in terms of the present panel-method, the above consideration amounts to no further influence of the panels betwen Region 1 and Region 2 other than the shock-jump kernel formula relating the adjacent panels '-' and '+'.

For a calculation example, we plan to compute the stability boundary for the hinge moment (see Figure 3, Reference 52). Since our formulation is not restricted to low-frequency computation, our result may then be compared with Lambourne's experimental data (k below 0.1).

Although Eckhaus' formulation is fairly general in the frequency range, his calculation scheme is subject to an approximation, which restricts the frequency to a higher range than 0.1. Furthermore, as the present MKF formulation is completely flexible in the steady flow input, little problem is expected to generalize the aileron-buzz model to one with a nonuniform mean flow. Clearly, studying this problem will certainly better our understanding of the mixed kernel function procedure leading to a general scheme for the supercritical flow computations.

Finally, it should be pointed out that the present shock-jump kernel function formulation only amounts to one which satisfies the shock jump condition, Eq. (B.1), at the foot of the shock, i.e., at $z = 0$. As the assumed mean shock wave is infinite in extent, Eq. (B.1) should be satisfied formally along the shock in z-direction. Landahl (Reference 57) proposed to use Fourier Transform in obtaining a general two-dimensional condition for a pulsating source and has obtained solutions in the upstream and the downstream sides of the shock wave in the transformed plane. Further investigations along this line are needed.

APPENDIX C

COEFFICIENTS FOR $C_{P_o} = \sum_{n=0}^{9} a_n \xi^n$

POLYNOMIAL COEFFICIENT	NACA64A006 AIRFOIL		WEDGE $M_\infty = 1.15$ $\tau = 0.05$	PARABOLIC-ARC AIRFOIL $M_\infty = 1.2$, $\tau = 0.0125$		GUDERLEY AIRFOIL $M_\infty = 1.0$ $\tau = 0.06$	PARABOLIC-ARC AIRFOIL $M_\infty = 1.0$ $\tau = 0.06$
	$M_\infty = 0.8$	$M = 0.825$		LINEAR THEORY	MODIFIED SPREITER		
a_0	-0.23302	-0.26342	0.881	0.1508	0.1956	-0.3944	0.4089
a_1	0.33363	0.35167	0	-0.3015	-0.3296	-0.9860	-2.5278
a_2	0.35350	0.40602	0	0	0	0	4.5893
a_3	-0.9777	-0.96755	0	0	0	0	-4.9746
a_4	0.5873	0.09087	0	0	0	0	2.0046
a_5	1.82620	1.55850	0	0	0	0	0
a_6	-0.76407	-0.88081	0	0	0	0	0
a_7	-1.19130	-0.79412	0	0	0	0	0
a_8	0.67934	0.73021	0	0	0	0	0
a_9	0.05657	-0.11261	0	0	0	0	0

REFERENCES

1. Ehlers, F.E., "A Finite Difference Method for the Solution of the Transonic Flow around Harmonically Oscillating Wings," NASA CR-2257, January 1974.

2. Traci, R.M., Farr, J.L., and Albano, E., "Perturbation Method for Transonic Flows about Oscillating Airfoil," AIAA Paper 75-877, June 1975.

3. Weatherill, W.H., Ehlers, F.E., and Sebastian, J.D., "Computation of the Transonic Perturbation Flow Fields around Two- and Three-Dimensional Oscillating Wings," NASA CR-2599, April 1975.

4. Beam, R.M., and Warming, R.F., "Numerical Calculations of Two-Dimensional Unsteady Transonic Flows with Circulation," NASA TN D-7605, February 1974.

5. Ballhaus, W.F., and Goorjian, P.M., "Implicity Finite-Difference Computations of Unsteady Transonic Flows about Airfoils, Including the Treatment of Irregular Shock-Wave Motions," AIAA Paper 77-205, January 1977.

6. Yu, N.J., Seebass, A.R., and Ballhaus, W.G., "An Implicit Shock Fitting Scheme for Unsteady Transonic Flow Computations," AIAA Paper 77-633, June 1977.

7. Chan, S.T.K., and Brashears, M.R., "Finite Element Analysis of Transonic Flow," AFFDL-TR-74-11, March, 1974, also AIAA Paper 75-875.

8. Küssner, H.G., "Allgemeine Tragflächentheorie," Luftfahrtforschung 17 (11/12), 1940, pp. 370-378.

9. Landahl, M.T., and Stark, V.J.E., "Numerical Lifting-Surface Theory: Problems and Progress," AIAA Journal, Volume 6, No. 11, November 1968, pp. 2049-2059.

10. Rodden, W.P., Giesing, J.P., and Kalman, T.P., "New Developments and Applications of the Subsonic Doublet-Lattice Method for Nonplanar Configurations," AGARD Symposium on Unsteady Aerodynamics for Aeroelastic Analyses of Interfering Surfaces, Paper No. 4, Norway, 1970.

11. Rowe, W.S., "Collocation Method for Calculating the Aerodynamic Pressure Distributions on a Lifting Surface Oscillating in Subsonic Compressible Flow," Proceedings of the AIAA Symposium on Structural Dynamics and Aeroelasticity, Boston, 1965, New York, 1965, pp. 31-45.

12. Cunningham, A.M., "Oscillatory Supersonic Kernel Function Method for Isolated Wings," Journal of Aircraft, Volume II, Number 10, October 1974, pp. 609-615.

13 Albano, E., and Rodden, W.P., "A Double-Lattice Method for Calculating Lift Distributions on Oscillating Surfaces in Subsonic Flows," AIAA Journal, No. 11, November 1969, p. 2192.

14. Tijdeman, H., "Investigation of the Transonic Flow around Oscillating Airfoils," NLR-TR-77090U, 1977.

15. Cunningham, A.M., "An Oscillatory Kernel Function Method for Lifting Surfaces in Mixed Transonic Flow," AIAA Paper No. 74-359, 1974.

16. Liu, D.D., "A Mixed Kernel Function Method for Unsteady Transonic Flow Calculations," Northrop Technical Brief, PC 20-59, March 1976.

17. Liu, D.D., and Winther, B.A., "Towards a Mixed Kernel Function Approach for Unsteady Transonic Flow Analysis," AGARD/FDP "Unsteady Aerodynamics" Symposium, Ottawa, Canada, September 1977 AGARD CPP-227, Paper No. 12.

18. Liu, D.D., "A Lifting Surface Theory Based on an Unsteady Linearized Transonic Flow Model," presented at the 19th AIAA/ASME Structure Dynamics and Material Conference in Bethesda, MD, April 1978, AIAA Paper No. 78-501.

19. Pi, W.S., Kelly, P.A., and Liu, D.D., "A Transonic Doublet Lattice Method for Unsteady Flow Calculations," AIAA Paper No. 79-0078, January 1979.

20. Murman, E.M., and Cole, J.D., "Calculation of Plane Steady Transonic Flows," AIAA Journal, Volume 9, No. 1, January 1971, pp. 114-121.

21. Landahl, M.T., Unsteady Transonic Flow, International Series of Monographs in Aeronautics and Astronautics, Pergamon Press, London, 1961.

22. Ruo, S.Y., Yates, E.C. Jr., and Theisen, J.G., "Calculation of Unsteady Transonic Aerodynamics for Oscillating Wings with Thickness," AIAA Paper No. 73-326, 1973.

23. Dowell, E.H., "A Simplified Theory of Oscillating Airfoils in Transonic Flow: Review and Extension," AIAA/ASME 18th Structural Dynamics Conference, San Diego, California, March 21-23, 1977, pp. 209-224.

24. Oswatitsch, K., and Keune, F., "Flow Around Bodies of Revolutions at Mach Number One," Paper presented at the Brooklyn Polytechnic's Conference on High-Speed Aeronautics, 1955.

25. Maeder, P.F., and Thommen, H.U., "Some Results of Linearized Transonic Flow about Slender Airfoils and Bodies of Revolution," J. Aero. Sci., No. 23, 1956, pp. 187-188.

26. Stahara, S.S., and Spreiter, J.R., "Development of a Nonlinear Unsteady Transonic Flow Theory," NASA CR-2258, 1973.

27. Rott, N., "Oscillating Airfoils at Mach Number 1," J. Aero. Sci. 16, No. 6, 1949, pp. 380-381.

28. Miles, J.W., "The Aerodynamics Forces on an Oscillating Airfoil at Supersonic Speeds," J. Aero. Sci. 14, 1947, pp. 351-358.

29. Possio, C., "L'azione aerodinamica sul profilo oscillante in un fluido compressibile a velocita iposonora," L'Aerotechnica, 18 (4), 1938, pp. 421-458.

30. Watkins, C.E., Runyan, H.L., and Woolston, D.S., "On the Kernel Function of the Integral Equations Relating the Lift and Downwash Distribution of Oscillating Finite Wings in Subsonic Flow," NACA RPT 1234, 1955.

31. Watkins, C.E., and Berman, J.H., "On the Kernel Function of the Integral Equation Relating Lift and Downwash Distributions of Oscillating Wings in Supersonic Flow," NACA RPT 1257, 1957.

32. Woodward, F.A., "Analysis and Design of Wing-Body Combination at Subsonic and Supersonic Speeds," Journal of Aircraft, Volume 5, November-December 1968, pp. 528-534.

33. Winther, B., "A Consistent Finite Element Approach to Linearized Unsteady Aerodynamics," Northrop Technical Brief NB 75-218, July 1975.

34. Shen, C.C., Lopez, M.L., and Wasson, N.F., "A Jet-Wing Lifting-Surface Theory Using Elementary Vortex Distributions," Journal of Aircraft, Volume 12, May 1975, pp. 448-456.

35. Fromme, J.A., and Halsteed, D.W., "Solutions to Küssner's Integral Equation in Unsteady Flow using Local Basis Functions," NASA CR-137719, September 1975.

36. Landahl, M., "Pressure-Loading Functions for Oscillating Wings with Control Surfaces," AIAA Journal, Volume 6, February 1968, pp. 345-348.

37. Oswatitsch, K., and Zierep, J., "Das Problem des Senkrechten Stossens an einer Gekruemmten Wand," ZAMM, Volume 40, Suppl. 1960, pp. T143-144.

38. Williams, M.H., "Linearization of Unsteady Transonic Flows Containing Shocks," AIAA Journal, Volume 4, Number 4, April 1979, pp. 394-397.

39. James, R.M., "On the Remarkable Accuracy of the Vortex Lattice Method," Computer Methods in Applied Mechanics and Engineering, Volume 1, June 1972, pp. 59-79.

40. Isogai, K., "Approximate Method for Calculating Aerodynamic Loadings on an Airfoil Oscillating in High Subsonic Flow," NAL TR-455T, 1976.

41. Tijdeman, H., and Schippers, P., "Results of Pressure Measurements on Airfoil with Oscillating Flap in Two-Dimensional High Subsonic and Transonic Flow (Zero Incidence and Zero Mean Flap Position)," NLR TR-73078U, 1973.

42. Fritz, W., "Transonische Strömung um Harmonisch Schwingende Profile," BMVg - Vertrag Nr. T/RF 41/RF 412/61420, Dornier GMBH, September 1978.

43. Chadwick, W.R., "Unsteady Supersonic Cascade Theory including Nonlinear Thickness Effects," PhD Thesis, Naval Postgraduate School, June 1975; also see AGARD CP-177, September 1975.

44. Jordan, P.F., "Aerodynamics Flutter Coefficients for Subsonic, Sonic and Supersonic Flow (Linear Two-Dimensional Theory)," Aeronautical Research Council R&M 2932, 1957.

45. Snyder, L.E. "Supersonic Torsional Flutter in Cascades," Final Technical Report PWA-4701, Pratt and Whitney Aircraft, E. Hartford, CT, April 1973.

46. Garrick, I.E., and Rubinow, S.J., "Flutter and Oscillating Air-Force Calculations for an Airfoil in Two-Dimensional Supersonic Flow," NACA Report 846, 1946.

47. Brix, C.W., "A Study of Supersonic Flow Past Vibrating Shells and Cascades," PhD Thesis, Naval Postgraduate School, June 1973; also see AIAA Paper No. 74-14.

48. Carrier, G.F., "The Oscillating Wedge in a Supersonic Stream," J. Aero. Sci., Volume 16, No. 3, March 1949, pp. 150-152.

49. Spreiter, J.R., and Alksne, A.Y., "Thin Airfoil Theory Based on Approximate Solution of the Transonic Flow Equation," NACA Report 1359, 1958.

50. Goodman, T.R., "An Integral Approach to Lifting Wing Theory at Mach One," AFOSR-TR-75-0822, June 1975.

51. Knechtel, E.D., "Experimental Investigation at Transonic Speeds of Pressure Distributions over Wedges and Circular Arc Airfoil Sections and Evaluation of Perforated Wall Interference," NASA TND-15, 1959.

52. Eckhaus, W., "A Theory of Transonic Aileron Buzz Neglecting Viscous Effects," J. Aero. Sci., June 1962, pp. 712-718.

53. Landahl, M.T., "Some Developments in Unsteady Transonic Flow Research," Symposium Transsonicum II (IUTAM), Gottingen, 1975, pp. 1-32.

54. Liepmann, H.W., and Roshko, A., Elements of Gasdynamics, GALCIT Aeronautical Series, John Wiley and Sons, Inc., 1975.

55. Teipel, I.,"Die Berechnung instationarer Luftkrafte im schallnahen Bereigh," Journal de Mecanique, Volume 4, No. 3, September 1965, pp. 335-360.

56. Landahl, M.T., "Linearized Theory for Unsteady Transonic Flow," Symposium Transsonicuum, Volume I, Edited by Oswatitsch, Springer-Verlag, Berlin, 1962, pp. 414-439.

57. Landahl, M.T., Private Communication, 1979.

*U.S.Government Printing Office: 1979 — 657-084/387